Condensation on rotating axisymmetric bodies

Mensah Ampadu Osei-Bonsu

CONDENSATION ON ROTATING AXISYMMETRIC BODIES

by

MENSAH AMPADU OSEI-BONSU, B.Sc.

Thesis submitted for the degree of

Doctor of Philosophy

in the

University of Durham

May 1974

Department of Engineering Science

University of Durham

Abstract

An analysis is made for the laminar film condensation on a rotating axisymmetrical general curved body of which the cylinder, the disc and the cones are special examples. The body rotates about a vertical axis and the film is assumed to drain under the influence of gravitational and centrifugal accelerations. The problem is formulated as a solution of the Navier-Stokes and energy equations. A differential equation which governs the growth of the condensate film is obtained and solved to yield one equation which is applicable to all rotating axisymmetrical bodies. The equation involves the geometry of the body and requires a single integration for the complete solution.

Theoretical results of condensate layer thickness and heat transfer coefficients are given for a curved body whose generator forms a circular arc of 90^{o} for a speed range of 0.1 to 10^{6} rev/min. It is shown that when the curvature is neglected, the analysis over-estimate the local film thickness by 71 per cent.

Experimental results for the curved body confirm the theoretical findings. However, due to the formation of roll-waves on the condensate layer and hence a departure from the laminar model, the experimental results for the heat transfer coefficient were 1.055 to 1.440 times greater than the theoretical predictions.

No detachment of drops from the film of condensate was observed at the experimental speed range of 0.0 to 1000 rev/min. and the condensate drained as a film along the generator. The criterion for the detachment of drops given by Howe is re-appraised and a new criterion which states that "the non-dimensional film thickness η, should be equal to or greater than 1.8 for the onset of the detachment of drops" is proposed.

Acknowledgements

The work reported here would not have been possible without the help of many people and I am greatly indebted to them.

My sincere thanks are extended to Professor Harry Marsh. Without his skilful direction and supervision throughout the work many of the findings in this report would not have been possible.

I am also extremely grateful to Dr. M. J. Holgate, who as a member of the research group at Durham, never failed with his advice and help when needed.

I would like to thank Dr. M. Howe for his help and advice, in particular for placing at my disposal information not contained in his thesis. Similar thanks are extended to Mr. D. B. Smith for making available to me his unpublished experimental findings.

My thanks are due to Chief technician Mr. C.J.F. Campbell and senior technicians D. James, A. Harker and W. Johnson for their help in the construction and running of the rig.

My thanks are also due to the Science Research Council for sponsoring this work.

I am grateful to Miss Rosemary Atkinson for patiently transforming pages of handwriting into typed script.

Finally I am indebted to Iris and the children who have had to be so patient and understanding.

Contents

List of Figures and Photographs

LIST OF SYMBOLS

A	$\frac{3\nu^2 C\theta}{Pr[h_{fg} + \frac{3}{8}C\theta]}$
$\hat{A}$	Surface area
D	As defined in section 3.2.1
F	$(\xi^2 Sin\lambda + \xi Cos\lambda)$; Body force
M	Correction factor as defined in equation (7.3.1)
N	Rotational speed
Q	Heat transfer per unit time
R	Radius of body as defined in fig. 1.
R_c	Radius of curvature
S	Co-ordinate, defined in fig. 1
T	Temperature
T_i	Cooling water-wall interfacial temp.
T_o	Condensate-wall interfacial temperature
T_{sat}	Saturation temperature
U	Velocity of vapour
V	Velocity of condensate
W	Condensate mass flow rate per unit perimeter ($\dot{m}/\pi d$)
X	Distance along the generator of cone
Y	Co-ordinate, as defined in fig. 1
a	As defined in text
b	As defined in text
c	Specific heat at constant pressure of condensate
d	Outside diameter (of cylinder, cone)
e_s	Unit vector in S direction
e_y	Unit vecton in Y direction

e_ϕ	Unit vector in ϕ direction
f	Frictional factor
g	Gravitational acceleration
h	Local heat transfer coefficient
$\bar{h}$	Average heat transfer coefficient
h_{fg}	Specific enthalpy of condensation
h_s, h_y, h_ϕ	Scale factors
i	Unit vector in x direction
j	Unit vector in y direction
k	Unit vector in z direction
k	Thermal conductivity of condensate
k_w	Thermal conductivity of body material
ℓ	Length as defined in fig. 2 or in text
$\dot{m}$	Mass flow rate
p	Pressure
q	Heat transfer per unit area and time
s	Distance in S direction
$\bar{v}$	Mean velocity of condensate
x	Cartesian Co-od.; length in x direction
y	Cartesian Co-od.; length in y direction
y	Film thickness in Y direction
z	Cartesian Co-od.; length in z direction
α	Non-dimensionalisation constant
$\hat{\alpha}$	Angle of inclination (half cone angle)
γ	Non-dimensionalisation constant
β	Angle as defined in fig. 2

η	Non-dimensional film thickness
ξ	Non-dimensional radius ($\xi=R_w^2/g$)
ρ	Density
μ	Dynamic viscosity
ν	Kinematic viscosity
δ	Condensate thickness
τ	Shear stress
σ	Surface tension; electrical conductivity
ω	Angular velocity
θ	Temperature difference ($T_{sat} - T_o$)
θ_w	Temperature difference ($T_o - T_i$)
ϕ	Co-ordinate, defined in fig. 1
λ	Short form of $\lambda(\xi)$, function of ξ, ($\beta = \lambda(\xi)$)
ψ	Short form of $\psi(s)$, function of s, ($\beta = \psi(s)$)
Φ	Short form of $\phi(s)$, function of s, ($\xi = \Phi(s)$)
$\mathfrak{F}$	$\xi/\mathrm{Sin}\lambda$
∇	Vector operator "nabla"
Subscripts	
i	Inside surface of body
o	Outside surface of body; origin
v	Vapour
w	Wall
m	Mean
sat	Saturated steam
s, y, ϕ	S, Y and ϕ directions
Nu_s	Nusselt number hs/k
Pr	Prandtl number $c\mu/k$

Re	Reynolds number $4W/\mu$
We	Weber number $d^3{}_{\rho\omega}{}^2/(4g_c)$

Unlisted symbols are as defined in the text.

1.0 INTRODUCTION

1.0 INTRODUCTION

This work is concerned primarily with the filmwise condensation of steam on rotating axisymmetrical curved bodies.

The need to investigate condensation on rotating bodies on the present scale arose in the 1950s when the Royal Navy showed interest in the phenomenon. Transient thermal stresses occur in all steam turbine rotors during cold starting and during the maneouvring of marine steam turbines. These thermal stresses result from the changes in rotor temperature on the admission of the steam to the turbine. If the rate of change of rotor temperature is not limited during these operations, the rotor can be overstressed and eventually suffer thermally induced fatigue which in turn leads to the risk of rotor disintegration. Thus a turbine has to be warmed up gradually until it attains the operating temperatures.

The warming up time can be several hours depending on the size of the turbine. This is tolerated in land based turbines and some marine steam turbines, but it is something the Navy could not entertain, hence the Navy's interest.

The present work therefore forms part of a wider investigation into the question of transient thermal stresses in steam turbine rotors during cold starting and during maneouvring.

The work reported here is not of interest to turbine operators only but also turbine and heat exchanger designers. Large acceleration fields created by rotating the condensing surface lead to improvements in the rate of condensation. In the field of condenser design such improvements could reduce the area of the condensing surface for a given thermal load and thus reduce the

size of the condenser. This advantage might be used in space-flight applications where the condition of zero gravity demands the creation of an acceleration field at the condensing surface to induce film drainage. Creating the field by rotating the surface, as opposed to vibrating it, has the operational advantage of being both silent and dynamically balanced. In large land based condensers however, the advantage gained by the improved rate of condensation as a result of the rotation might be cancelled by the initial and running costs. However, in plants where space conservation is of critical importance rotating surface condensers could be a practical proposition.

The question of thermal stresses in turbine rotors is not a problem for the turbine operator only. It is a primary concern to the turbine designer. With the advent of the large rotors used in land based turbines and the use of steam turbines in nuclear submarines, there has been the need for the turbine designer to reduce the warm through period while maintaining safe levels of stresses in the rotor. With steam turbines the problem of finding the rotor temperature at a given time is complicated by the deposition of condensate on the rotor whenever the saturation temperature of the steam is higher than the rotor outer surface temperature. The behaviour of the film as a heat transfer barrier depends on the thickness of the film which increases until the rates of condensation and drainage are equal. The rates of drainage are governed by the geometry of the condensing surface and by the magnitude and direction of the acceleration field produced by the rotor. In this report an equation has been derived which enables the behaviour of the condensate film to be predicted when the geometry and the speed of rotation of the condensing surface are known.

A considerable amount of work, both theoretical and experimental, has been done in the field of condensation on rotating bodies by other workers. In the main however, the published work covers the cylinder, the disc and the cones. The general curved body of which the cylinder, the disc and the cones are special cases has not been studied in depth. In the present work, the general curved body has been studied in detail. A laminar model of the condensation process on the general curved body has been studied and equations developed to predict the behaviour of the condensate film and hence the heat transfer coefficients on the body. To test the theory, an experimental curved body (fig. 9) was designed and used to obtain a complete set of experimental results over a wide range of operating conditions. The experimental heat transfer coefficients are in good agreement with the values predicted by the theory.

2.0 PREVIOUS WORK

2.0 INTRODUCTION

The understanding of the mechanism of condensation has been of interest to engineers for many years because of its importance in the running of steam engines and in the chemical manufacturing processes. With the aid of the modern computers tremendous advances in the techniques of theoretical analysis and of modelling condensation have been made. In addition, the amount of experimental work to verify the mathematical models and to fill in the gaps where the models have been inaccurate has been increasing. In this section a review of those advances with bearing on the present work is made by considering the different modes of condensation, the enhancement of condensation and lastly, the condensation on rotating surfaces.

2.1 Modes of Condensation

Condensation occurs when saturated vapour comes in contact with a colder surface whose temperature is below the saturation temperature of the vapour. Liquid is formed and if the liquid wets the surface (hydrophilic) then a continuous film of liquid is formed and the process is called "filmwise condensation". If the liquid does not wet the surface (hydrophobic) droplets are formed which coalesce and run down the surface. This is called "dropwise condensation". In practice both modes of condensation can occur on the same cooling surface and this is referred to as "mixed condensation". If efforts are not made to keep the more common metals hydrophobic, then dropwise and mixed condensation will give way eventually to filmwise condensation.

It is for this reason that the majority of condensers are designed for filmwise condensation and that the present work deals only with filmwise condensation.

2.2 Dropwise condensation

This review concentrates on filmwise condensation and only a brief mention of dropwise condensation will be made in section 2.4.1 when dealing with the enhancement of condensation. However, one can direct the reader whose interest lies in dropwise condensation to papers by Tanner, Potter, Pope and West (1, 2) who report their own experimental findings on the effects of heat flux, of vapour velocity, of non-condensable gas concentration and of surface chemistry on dropwise condensation. The physical chemistry and performance of promoters of dropwise condensation have been studied by Osment et al (3). Improved performance of industrial plants by the use of dropwise promoters is reported by Poll et al (4). The density of nucleation sites has been studied by McCormick and Westwater (5, 6). Dropwise condensation is not a "steady-state" process and is much more difficult to model theoretically than is the case with filmwise condensation. A successful attempt to predict heat transfer coefficients is that of Le Fevre and Rose (7) and Rose (8). Here the model used is one in which drops grow at preferred sites on the metal surface, and heat-transfer rates are calculated for conduction through the drops.

2.3 Filmwise Condensation

2.3.1 The Nusselt theory

Filmwise condensation was first tackled theoretically by Nusselt (9) in 1916 and the equations derived in the analysis are still widely used to predict condensation rates.

Nusselt combined the laws of laminar flow of a liquid film with heat transfer by conduction through it. The following assumptions were used:

a) the energy given up by the vapour was latent heat, the specific enthalpy of condensation

b) the film drained from the surface in laminar flow.

c) heat was transferred through the film by conduction.

d) the temperature gradient through the film was linear

e) the surface of the solid was smooth and clean.

f) the temperature of the solid surface was constant, an isothermal surface.

g) the only vapour flow was towards the condensing surface.

h) the vapour was free from non-condensable gases.

The implication of assumption (b) was that the thickness of the film was small compared with the radius of curvature of the condonsing surface and that fluid accelerations and hence the inertia effects were negligible. Nusselt proceeded to obtain the following equations for condensation on plain and cylindrical surfaces for vertical drainage under gravity:

i) plain surface,

$$\bar{h} = 0.943 \left[\frac{k^3 \rho^2 g h_{fg} \operatorname{Sin} \hat{\alpha}}{\mu \times \theta} \right]^{\frac{1}{4}} \qquad (2.3.1)$$

(ii) cylindrical surface (axis horizontal),

$$\bar{h} = 0.725 \left[\frac{k^3 \rho^2 g h_{fg}}{\mu d \theta} \right]^{\frac{1}{4}} \qquad (2.3.2)$$

The analysis of Nusselt for the laminar film condensation neglected the contribution to the energy flow from the sub-cooling of the condensate below the vapour saturation temperature. For the condensation of vapours at low pressures, for example the condensation of steam under vacuum conditions, the specific enthalpy of vaporisation is large compared with the energy associated with sub-cooling and the latter may be ignored. However, for organic vapours at high pressures with large temperature differences across the condensate the contribution of the sub-cooling term is significant and cannot be ignored. Nusselt derived an alternative expression for equation (2.3.1) which included this effect. However, due to an error in the analysis the additional sub-cooling term is incorrect both in sign and in magnitude. Bromley (10) corrected the Nusselt analysis and the result was later verified by Rohsenow (11)

If a linear temperature distribution through the condensate is assumed in the manner of Nusselt, the mean heat transfer coefficients given by equations (2.3.1) and (2.3.2) can be corrected for sub-cooling by multiplying by the correction factor:

$$[1 + 0.375\ c\theta/h_{fg}]^{\frac{1}{4}}$$

Rohsenow improved this correction factor by calculating the actual non-linear temperature distribution in a thick film to give:

$$[1 + 0.68\ c\theta/h_{fg}]^{\frac{1}{4}}$$

Hampson and Ozisik (12) have compared the mean experimental heat transfer coefficient for steam condensing on inclined plates with the Nusselt value. The experimental heat transfer coefficients were shown to be between 1.18 and 1.28 times the Nusselt values for all angles of inclination away from the horizontal. However, experimental heat transfer coefficients for condensation on the underside of a horizontal plate were shown to be 1.5 times the

Nusselt values. This increase in the experimental heat transfer coefficients was attributed to the formation and detachment of pendant drops from the surface of the film.

2.3.2 The effect of vapour velocity on condensation

The general conclusion from the work on the effects of vapour velocities on condensation and heat transfer rates is that the effect is small for many fluids. Sparrow and Gregg (13) considered the effect of vapour velocity on heat transfer in connection with their work on condensation on a rotating disc and showed that the effect is small, particularly for Prandtl numbers greater than unity. They further concluded that depending on the operating conditions and on the film thickness, vapour drag may retard or augment the condensate drainage and hence may increase or decrease the heat transfer rate.

Chen (14) and Koh, Sparrow and Hartnett(15) published studies of the influence of shear stresses at the liquid-vapour interface due to induced vapour velocity, Both studies were carried out for laminar films and both utilised two-phase boundary layer theory. Chen used the equations of momentum and of energy in a modified integral form and provided a solution using a perturbation method for vertical flat plates and horizontal tubes. Koh et al used the partial differential form of the boundary layer equations and provided a solution through the use of similarity transforms.

Both studies showed that the effect of induced vapour velocity increased film thickness and reduced the heat transfer coefficient by causing a negative velocity gradient at the liquid-vapour interface with the maximum velocity occurring inside the film. The reduction in heat transfer coefficient was negligible at Prandtl numbers greater than 10, but the reduction reached 0.91 of the value without shear at Prandtl number of unity. In the liquid metal range, the adverse

effect of interfacial shear is maintained even in thin films and the heat transfer coefficient is reduced to 0.75 of the value without shear.

Nusselt (9) is analysing laminar condensation considered the effect of a shear stress on the film surface caused by vapour flow. From this consideration, his mean film velocity was modified,

from $\bar{v} = \frac{\rho g(\mathrm{Sin}\ \alpha)\ \delta^2}{3\mu}$ to $\bar{v} = \frac{\rho g(\mathrm{Sin}\ \alpha)\ \delta^2}{3\mu} + \frac{\tau_{(y\ =\ \delta)} \cdot \delta}{2\mu}$

where τ is the shear stress.

Shekriladze and Gomelauri (16) obtained analytical expressions for the mean heat transfer coefficients on a flat plate in the horizontal and vertical planes and also for a horizontal tube. They assumed that the shear stress on the condensate surface depends mainly on the momentum transfer across the liquid vapour interface. This assumption differs from that of Sugawara et al (17) who estimated the shear stress from the consideration of a non-condensing gas flow over an impermeable surface and estimated up to 35% reduction in the heat transfer coefficient.

2.3.3 Inertia effects

For water and organic liquids Chen (14) and Sparrow and Gregg (18) using a boundary layer analysis have shown that the inertia effects in the condensate film are insignificant. However, for liquid metals, the inertial effects were shown to be significant. The solutions of Sparrow and Gregg show that for a Prandtl number of 0.003 and a value of $c\theta/h_{fg} = 0.1$, the Nusselt model which neglects both inertia and convective effects, predicts heat transfer coefficients 1.75 times that of their own predictions.

2.3.4 Film flow behaviour on heat transfer rates

Several workers have measured significantly higher heat transfer coefficients for conditons where Nusselt theory should apply.

This discrepancy is attributed to the turbulent flow characteristics of the film which has been demonstrated as occurring at very low Reynolds numbers. Zozula (19) defined a condensate film Reynolds number by $Re = 4W/\mu$ and classified the flow regimes on a vertical surface into:

a) laminar for $Re < 30$

b) laminar flow but disturbed by waves for $30 < Re < 1600$

c) turbulent or wave flow for $Re > 1600$

Kirkbride (20) made measurements of the maximum film thickness for oil and water films flowing down vertical tubes. The films at Reynolds numbers $4W/\mu$ up to 8 were observed to be smooth and the measured maximum film thickness agreed with the theoretical laminar value. At Reynolds numbers between 8 and 1800, the film was observed to support waves. The maximum film thickness was found to be larger than the theoretical laminar values by a factor of approximately two at a Reynolds number of 1000.

Friedman and Miller (21) and Dukler and Bergelin (22) published mean film thicknesses for kerosene, toluene and water films flowing down vertical tubes. The mean film thicknesses were found to agree with the theoretical laminar film thicknesses.

Ginabit (23) as early as 1924 estimated that the effect of surface waves on the condensate film would be to increase the condensate film heat transfer coefficient by 20 per cent. Kapitza (24) made theoretical study of wave flow of thin layers of a viscous fluid and predicted 21 per cent greater heat transfer rate in a wavy film than that for the equivalent smooth film. Kapitza attributed this to the decrease in the average film thickness due to the wave shape.

More recently Leonard and Estrin (25) published their investigations into heat transfer through a wavy film on a vertical surface. They studied the sinusoidal wave and a steep crested and elongated trough wave.

They concluded that the shape of the wave influences the heat transfer considerably. They also noted that for low Reynolds numbers where wave amplitudes are near zero, the wavy model predictions corresponded to the laminar film model.

Colburn (26) in 1934 was the first to develop an expression for the average heat transfer coefficient under turbulent flow conditions:

$$\frac{\bar{h}}{k}\left[\frac{\nu^2}{g}\right]^{1/3} = \frac{Re}{22\ (Pr)^{-1/3}\ (Re^{0.8} - 364) + 12800}$$

Labuntsov (27) in a more recent study correlated a large amount of turbulent flow data using:

$$\frac{\bar{h}}{k}\left[\frac{\nu^2}{g}\right]^{1/3} = \frac{Re}{58(Pr)^{-\frac{1}{2}}\ (Re^{0.75} - 253) + 9200}$$

2.3.5 Influence of vapour superheat

The literature contains a lot of contradictory evidence about the belief that it is more difficult to transfer energy from superheated steam compared to saturated steam. Information about the problems associated with the use of superheated steam can be found in the proceedings of a conference held at NEL in 1961 (28).

2.3.6 Effect of non-condensable gases

When a pure saturated vapour condenses on a surface, the difference in temperature between the surface of the condensate and the bulk of the vapour is, in nearly all practical cases, very small and the resistance to heat and mass transfer at the interface is negligible. Such is not the case when the bulk of the vapour contains some gas which cannot condense under the operating conditions. In these circumstances the condensing vapour must diffuse through the stationary non-condensable gas surrounding the condensing surface.

Othmer (29) estimated that the presence of only 1% by volume of air in the vapour decreased the heat transfer coefficient by 60% when compared with the case of no air. Hampson (30) studied the above phenomenon using nitrogen, air and carbon dioxide. He presented the results for nitrogen from which it was deduced that 2.0 per cent by weight of nitrogen in steam reduced the heat transfer coefficient by a third when compared with the case of no nitrogen.

There has been a number of boundary layer solutions to the problem of condensation of a mixture of vapour and non-condensable gases. Recent examples include those of Sparrow and Eckert (31), Baasel and Smith (32), Sparrow and Lin (33), Sparrow, Minkowyez and Saddy (34), Tamir and Taitel (35) and Denny, Mills and Jusionis (36).

2.3.7 The effect of non-uniform gravity

The effects of non-uniform gravity fields on film condensation were considered by Dhir and Leinhard (37) in connection with their work on boiling heat transfer. The gravitational constant "g" which appears in the Nusselt equation for heat transfer coefficients was replaced by an effective gravitational constant "$g"_{eff}$ given by:

$$g_{eff} = \frac{x(gR)^{4/3}}{\int_0^x g^{1/3} R^{4/3} dx}$$

where R is the local radius of the body. For a vertical flat plate $g_{eff} = g$ and for a stationary cone $g_{eff} = \frac{7}{3} g \cos \hat{\alpha}$ where $2\hat{\alpha}$ is the cone angle.

Gerstmann and Griffith (38) observed the condensation of freon 113 onto the underside of horizontal and inclined plane surfaces. A random array of drops ~~were~~ was observed to form at the free surface of the film on the underside of the horizontal surface.

At small angles of inclination, the drops ran down the surface and became elongated. As the angle of inclination increased, the nature of the interface changed. They observed four basically different regimes of flow:

(i) a regime where the flow was dominated by the presence of pendant drops.

(ii) a glassy smooth flow which existed at the leading edge of the plate.

(iii) a developing wave state where the disturbances were of appreciable amplitude but there was no rupture of the interface (i.e. no drops).

(iv) a regime where the interface ruptured.

They also observed that although the heat flux was the same, no drops detached from the interface when the angle of inclination was greater than 13^{o}. Instead, all the condensate ran off the end of the test surface. The heat transfer data for 20^{o} to 90^{o} inclination were all 10 per cent greater than the theoretical values, suggesting that in the roll-wave regime, the net effect of interfacial waves remained roughly constant.

2.3.8 Evaluation of condensate film physical properties

Labuntsov (39) in his earlier work on fluids under conditions of wave flow, evaluated the physical properties at the vapour saturation temperature and then corrected for the physical property variations. McAdams (40) recommended that the viscosity should be evaluated at a temperature:

$$T = T_{sat} - 0.75\theta$$

Poots and Miles (41) made a theoretical study of the effects of temperature dependent physical properties on the condensation of steam on a plane vertical surface.

They compared their results with those of Nusselt (9), Rohsenow (11) and Chen (14) and recommended the Drew reference temperature:

$$T = T_{sat} - 0.75\theta$$

for the evaluation of the physical properties for the laminar model.

2.4 Enhancement of condensation

The amount of surface required for a given duty in a condenser is a function of many variables. Studies in condensation have shown that for a given duty the combination of filmwise condensation and the plain cylindrical metal tube is not the optimum. In this section some of the studies are reported.

2.4.1 Dropwise condensation

A few years ago, the Central Electricity Generating Board in collaboration with the Warren Spring Laboratory (42) used regular injections of stearic acid to promote dropwise condensation in a large triple effect evaporator (3 evaporators in series) producing boiler feed water for Tilbury Power Station. There was a 15 per cent improvement in the net output of the evaporator and the feed water produced was of acceptable purity. The authors estimated that with some redesign, the plant could produce 35 per cent more water with the same surface area, using stearic acid promoter.

Hampson (30) has shown that even with non-condensable gases, dropwise condensation gives an improvement over filmwise condensation. Rigorous studies have been carried out into the ways of promoting dropwise condensation by Osment and Tanner (43), Brown and Thomas (44) and Erb and Thielen (45) who considered gold plating.

2.4.2 Fluted tubes

In the film condensation of pure vapours, the only resistance to heat transfer of any importance between the vapour and the cold surface, is that through the film of condensate. On a flat or

cylindrical vertical surface the film, at any horizontal section, is uniformly distributed across the surface. If means can be found to disturb this uniformity, it is likely to improve the mean film coefficient of heat transfer.

Gregorig (46) was the first to suggest that the forces of surface tension could be used to disturb the normal uniformity of the condensate film across the surface. By suitably shaping the surface into ridges and grooves, the condensate could be made to flow rapidly off the ridges into the grooves. This would leave a very thin film on the ridges where very high local coefficients of heat transfer could be obtained.

Hawes (47) has analysed the case where the grooves are made cylindrical and Thomas and Alexander (48) have discussed alternative profiles. Experimental evidence shows that overall heat transfer coefficients of up to 2.5 times that obtained from a plain tube of the same length and under the same conditions, could be obtained.

2.4.3 Finned tubes

When pure steam condenses on a water cooled tube, the steam-side heat transfer coefficient predicted by the Nusselt equation and measured in practice exceeds the water-side heat transfer coefficient, typically by some 50 per cent. Water is exceptional however, in having a high thermal conductivity, a high latent heat and a moderate viscosity so that for a given mass condensing rate, the condensate film is thin and highly conducting. Many hydrocarbons, however, have relatively low latent heats and poorly conducting and sometimes viscous phases so that, for the same mass condensing rate the condensate film is thick and poorly conducting, giving rise to vapour-side coefficients much lower than on the water side.

In such circumstances it may pay to use an extended surface on the condensing side.

Katz et al (49) studied condensation on extended surfaces and produced the equation:

$$h = 0.728 \left[\frac{k^3 \rho^2 g h_{fg}}{\mu \theta d}\right]^{\frac{1}{4}} \left\{\frac{a_t}{a} + 1.10 \left[\frac{d}{H}\right]^{\frac{1}{4}} \frac{a_f}{a}\right\} \qquad (2.4.1)$$

where H is the effective height of the fin, a_t is the exposed primary surface of the tube between the fins, a_f the area of the fins and $a = a_t + a_f$. Henrici (50, 51) tested a number of finned tubes using refrigerants and found a good agreement with equation (2.4.1).

2.4.4 Reduction of coolant-side resistance

In steam condensers the steam-side heat transfer coefficient is typically some 50 per cent greater than the water-side heat transfer coefficient. Thus there is a need to reduce resistance to heat transfer on the water side. Special shaped tubes have been developed to improve the water-side coefficient. These tubes usually have helical ridges inside the tube and the ridges have the effect of roughening the inside wall. The tube-side heat transfer coefficients for these tubes are reported by Ashraf (52). Experimental work at NEL on such tubes indicate that the effect of the ridges is to double the heat transfer coefficient on the water-side but to have only a small effect on the steam side.

2.4.5 Use of electric fields

In 1965, Velkoff and Miller (53) presented experimental heat transfer coefficients for freon 113 condensing in the prosence of uniform electrostatic fields created between the condensing surface and an anode grid held in the vapour. The field strength was varied by applying voltages up to 50 kV. and currents up to 14μA. Applying

the electrostatic field induced waves in the film and caused jets of condensate to be emitted from the film. Experimental heat transfer coefficients 2.5 times the value without the field were measured for these low electrical power inputs.

Recently Holmes and Chapman (54) published experimental heat transfer coefficients for freon 114 condensing in the presence of alternating electric fields. The fields were created between the condensing surface and a plate held in the vapour by the application of voltages up to 60kV. at 60 Hz. Experimental heat transfer coefficients with the field applied were found to be as much as 10 times the value without the field.

2.5 Filmwise condensation on rotating surfaces

The experimental and theoretical studies of the heat transfer between rotating surfaces and either single or two-phase fluids have been undertaken for two main reasons. The first is to gain some knowledge of the beneficial effects of rotation on heat transfer with a view to improving the performance of evaporators and condensers. The second reason for the study is to enable calculations to be made for the heat transfer between working fluid and the rotating parts of power producing machines. A considerable amount of work has been done by others on the rotating disc, the rotating cylinder and the rotating cone and these are reviewed in the following section. The general curved body is also reviewed although there is very little published information.

2.5.1 Filmwise condensation on rotating disc

The theoretical understanding of the filmwise condensation on rotating surfaces took a major step forward in 1959 when Sparrow and Gregg (55) published their work "A theory of rotating condensation."

Starting from the Navier-Stokes, energy and continuity equations, Sparrow and Gregg used boundary layer techniques to derive equations for heat tranfer coefficient for the condensation on a rotating disc. They analysed the case where convection and inertia terms were assumed important and compared their solution with the case where such terms were neglected. They showed that for thin condensate layers such terms could be ignored. This finding has been used in the author's analysis of the condensation on the rotating curved body.

Sparrow and Gregg presented their results in terms of $c\theta/h_{fg}$ and showed that for small values of $c\theta/h_{fg}$, which imply small film thicknesses, and over the range of Prandtl number 1 to 100, the heat transfer coefficient is given by:

$$\frac{h}{k}\left[\frac{\nu}{\omega}\right]^{\frac{1}{2}} = 0.904 \left[\frac{Pr\ h_{fg}}{c\theta}\right]^{\frac{1}{4}}$$

and the non-dimensional film thickness

$$\eta_\delta = \delta\left[\frac{\omega}{\nu}\right]^{\frac{1}{2}} = 1.107\left[\frac{c\theta}{Pr\ h_{fg}}\right]^{\frac{1}{4}}$$

Thus for a given fluid and a fixed temperature difference between the fluid and the disc, the local heat transfer coefficient and the film thickness are determined by the speed of rotation of the disc, i.e. $h \sim \omega^{\frac{1}{2}}$ and $\delta \sim \omega^{-\frac{1}{2}}$

It should therefore be possible to achieve high values of the heat tranfer coefficient by rotating the disc at high speed. Finally, Sparrow and Gregg showed that for liquid metals (low Prandtl number fluids), the effects of inertia and convection were very important.

Later in 1959, Nandapurka and Beatty (56) published experimental heat transfer coefficients for methanol, ethanol and freon 113 on a horizontal rotating disc. They compared their heat transfer coefficients with the predictions of Sparrow and Gree (55) and observed that experimental values were 25% less than the theoretical predictions. They attributed this to the effects of ripples they had observed when dye was introduced onto the rotating disc.

Espig and Hoyle (57) published experimental heat tranfer coefficients for steam condensing onto a smooth rotating disc. This was in connection with their work on transient thermal stresses in rotating axisymmetrical bodies. The disc is considered as a cone with an apex angle of 180^{o}. Espig and Hoyle predicted theoretically that, for the laminar model the heat transfer coefficient is given by:

$$h = 0.903 \left[\frac{k^3 \rho^2 h_{fg}}{\mu \theta} \right]^{\frac{1}{4}} . \omega^{\frac{1}{2}}$$

They compared their experimental findings with the above theory and found that the experimental values for the heat transfer coefficient were 1.5 to 2.0 times greater.

In an earlier work into the behaviour of water films on rotating discs, Espig and Hoyle (58) observed waves and they argued that such waves would be present on a film of condensate forming on a rotating disc. The discrepancy in the experimental and theoretical results was then attributed to the presence of waves on the film of condensate.

2.5.2 Filmwise condensation on rotating cylinders

Filmwise condensation on a rotating cylinder was studied by Yeh (59) and by Singer and Preckshot (60). Similar results were obtained in both studies which indicated that for Weber number less than 1800, there was an increase in the heat transfer coefficient.

For Weber numbers greater than 1800, the heat transfer coefficient decreased to almost the stationary value. Doubts have however been expressed about the validity of the findings because a faulty mechanical seal was suspected of leaking air and oil into the steam space.

Hoyle and Matthews (61) studied the heat transfer from steam condensing onto rotating cylinders. They studied three cylinders of diameters 0.10m., 0.20m. and 0.254m. to find the effect of the different diameters on the heat transfer coefficient. Hoyle and Matthews did not observe any decrease in heat transfer coefficient when the Weber number increased beyond 1800 as reported by Yeh, and by Singer and Preckshot. Hoyle and Matthews correlated mean heat transfer coefficient for their three rotating cylinders by expressing the Nusselt equation thus,

$$\bar{h} = B \left[\frac{k^3 \rho^2 g h_{fg}}{\mu \theta d} \right]^{\frac{1}{4}}$$

where $$B = \frac{1.5}{\left[d\sqrt{\rho/\sigma} \right]^{0.19}} \left[1.9 - \frac{0.9}{1.095\, d\omega^2/2g} \right]$$

In 1970 Nicol and Gacesa (62) published their experimental work on the condensation of steam onto a rotating vertical cylinder. They observed no decrease in heat tranfer coefficient even with Weber numbers in excess of 5000. This agreed with the findings of Hoyle and Matthews (61). Nicol and Gacesa found the Nusselt number to remain constant at 110 for Weber numbers up to 430 and thereafter increased according to:

$$Nu_a = 6.13\, We^{0.496}, \text{ where } Nu_a = \bar{h} \cdot d/2k$$

Experimental studies have recently been carried out by Williams et al (63) into the condensation on a vertical rotating radially finned tube. Their data for methanol and isopropanol shows that the condensate film heat transfer coefficient could be signficantly increased by the use of centrifugal force. They propose the empirical equation:

$$h_e = 0.655 \left[\frac{k^3 \rho^2 h_{fg}}{\mu\theta}\right]^{\frac{1}{4}} \left[\frac{G}{L}\right]^{\frac{1}{4}}$$

where h_e is the condensate film heat transfer coefficient based on the effective outside area of the tube, G the drainage acceleration $[g^2 + (d\omega^2/2)^2]^{\frac{1}{2}}$ and L length of condenser tube between adjacent fins.

2.5.3 Filmwise condensation on rotating cones

Rotating conical boilers have been used in desalination and in food processing for some years. This perhaps, partially accounts for the amount of investigation that has gone into the heat transfer and fluid flow on rotating cones.

Hickman (64) in 1957 described and gave performance data for centrifugal boiler and compression still in which the evaporating liquid flowed in a thin film along the inner surface of a rotating inverted cone. Vapour from the inner surface of the cone was collected and compressed before being condensed onto the outer surface of the cone. Energy liberated at the outer surface during condensation was transferred by conduction to maintain the evaporation process. Bromley (65) studied the above boiler analytically and provided equations for predicting its performance.

Starting from the Navier-Stokes equations, Bruin (66) has predicted the velocity distributions in a liquid film flowing along the inner surface of an inverted cone. Wu (67) made use of the Karman-Cochran solution of the Navier-Stokes equations in his study of the laminar motion of an incompressible viscous fluid induced by a spinning cone.

In 1960 Tien (68) indicated that the heat transfer results for a rotating disc could also be used for rotating cones under boundary layer approximations. Sparrow and Hartnett (69) used the findings of Wu and Tien to modify their theory for condensation on rotating discs and extended the analysis to condensation on rotating cones. Comparing the heat transfer coefficients for rotating discs and for rotating cones, Sparrow and Hartnett gave the equation:

$$\frac{h_{cone}}{h_{disc}} = (\mathrm{Sin}\,\hat{\alpha})^{\frac{1}{2}}$$

where $2\hat{\alpha}$ is the cone angle. It should be appreciated that Sparrow et al have not considered gravity in any of their analyses.

Heat transfer by steam condensing onto a rotating 60° cone was studied by Howe and Hoyle (70). Their conclusions were that:

(i) the rate of heat transfer was dependent on $d\omega^2/2g$ when $d\omega^2/2$, the centrifugal acceleration, was of the same order of magnitude as the gravitational acceleration.

(ii) the rate of heat transfer was independent of $d\omega^2/2g$ when $d\omega^2/2$ was large compared with the gravitational acceleration.

(iii) the heat transfer behaviour on the 60° cone was more comparable to the cylinder than to the disc.

Howe and Hoyle correlated their results by the empirical fomulae:

$$\frac{hd}{k} = 2000 \left[\frac{d\sigma\rho}{2.5\,\mu^2\,10^8}\right]$$

for the case of no rotation,

$$\text{and } \frac{hd}{k} = 3700.0 \left[\frac{d\sigma\rho}{2.5\mu^2 10^8}\right]^{\frac{0.16d\omega^2}{2g}}$$

$$\text{for } d\omega^2/2g > 2.45$$

More recently, Howe (71) carried out an extensive study of the heat transfer by condensation onto rotating cones in which he considered the 10^o and the 20^o cones in addition to the 60^o cone. Howe assumed the laminar model and examined the effects of rotation and gravity on the heat transfer rate. He made a comparison between the cone and the disc and showed that when the acceleration force acting on the condensate was predominantly gravitational,

$$\frac{h_{cone}}{h_{disc}} \text{ was asymptotic to } 0.976 \left[\frac{g \cos \hat{\alpha}}{x\omega^2}\right]^{\frac{1}{4}}$$

but when centrifugal acceleration dominated the drainage the asymptote was $(\sin \hat{\alpha})^{\frac{1}{2}}$ which agreed with Sparrow and Hartnett (69). Howe did not verify the above quotient experimentally.

Experimental local heat transfer coefficients were observed by Howe to be 1.2 and 1.9 times the value predicted by the laminar model. He observed waves and the detachment of drops from the condensate in a photographic study and he explained the discrepancy by their effects. He correlated his experimental results with the equation:

$$Nu(3H)^{\frac{1}{4}} \left[\frac{\omega \sin \hat{\alpha}}{g \cos \hat{\alpha}}\right]^{3/2} = A_1 \left[\frac{x^2\omega^2 \sin^2 \hat{\alpha}}{g \cos \hat{\alpha}}\right]^{A_2}$$

$$\text{where } H = \left[\frac{c\,\theta\,\nu^2}{Pr(h_{fg} + \frac{3}{8}c\theta)}\right]$$

and A_1 and A_2 are constants.

Howe observed closer agreement between the laminar model and the experimental results at high rotational speeds.

The constants A_1 and A_2 therefore vary with speed and are determined according to the value of $\frac{X\omega^2 \text{Sin}^2 \hat{\alpha}}{g \text{ Cos } \hat{\alpha}}$. He provided a table of such values.

2.5.4 Filmwise condensation on rotating curved bodies

A considerable amount of work has been done on the filmwise condensation on rotating discs, cylinders and cones. However, this is not the case with the general curved body of which the disc, the cylinder and the cone are special cases.

Howe (71) was the first to tackle the problem of condensation on bodies with curved generators. Working with the laminar model, Howe extended his analysis for condensation onto rotating cones to cover the curved generator. His findings indicated that the curvature of the generator had a significant effect on condensation. Howe analysed three bodies with shaft diameters of 0.002m., 0.2m. and 0.6m., but each with a radius of curvature of 0.2m. Each body was given speeds of rotation over the range zero to 10,000 rev/min, together with common values of temperature difference $\theta = 10^{\circ}C$ and Prandtl number Pr = 1.37. The conclusion from the analyses was that the film thickness and the heat transfer coefficients were very much dependent on the choice of radius of curvature and the diameter of the cylindrical part of the bodies. From the photographic studies of the condensation process on his cones, Howe predicted that drop detachment should occur at the shaft and of a body with a curved generator where the angle $\hat{\alpha}$ is small and that the detachment of drops should cease as the angle $\hat{\alpha}$ increases beyond 20°.

2.6 Present work

The present work is concerned with the filmwise condensation

of steam onto rotating axisymmetrical curved bodies. It is the final phase of the investigation into the condensation of steam onto rotating bodies undertaken by Hoyle and his colleagues as part of their wider investigation into the question of thermal stresses in steam turbine rotors during cold starting and during maneouvring. The problems involved during these operations have been given by Terrel (72), Hall and Britten (73) and more recently by Moore (74)

Hoyle and his colleagues studied the condensation of steam onto rotating discs, rotating cylinders and rotating cones. As part of the same research, Robson (75) studied the behaviour of a film of condensate on the surface of a rotating 60° cone; and Holgate (76) the stability of a fluid film on such a cone. Measurements of the condensate film thickness on the 10° and 20° cones used by Howe (71) have been made by Smith (77).

The work with the rotating discs, cylinders and cones had provided much useful information about condensation on a rotating body but these shapes were not representative of a steam turbine disc. One school of thought at the onset of the research programme was that any axisymmetrical body could be simulated by a combination of truncated cones as shown below.

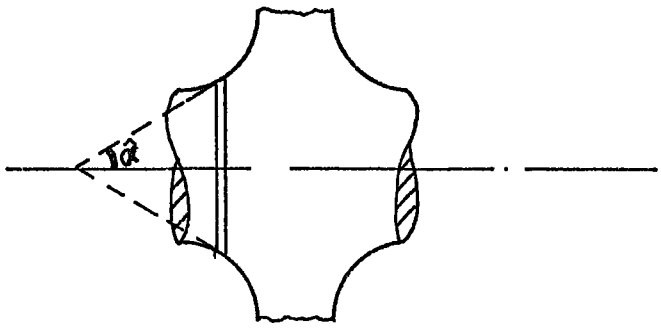

Thus the knowledge gained from discs (180° cones), cylinder (0° cones) and cones should enable one to formulate a theory for the curved body.

There is one difficulty however with the above idea. A cone is a curve with an infinite radius of curvature and any thoories based on the above assumption undoubtedly neglect the curvature effects

in the analysis. This became apparent when Howe (71) extended his theory of the laminar condensation of steam onto rotating cones to cover the surface with the curved generator. It became clear from the theory, that the final phase of the research programme should examine in detail the condensation of steam onto a rotating curved body, and in particular, the effects of curvature.

In view of Howe's (71) findings, a fresh approach to the problem of condensation of steam onto rotating curved body was adopted. Instead of considering a curved body as being made up of series of cones, the reverse was considered. Thus the general curved body of which the disc, the cylinder and the cone are special cases is considered. The theory of filmwise condensation onto the rotating asixymmetrical general curved body is developed. The Navier-Stokes and the energy equations are solved for the laminar model of condensation on such a body. The body is assumed to rotate with the axis of symmetry vertical. The analysis considers pure vapours only and the vapour-condensate interfacial shear, convective and inertia effects are neglected. Gravity, rotational speed and curvature are considered and the importance of the curvature effect is examined. The analysis presented in this thesis was developed independently of that given by Howe.

To provide an experimental verification of the theory, a circular curved body with a generator which forms a circular arc of 90^{o} is designed and used. Any curved generator could have been used. The choice was a compromise between theoretical considerations, the existing equipment and the cost of manufacture.

Finally, a photographic study of the condensation process is undertaken and the onset of the detachment of drops predicted.

3.0 THEORY

3.0 Introduction

This section deals with the development of the laminar theory for the condensation of a vapour onto a general curved body rotating with the axis of symmetry vertical. The co-ordinate system employed in the theoretical and the experimental analyses is introduced. This is followed by the transformation of the Navier-Stokes and the energy equations into the new co-ordinate system. The governing equations are developed and analysed and a single differential equation which describes the condensation process is produced. A non-dimensionalisation procedure is employed which simplifies the equation and facilitates a solution by a single numerical integration. Expressions for the behaviour of the condensate film thickness and the heat transfer coefficients with respect to the variation of centrifugal acceleration and the variation of distance from the start of the film are developed. The final equations are then applied to the experimental curved body. The predicted results are finally discussed.

The assumptions made - some of which have been stated earlier - are:

i) a laminar film flow, which implies that the thickness of the film of condensate is small compared with the radius of the body and with the radius of curvature.

ii) the film drains along the generator of the body; i.e. in a direction parallel to the condensing surface, by the action of both gravitational and centrifugal accelerations.

iii) the inertia and convective effects are neglected.

iv) the vapour-condensate interfacial shear is neglected.

v) pure vapour, i.e. no non-condensable gases.

vi) angular symmetry and steady state conditions prevail.

vii) the fluid is incompressible.

viii) no axial conduction, i.e. conduction along the generator, at the steady state is neglected.

For completeness, the full mathematical manipulations are carried out and the above assumptions and any others are brought in at the appropriate stage.

3.1 Derivation of equations

3.1.1 The co-ordinate system

The cartesian co-ordinate system of x, $\underset{\sim}{y}$ and z could not conveniently be used in the present work because of the rotational motion. Different othogonal co-ordinate systems were considered and the most convenient was chosen. Consider the general curved body shown in fig. 1. The curved surface is described by the rotation of a defined curved generator about the vertical axis. The angle of rotation is denoted by ϕ. The direction along the generator is denoted by S and the distance from the leading edge to some point on the generator in this direction by s. Y is the direction normal to the surface S at the point of consideration. Y is positive in a direction away from the axis of rotation. The thickness of the film of condensate in the Y direction is denoted by y as shown in fig. 2. In fig. 1, e_y, e_ϕ and e_s denote unit vectors in the directions Y, ϕ and S respectively.

3.1.2 Derivation of the Navier-Stokes equation in terms of S, Y and ϕ

Scale factors

Following Spiegel (78 p.135), the scale factors for the orthogonal co-ordinate system S, Y and ϕ are obtained as follows:

From fig. 1 and fig. 2, consider a particle of condensate at a point P, a small distance away from the surface of the body,

$$x = (R+y\text{Cos}\beta)\ \text{Cos}\ \phi$$

$$y = (R+y\text{Cos}\beta)\ \text{Sin}\ \phi$$

$$z = (\ell - y\text{Sin}\beta)$$

Let the vector

$$\tilde{r} = (R+y\text{Cos}\beta)\ \text{Cos}\phi i + (R+y\text{Cos}\beta)\ \text{Sin}\phi j + (\ell - y\text{Sin}\beta)\ k$$

Let h_s, h_y and h_ϕ be the scale factors.

$$h_s = \left|\frac{\partial \tilde{r}}{\partial s}\right| \qquad h_y = \left|\frac{\partial \tilde{r}}{\partial y}\right| \qquad h_\phi = \left|\frac{\partial \tilde{r}}{\partial \phi}\right|$$

For thin films of fluid, y is small compared with R or ℓ, hence any contributions by y can be neglected. For such a case,

$$h_s = \sqrt{\{(R')^2 + (\ell')^2\}}$$

where $R' = \partial R/\partial s = \text{Sin}\beta$ and $\ell' = \partial \ell/\partial s = \text{Cos}\beta$

Hence $h_s = 1$ and similarly $h_y = 1$ and $h_\phi = R$.

The Navier-Stokes equation

The general vectorial form of the Navier-Stokes equation for an incompressible fluid is:

$$\rho \frac{DV}{Dt} = F - \text{grad.}p + \mu \nabla^2 V$$

where V is the vectorial velocity and F the vectorial body force.

Referring to fig. 1

$$V = V_s e_s + V_y e_y + V_\phi e_\phi$$

The acceleration force terms

Following Lamb (79) and applying assumption (vi), namely that angular symmetry and steady state conditions prevail, the expansion of the acceleration term of the Navier-Stokes equation in the S-direction is given by equation (3.1.1) below.

$$\rho \frac{DV_s}{Dt} = \rho \left[\frac{V_s}{h_s} \frac{\partial V_s}{\partial s} + \frac{V_y}{h_y} \frac{\partial V_s}{\partial y} + \frac{V_y}{h_s h_y} \left\{ V_s \frac{\partial (h_s)}{\partial y} - V_y \frac{\partial (h_y)}{\partial s} \right\} - \frac{V_\phi^2}{h_s h_\phi} \frac{\partial (h_\phi)}{\partial s} \right] \qquad (3.1.1)$$

Substituting for h_s, h_y and h_ϕ in equation (3.1.1) and simplifying,

$$\rho \frac{DV_s}{Dt} = \rho \left[V_s \frac{\partial V_s}{\partial s} + V_y \frac{\partial V_s}{\partial y} - \frac{V_\phi^2}{R} \text{Sin}\beta \right] \qquad (3.1.2)$$

Equation (3.1.2) indicates the acceleration force acting on the film of fluid in the S-direction. The centrifugal effect given by $\rho \frac{V_\phi^2}{R} \text{Sin}\beta$ is easily recognised.

Body force terms

The body force, as implied here, is the force due to gravity only. For a body with its axis of symmetry vertical, the body forces in the S, Y and ϕ directions are given by:

$F_s = \rho g \text{Cos}\beta$

$F_y = -\rho g \text{Sin}\beta$

$F_\phi = 0$

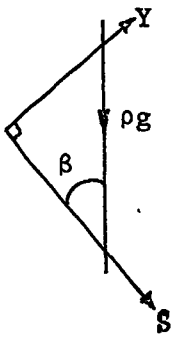

Pressure force terms

$$\text{grad.}p = \frac{1}{h_s} \frac{\partial p}{\partial s} e_s + \frac{1}{h_y} \frac{\partial p}{\partial y} e_y$$

Hence in the S-direction, pressure force term is $\partial p/\partial s$.

The viscous force terms

The viscous force terms in the Navier-Stokes equation are given by $\mu\nabla^2 V$.

By general vectorial notation,

$$\nabla^2 V = \nabla(\nabla.V) - \nabla x(\nabla x V) \qquad (3.1.3)$$

$(\nabla.V) = 0$ is the continuity equation. Hence at the steady state,

$$\nabla^2 V = - \nabla x(\nabla x V) \qquad (3.1.4)$$

From assumption (vi), $\frac{\partial}{\partial \phi} = 0$

$$(\nabla x V) = \frac{1}{h_s h_y h_\phi} \begin{vmatrix} h_s e_s & h_y e_y & h_\phi e_\phi \\ \frac{\partial}{\partial s} & \frac{\partial}{\partial y} & 0 \\ h_s V_s & h_y V_y & h_\phi V_\phi \end{vmatrix}$$

Substituting for h_s, h_y and h_ϕ and simplifying,

$$(\nabla x V) = \left[\frac{\partial V_\phi}{\partial y}\right] e_s + \left[-\frac{V_\phi \sin\beta}{R} - \frac{\partial V_\phi}{\partial s}\right] e_y + \left[\frac{\partial V_y}{\partial s} - \frac{\partial V_s}{\partial y}\right] e_\phi$$

$$(\nabla x V) = E_s e_s + E_y e_y + E_\phi e_\phi$$

where E represents the terms in the brackets

$$\nabla x(\nabla x V) = \frac{1}{R} \begin{vmatrix} e_s & e_y & Re_\phi \\ \frac{\partial}{\partial s} & \frac{\partial}{\partial y} & 0 \\ E_s & E_y & RE_\phi \end{vmatrix}$$

$$\nabla x(\nabla xV) = \left[\frac{\partial E_\phi}{\partial y}\right] e_s + \left[-\frac{E_\phi \mathrm{Sin}\beta}{R} - \frac{\partial E_\phi}{\partial s}\right] e_y + \left[\frac{\partial E_y}{\partial s} - \frac{\partial E_s}{\partial y}\right] e_\phi \qquad (3.1.5)$$

For the S-direction only,

$$-\nabla x(\nabla xV) = -\frac{\partial E_\phi}{\partial y}$$

$$= -\frac{\partial}{\partial y}\left[\frac{\partial V_y}{\partial s} - \frac{\partial V_s}{\partial y}\right]$$

$$\text{or } \nabla^2 V_s = \frac{\partial^2 V_s}{\partial y^2} - \frac{\partial}{\partial y}\left\{\left(\frac{\partial V_y}{\partial s}\right)\right\} \qquad (3.1.6)$$

Hence in the S-direction, the momentum equation is given by:

$$\left[V_s \frac{\partial V_s}{\partial s} + V_y \frac{\partial V_s}{\partial y} - \frac{V_\phi^2 \mathrm{Sin}\beta}{R}\right] = g\mathrm{Cos}\beta - \frac{1}{\rho}\frac{\partial P}{\partial s} + \nu\left[\frac{\partial^2 V_s}{\partial y^2} - \frac{\partial}{\partial y}\left(\frac{\partial V_y}{\partial s}\right)\right] \qquad (3.1.7)$$

Equation (3.1.7) is the transformed Navier-Stokes equation for the S-direction only. It describes the motion of an axially symmetric thin film of incompressible fluid along the generator of the general curved body shown in fig. 1. From assumption (ii), equation (3.1.7) is the equation of interest and the momentum equation for the Y and ϕ directions will not be presented. However, before any analysis and hence a solution for equation (3.1.7) could be contemplated, the transformation will be completed by considering the energy equation.

The energy equation

Neglecting the mechanical and frictional energy dissipation, the energy equation becomes:

$$\frac{DT}{Dt} = \frac{k}{\rho c}\nabla^2 T$$

$$\frac{DT}{Dt} = \frac{\partial T}{\partial \tau} + (V.\nabla T)$$

and from assumption (vi)

$$\frac{DT}{Dt} = V_s \frac{\partial T}{\partial s} + V_y \frac{\partial T}{\partial y} \qquad (3.1.8)$$

$$\nabla^2 T = \text{div. grad } T$$

$$= \frac{1}{R}\left[\frac{\partial}{\partial s}\left\{(R \frac{\partial T}{\partial s})\right\} + \frac{\partial}{\partial y}\left\{(R\frac{\partial T}{\partial y})\right\}\right]$$

$$\nabla^2 T = \frac{\text{Sin}\beta}{R} \frac{\partial T}{\partial s} + \frac{\partial^2 T}{\partial s^2} + \frac{\partial^2 T}{\partial y^2} \qquad (3.1.9)$$

From (3.1.8) and (3.1.9)

$$V_s \frac{\partial T}{\partial s} + V_y \frac{\partial T}{\partial y} = \frac{k}{\rho c}\left[\frac{\text{Sin}\beta}{R} \frac{\partial T}{\partial s} + \frac{\partial^2 T}{\partial s^2} + \frac{\partial^2 T}{\partial y^2}\right] \qquad (3.1.10)$$

3.1.3 Analysis of the governing equations

From the assumption that for steady flow the inertia and convective effects are negligible, equations (3.1.7) and (3.1.10) reduce respectively to:

$$-\frac{V_\phi^2 \text{Sin}\beta}{R} = g\text{Cos}\beta - \frac{1}{\rho}\frac{\partial P}{\partial s} + \nu\left[\frac{\partial^2 V_s}{\partial y^2} - \frac{\partial}{\partial y}\left\{(\frac{\partial V_y}{\partial s})\right\}\right] \qquad (3.1.7i)$$

$$0 = \left[\frac{\text{Sin}\beta}{R} \frac{\partial T}{\partial s} + \frac{\partial^2 T}{\partial s^2} + \frac{\partial^2 T}{\partial y^2}\right] \qquad (3.1.10i)$$

For a thin film, the component of velocity in the Y-direction is small compared with that in the S-direction and the variation of velocity in the S-direction is small compared with that in the Y-direction. On this basis equation (3.1.7i) may be approximated by:

$$-\frac{V_\phi^2 \text{Sin}\beta}{R} = g\text{Cos}\beta - \frac{1}{\rho}\frac{\partial P}{\partial s} + \nu \frac{\partial^2 V_s}{\partial y^2} \qquad (3.1.7ii)$$

It is assumed that the external pressure acting on the fluid is constant. Hence pressure variations in the film are of the simple hydrostatic form

produced by the gravitational force. As the film is thin, the variations in pressure in the S and ϕ directions are small compared with the variations in the Y-direction. Hence the variations in pressure in the S-direction can be neglected and equation (3.1.7ii) then approximates to:

$$-\frac{V_\phi^2 \mathrm{Sin}\beta}{R} = g\mathrm{Cos}\beta + \nu\frac{\partial^2 V_s}{\partial y^2} \qquad (3.1.11)$$

Furthermore, from assumption (viii) namely that at the steady state there is no axial conduction, i.e. no conduction in the S-direction, $\partial T/\partial s = 0$. Hence equation (3.1.10i) reduces to:

$$\frac{\partial^2 T}{\partial y^2} = 0 \qquad (3.1.12)$$

Solutions of the governing equations

Equations (3.1.11) and (3.1.12) are the governing equations. Their solutions yield the drainage velocity, V_s and the temperature distribution, T in the film. For the condensation of pure vapour, the following boundary conditions will prevail:

$$\left.\begin{aligned} V_s &= 0 \\ V_\phi &= R\omega \\ V_y &= 0 \\ T &= T_o \end{aligned}\right\} \quad y = 0$$

At the vapour-condensate interface, there will be negligible shear (assumption (iv)), and the interfacial temperature will be common to both fluids.

Thus,

$$\left.\begin{aligned} \tau_s &= 0 \\ \tau_\phi &= 0 \\ T &= T_{sat} \end{aligned}\right\} \quad y = \delta$$

Drainage velocity

It follows from assumption (iv) there is negligible slip; hence equation (3.1.11) becomes:

$$\frac{d^2V_s}{dy^2} = -\frac{1}{\nu}\left[R\omega^2 \sin\beta + g\cos\beta\right]$$

This yield:

$$V_s = -\frac{1}{\nu}\left[R\omega^2 \sin\beta + g\cos\beta\right]\frac{1}{2}y^2 + B_y + D$$

where B and D are constants of integration.

When $y = 0$, $V_s = 0$ hence $D = 0$

$$\therefore V_s = -\frac{1}{2\nu}\left[R\omega^2 \sin\beta + g\cos\beta\right] y^2 + By \qquad (3.1.13)$$

From the boundary condition at $y = \delta$

$$\left[\frac{dV_s}{dy}\right]_{y=\delta} = 0 = \left[\frac{dV_y}{ds}\right]_{y=\delta}$$

$$\text{and } V_s = \frac{1}{2\nu}\left[R\omega^2 \sin\beta + g\cos\beta\right]\left[2\delta y - y^2\right] \qquad (3.1.14)$$

The drainage velocity, V_s, has a parabolic distribution for a given rotational speed. This is what one would expect of a laminar model such as assumed here.

Temperature distribution

Equation (3.1.12) becomes,

$$\frac{d^2T}{dy^2} = 0$$

$$\therefore T = ay + b$$

where a and b are constants of integration.

At $y = 0$, $T = T_o$ hence $b = T_o$

At $y = \delta$, $T = T_{sat}$

$$\therefore \quad T_{sat} - T_o = a\delta = \theta \qquad \text{hence } a = \theta/\delta$$

$$\therefore \quad T = \theta y/\delta + T_o \tag{3.1.15}$$

and
$$\frac{dT}{dy} = \frac{\theta}{\delta} \tag{3.1.16}$$

$$(T_{sat} - T) = \theta(1-y/\delta)$$

Equation (3.1.15) shows that the temperature distribution in the film is linear. It is worth noting from equation (3.1.10i) that a different temperature distribution would have been obtained if axial conduction had been considered. It is important to note therefore, that where a comparatively thicker film of condensate is concerned, equation (3.1.10i) will have to be solved as it stands as the assumption about axial conduction may not hold.

3.1.4 The governing equation of laminar film condensation on a rotating curved body

In the preceeding section, equations (3.1.14 - 3.1.16) are used to obtain the governing equation of laminar film condensation on the rotating general curved body. This is achieved by considering the conservation of energy in a control volume of the condensate.

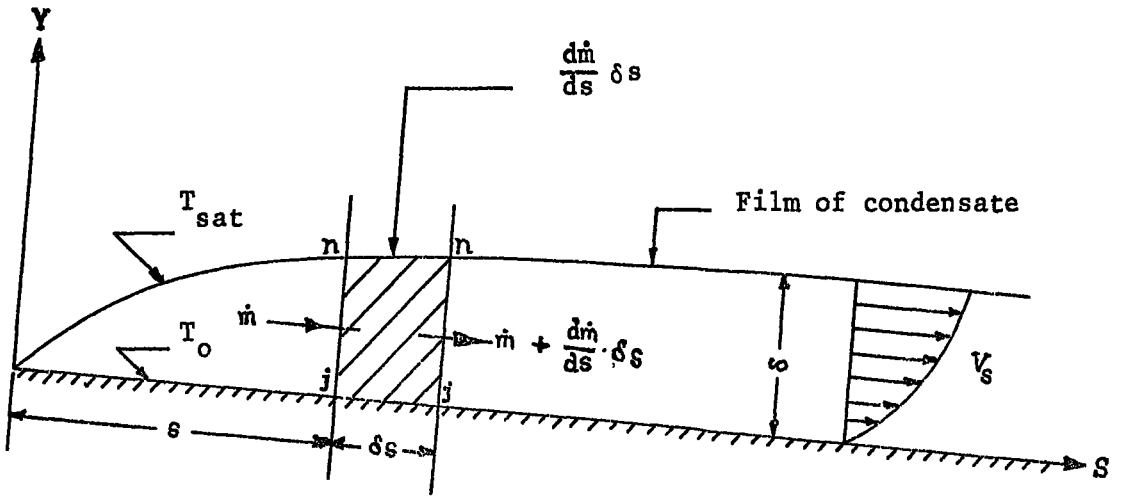

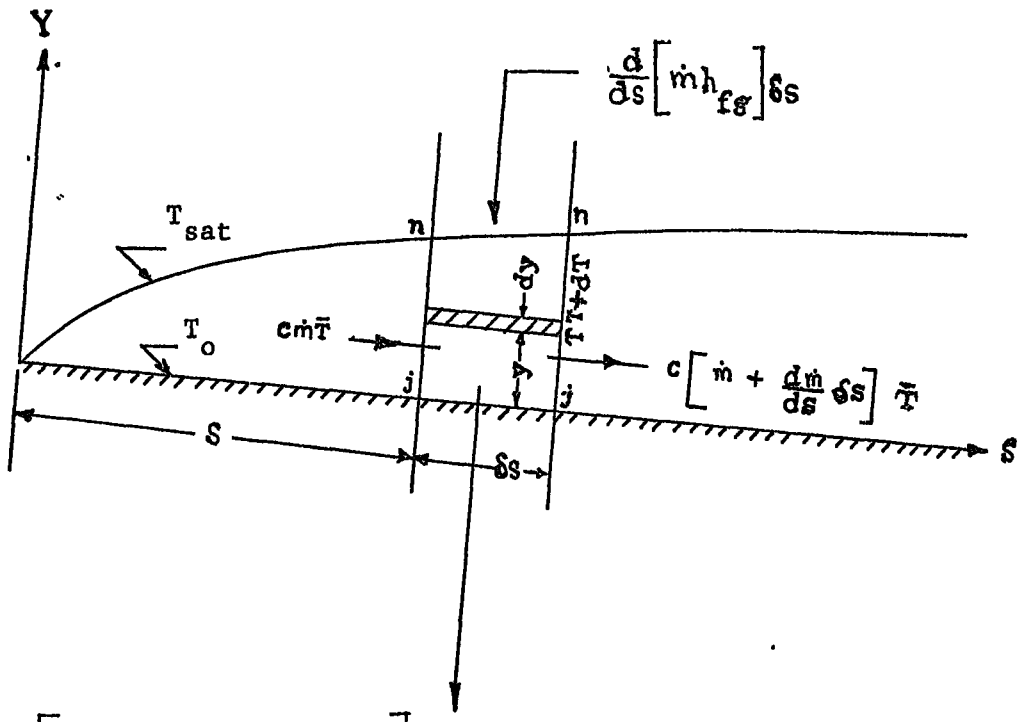

$$dQ = \frac{d}{ds}\left[\dot{m}h_{fg} + \dot{m}c\,(T_{sat} - \bar{T})\right]\delta s$$

Consider the element of condensate jnnj of width δs, which when rotated about the axis of symmetry of the body forms a control volume of the condensate film. The energy dQ crossing the boundary jj is given by the condensation of the vapour of mass $\frac{d\dot{m}}{ds}\,\delta s$ and the sub-cooling of that mass of condensate from the saturation temperature T_{sat} to the mean temperature $\bar{T}$ which is between that of the wall and the steam. Assuming that the energy is transferred to the boundary jj by conduction only through the film of condensate, we can invoke an over-all energy balance as follows:

$$dQ = kd\hat{A}\left[\frac{dT}{dy}\right]_{y=0} = \frac{d}{ds}\left[\dot{m}h_{fg} + \dot{m}c\,(T_{sat} - \bar{T})\right]\delta s \qquad (3.1.17)$$

In equation (3.1.17) the term involving dT/dy represents the energy transfer by conduction to the inner surface of the control volume denoted by jj.

On the extreme right hand side of equation (3.1.17), the term involving $\dot{m}h_{fg}$ represents the energy liberated by the vapour condensing on the outer surface of the control volume denoted by nn. The term involving $(T_{sat} - \bar{T})$ represents the energy liberated by the sub-cooling of the condensate to the mean temperature $\bar{T}$.

The effective conducting area of the control volume is given by $d\hat{A} = 2\pi R\delta s$. Substituting for $d\hat{A}$ and dT/dy from equation (3.1.16) into equation (3.1.17) and simplifying yield:

$$2\pi Rk\,\frac{\theta}{\delta} = \frac{d}{ds}\left[\dot{m}h_{fg} + \dot{m}c\cdot(T_{sat} - \bar{T})\right] \qquad (3.1.18)$$

Now $\dot{m} = \rho \int_0^{\delta} 2\pi Rh_y dy V_s$

$= 2\pi R\rho \int_0^{\delta} V_s dy$

Substituting for V_s from equation (3.1.14) and integrating,

$$\dot{m} = \frac{2\pi R\rho\delta^3}{3\nu}\left[R\omega^2 Sin\beta + gCos\beta\right] \qquad (3.1.19)$$

$$\therefore\ \dot{m}h_{fg} = \frac{2\pi R\rho\delta^3 h_{fg}}{3\nu}\left[R\omega^2 Sin\beta + gCos\beta\right] \qquad (3.1.20i)$$

From equation (3.1.16),

$$\dot{m}c\,(T_{sat} - \bar{T}) = 2\pi R\rho \int_0^{\delta} V_s\, c\,\theta\,(1-y/\delta)\,dy$$

$$= 2\pi R\rho\, c\theta \int_0^{\delta} V_s\,(1-y/\delta)\,dy$$

$$= \frac{2\pi R\rho\, c\theta}{8\nu}\left[R\omega^2 Sin\beta + gCos\beta\right] \qquad (3.1.20ii)$$

Substituting (3.1.20i) and (3.1.20ii) into (3.1.18),

$$2\pi Rk\,\frac{\theta}{\delta} = \frac{d}{ds}\left[\frac{2\pi R\rho\delta^3}{\nu}\left\{\frac{h_{fg}}{3} + \frac{c\theta}{8}\right\}\left\{R\omega^2 Sin\beta + gCos\beta\right\}\right]$$

$$Rk \cdot \frac{\theta}{\delta} = \frac{\nu\rho c\theta}{3\nu^2} \left[\frac{h_{fg}}{c\theta}\right] \left[1 + \frac{3c\theta}{8h_{fg}}\right] \frac{d}{ds} \left[R\delta^3(R\omega^2 Sin\beta + gCos\beta)\right]$$

$$\frac{R}{\delta} = \frac{Pr\, h_{fg}}{3\nu^2 c\theta} \left[1 + \frac{3c\theta}{8h_{fg}}\right] \frac{d}{ds} \left[R\delta^3(R\omega^2 Sin\beta + gCos\beta)\right]$$

Now let $A = \dfrac{3\nu^2 c\theta}{Pr\left[h_{fg} + \frac{3c\theta}{8}\right]}$

Then,

$$A = \frac{\delta}{R} \frac{d}{ds} \left[R\delta^3(R\omega^2 Sin\beta + gCos\beta)\right] \qquad (3.1.21)$$

Equation (3.1.21) is the differential form of the equation governing the filmwise condensation on a rotating general curved body. However, before a solution is attempted, the equation will be examined in detail.

It was stated earlier that,

$$dR/ds = Sin\beta$$
$$d\beta/ds = \beta' = 1/Rc \qquad (3.1.22)$$

From equation (3.1.21),

$$A = \frac{\delta}{R}\left[\delta^3(2R\omega^2 Sin\beta + gCos\beta)\frac{dR}{ds} + \delta^3(R^2\omega^2 Cos\beta - gRSin\beta)\frac{d\beta}{ds}\right.$$
$$\left. + 3\delta^2(R^2\omega^2 Sin\beta + gRCos\beta)\frac{d\delta}{ds}\right]$$

Substituting from (3.1.22) and simplifying,

$$A = \frac{\delta^4}{R} Sin\beta(2R\omega^2 Sin\beta + gCos\beta) + \frac{\delta^4}{R_c}(R\omega^2 Cos\beta - gSin\beta)$$
$$+ 3\delta^3 (R\omega^2 Sin\beta + gCos\beta)\frac{d\delta}{ds}$$

Now, $\frac{3}{4}(R\omega^2 Sin\beta + gCos\beta)\frac{d\delta^4}{ds} = 3\delta^3(R\omega^2 Sin\beta + gCos\beta)\frac{d\delta}{ds}$

$$\therefore A = \frac{\delta^4}{R} Sin\beta(2R\omega^2 Sin\beta + gCos\beta) + \frac{\delta^4}{R_c}(R\omega^2 Cos\beta - gSin\beta)$$
$$+ \frac{3}{4}(R\omega^2 Sin\beta + gCos\beta)\frac{d\delta^4}{ds}$$

Hence re-arranging,

$$\frac{3}{4}\frac{d\delta^4}{ds} = \frac{A - \{\delta^4 Sin\beta(2R\omega^2 Sin\beta + gCos\beta)/R + \delta^4(R\omega^2 Cos\beta - gSin\beta)/R_c\}}{(R\omega^2 Sin\beta + gCos\beta)} \quad (3.1.23)$$

The final term in the numerator of equation (3.1.23) includes R_c, the radius of curvature of the generator of the body. Thus $(R\omega^2 Cos\beta - gSin\beta)/R_c$ represents the curvature effect.

Now consider the case where there is no rotation and angle β is zero. Assume that R_c is infinite. This is the case of condensation on a stationary vertical cylinder. Equation (3.1.23) reduces to:

$$\frac{3}{4}\frac{d\delta^4}{ds} = \frac{A}{g} \quad (3.1.24)$$

$$\text{and } \delta^4 = 4As/3g \quad (3.1.24a)$$

$$\text{or } \delta^4 = \frac{4\mu k s\theta}{\rho^2 g h_{fg}}$$

This is easily recognised as the Nusselt (9) expression for the condensation on a vertical plate. It shows that for such a body $\delta \propto s^{\frac{1}{4}}$.

In equation (3.1.23), let $\delta^4(a+b)$ represent the terms in the external brackets of the numerator.

$$\text{i.e. } a = \frac{R\omega^2\left[1-Cos(2\beta)\right] + \frac{1}{2}gSin(2\beta)}{R}$$

$$b = \frac{R\omega^2 Cos\beta - gSin\beta}{R_c}$$

When there is no rotation, i.e. $\omega=0$

$$\left.\begin{aligned} a = a_1 &= \left[gSin(2\beta)\right]/2R \\ b = b_1 &= -(gSin\beta)/R_c \end{aligned}\right\} \quad (3.1.25)$$

At high speeds of rotation, i.e. $\omega \gg 0$ and $g \to 0$

$$\left.\begin{aligned} a &= a_2 = \omega^2(1-\text{Cos}(2\beta)) \\ b &= b_2 = (R\omega^2\text{Cos}\beta)/R_c \end{aligned}\right\} \qquad (3.1.26)$$

The numerator of equation (3.1.23) becomes

$A - \delta^4(a_1 + b_1)$ when $\omega=0$ and $\beta \leqq 90^o$

and $A - \delta^4(a_2 + b_2)$ when $\omega>>0$ and $\beta \leqq 90^o$

Thus the curvature effect (represented by the curvature term b above), can assist or retard the growth of the film. From (3.1.25), the magnitude of the net effect (i.e. in relation to the other terms) is given by:

$$\left| \frac{b_1}{a_1} \right| = \frac{R}{R_c} \cdot \frac{2\text{Sin}\beta}{\text{Sin}(2\beta)}$$

and from (3.1.26) by:

$$\left| \frac{b_2}{a_2} \right| = \frac{R}{R_c} \cdot \frac{\text{Cos}\beta}{(1-\text{Cos}(2\beta))}$$

Thus, for all speed of rotation and a given value of the angle β such that $90^o>\beta>0^o$, the magnitude of the effect of curvature is governed by the ratio of the radii R/R_c.

In equation (3.1.23), if the radius of curvature becomes infinite ($R_c=\infty$) and the angle $\beta = 90^o$, then when $\omega>>0$ and $g \to 0$

$$\frac{3}{4} \cdot \frac{d\delta^4}{ds} = \frac{A - 2\delta^4\omega^2}{R\omega^2}$$

and has the solution $\delta^4 = A/2\omega^2$ (3.1.27)

But $R_c = \infty$ and $\beta = 90^o$ is the rotating disc. Equation (3.1.27) compares exactly with the Sparrow and Gregg (55) solution for the condensation on rotating discs.

If in the above case, the angle β remained variable and unspecified, then

$$\frac{3}{4}\cdot\frac{d\delta^4}{ds} = \frac{A - 2\delta^4\omega^2\,Sin^2\beta}{R\omega^2 Sin\beta}$$

which when β is constant has the solution

$$\delta^4 = \frac{A}{2\omega^2 Sin^2\beta} \qquad (3.1.28)$$

It should be recognised that when R_c is infinite and β equals some constant angle other than 0^o and 90^o, is the case of the rotating cone. Equation (3.1.28) compares exactly with the solution of Sparrow and Hartnett (69) for the condensation on rotating cones.

It is important to note that equation (3.1.28) is only obtained when β is assumed constant. This implies that equation (3.1.28) is applicable to individual cones only. For a given cone and hence a given β, equation (3.1.28) gives the assymptote to which the film of condensate grows as the speed of rotation is increased and the effects of gravity are diminished.

It should be appreciated that if β varies with respect to the distance (s), then this represents the case where the generator is made up of a series of truncated cones since the radius of curvature at any given point is infinite. The problem becomes different in such a case and the solution requires the exact mathematical relationship between β and s, or a technique to link one cone to another without causing any discontinuities in the film of condensate.

In equation (3.1.23) if gravity, rotation and the angle β are finite but R_c infinite, then

$$\frac{3}{4}\cdot\frac{d\delta^4}{ds} = \frac{A - \delta^4 Sin\beta(2R\omega^2 Sin\beta + gCos\beta)/R}{(R\omega^2 Sin\beta + gCos\beta)} \qquad (3.1.29)$$

Equation (3.1.29) requires a numerical solution. It compares exactly with Howe's (71) solution for condensation on rotating cones including the effect of gravity.

Lastly, consider R_c to be infinite and the angle β to be zero. This represents the rotating vertical cylinder. Equation (3.1.23) becomes

$$\frac{3}{4} \cdot \frac{d\delta^4}{ds} = \frac{A}{g} \qquad (3.1.30)$$

Equations (3.1.30) and (3.1.24) are identical. It can be seen from this that the growth of the film of condensate on a rotating vertical cylinder is not governed by the rotation. Any improvement in the heat transfer coefficient such as reported by others, is the result of surface disturbances and the detachment of drops.

3.1.5 Solution of equation (3.1.21) in non-dimensional form

The equation:

$$A = \frac{\delta}{R} \frac{d}{ds} \left[R\delta^3 \, (R\omega^2 \mathrm{Sin}\beta + g\mathrm{Cos}\beta) \right] \qquad (3.1.21)$$

is the governing equation of filmwise condensation on the rotating general curved body. In the previous section, this equation was examined in detail. In this section, a solution of the equation is presented. The non-dimensionalisation of equation (3.1.21) facilitated the solution.

Let ξ be the non-dimensional radius of the body, and η be the non-dimensional condensate thickness. Then,

$R = \alpha\xi$ and $\delta = \gamma\eta$

where α and γ are constants and have the dimensions of length.

Let angle β be a function of ξ

i.e. $\beta = \lambda(\xi)$, (and be denoted by λ)

Now $ds = dR/\mathrm{Sin}\beta = \alpha d\xi/\mathrm{Sin}\lambda$

Substituting into equation (3.1.21), it becomes:

$$A = \frac{\gamma\eta}{\alpha\xi} \mathrm{Sin}\lambda \frac{d}{\alpha d\xi} \left[\alpha\xi\gamma^3\eta^3(\alpha\xi\omega^2\mathrm{Sin}\lambda + g\mathrm{Cos}\lambda) \right]$$

$$A = \frac{\eta}{\xi} \mathrm{Sin}\lambda \frac{d}{d\xi} \left[\eta^3(\omega^2\gamma^4\xi^2 \, \mathrm{Sin}\lambda + g\frac{\gamma^4\xi}{\alpha} \, \mathrm{Cos}\lambda \right] \qquad (3.1.31)$$

Suitable values of α and γ are:

$$\alpha = g/\omega^2 \quad \text{and} \quad \gamma = \omega^{-\frac{1}{2}} A^{\frac{1}{4}}$$

Hence $\xi = R/\alpha = R\omega^2/g$, the ratio of centrifugal acceleration to gravitational acceleration. Substituting for α and γ, equation (3.1.21) becomes:

$$1 = \frac{\eta}{\xi} \operatorname{Sin}\lambda \cdot \frac{d}{d\xi} \left[\eta^3 (\xi^2 \operatorname{Sin}\lambda + \xi \operatorname{Cos}\lambda) \right] \qquad (3.1.32)$$

$$\text{or,} \quad \frac{\xi}{\operatorname{Sin}\lambda} = \eta \frac{d}{d\xi} \left[\eta^3 (\xi^2 \operatorname{Sin}\lambda + \xi \operatorname{Cos}\lambda) \right] \qquad (3.1.32)$$

Let $\xi/\operatorname{Sin}\lambda = \mathcal{F}(\xi)$ and $(\xi^2 \operatorname{Sin}\lambda + \xi \operatorname{Cos}\lambda) = F(\xi)$

Substituting $\mathcal{F}$ and F, equation (3.1.32) becomes:

$$\mathcal{F} = \eta \frac{d}{d\xi} (\eta^3 F)$$

$$\therefore \quad \frac{4}{3}\mathcal{F} = 4\eta^3 F\eta' + \frac{4}{3}\eta^4 F' \quad \text{where } \frac{d}{d\xi} = ' \qquad (3.1.33)$$

Let $Z = \eta^4$. Then equation (3.1.33) becomes:

$$Z' + \frac{4}{3}\frac{F'Z}{F} = \frac{4}{3} \cdot \frac{\mathcal{F}}{F} \qquad (3.1.34)$$

which has the solution:

$$Z = \frac{4}{3} \frac{\int_{\xi_0}^{\xi} \mathcal{F} F^{1/3} \, d\xi}{F^{4/3}}$$

$$\text{and} \quad \eta^4 = \frac{4}{3} \frac{\int_{\xi_0}^{\xi} \mathcal{F} F^{1/3} \, d\xi}{F^{4/3}} \qquad (3.1.35)$$

Equation (3.1.35) is the solution of equation (3.1.21) in a non-dimensionalised form. This form of the solution has the advantage that only one integration is required for any given body. There are only two functions in the equation, namely, F and $\mathcal{F}$, and these are easily determined when the geometry of the body is known. Equation (3.1.35) applies to any axisymmetrical curved body, including cones, discs and cylinders.

Solution in terms of s

When $\mathcal{F}$ and F are substituted for, equation (3.1.35) becomes:

$$\eta^4 = \frac{4}{3} \frac{\int_{\xi_0}^{\xi} (\xi^2 \mathrm{Sin}\lambda + \xi \mathrm{Cos}\lambda)^{1/3} (\xi/\mathrm{Sin}\lambda) d\xi}{(\xi^2 \mathrm{Sin}\lambda + \xi \mathrm{Cos}\lambda)^{4/3}} \qquad (3.1.36)$$

It will be observed that when Sinλ is zero the integrand goes to infinity. In a computer programme to solve equation (3.1.36), λ can be given a small starting value to overcome the difficulty. If, on the other hand, equation (3.1.36) is expressed in terms of the distance (s), this problem does not arise.

If ξ and λ are functions of s, i.e. $\xi = \Phi(s)$, (and denoted by Φ) and $\lambda = \psi(s) = \beta$, (and denoted by ψ) then since $\mathrm{Sin}\beta = dR/ds = \alpha d\xi/ds$, equation (3.1.36) becomes:

$$\eta^4 = \frac{4}{3\alpha} \frac{\int_{s_0}^{s} \Phi(\Phi^2 \mathrm{Sin}\psi + \Phi \mathrm{Cos}\psi)^{1/3} ds}{(\Phi^2 \mathrm{Sin}\psi + \Phi \mathrm{Cos}\psi)^{4/3}} \qquad (3.1.37)$$

Equations (3.1.36) and (3.1.37) give identical results in practice and either can be used depending on the problem. If the geometry of the body is such that angle β becomes zero at some point, then equation (3.1.27) is preferred. On the other hand, when treating a curved body as made up of series of cones, angle β does not go to zero and equation (3.1.36) is preferred, since ξ is the same for either cone at the point of interesection and allows the linking of one cone to the other more easily without introducing any discontinuities in the growth of the film.

When dealing with the curved generator made up of series of cones, the integral part of the equation (3.1.36) or (3.1.37) is evaluated thus:

$$\int_a^z = \int_a^b + \int_b^c \ .... + \int_y^z$$

If it is imagined that each integral on the right hand side of the above equation represents the integration for a single trucated cone, then apart from the leading cone, some difficulties arise when integrating with respect to s as to what the lower limits of the integration should be for

each cone. This difficulty does not arise when the integration is with respect to ξ.

The heat transfer coefficients

When the geometry of the body on which the condensation is taking place is known, equation (3.1.36) or (3.1.37) can be integrated to give η.

Now $\delta = \gamma\eta = \omega^{-\frac{1}{2}} A^{\frac{1}{4}}\eta$

The local heat transfer coefficient is then given by:

$$h = \frac{k}{\delta} = \left[\frac{k}{\omega^{-\frac{1}{2}}A^{\frac{1}{4}}}\right] \frac{1}{\eta} \qquad (3.1.38)$$

$$\text{or} \quad h \left[\frac{\omega^{-\frac{1}{2}} A^{\frac{1}{4}}}{k}\right] = \frac{1}{\eta} \qquad (3.1.38a)$$

and the local Nusselt number by:

$$Nu_s = \frac{hs}{k} = \left[\frac{1}{\omega^{-\frac{1}{2}}A^{\frac{1}{4}}}\right] \frac{s}{\eta} \qquad (3.1.39)$$

$$\text{or} \quad Nu_s \left[\omega^{-\frac{1}{2}} A^{\frac{1}{4}}\right] = s/\eta \qquad (3.1.39a)$$

From the point of view of the heat exchanger designer, average heat transfer coefficients are of more interest than the local heat transfer coefficients. This is usually obtained by integrating the local heat transfer coefficient with respect to the distance from the start of the condensate film and dividing the results by area per unit depth. This is acceptable when dealing with bodies such as cylinders which have a constant diameter. When dealing with a body whose diameter varies with distance from the leading edge, it becomes necessary to integrate with respect to the area. The average heat transfer coefficient is thus based on area instead of length.

Considering the general axisymmetrical body of fig. 1, the surface area is given by,

Area $\hat{A} = 2\pi \int_{so}^{s} R ds$

The average heat transfer coefficient $\bar{h}$ over the distance so to s is given by:

$$\bar{h} = \frac{2\pi \int_{so}^{s} hR ds}{2\pi \int_{so}^{s} R ds}$$

$$= \frac{\left[k/(\omega^{-\frac{1}{2}}A^{\frac{1}{4}})\right] \int_{so}^{s} (R/\eta) ds}{\int_{so}^{s} R ds}$$

$$\bar{h}\left[\frac{\omega^{-\frac{1}{2}}A^{\frac{1}{4}}}{k}\right] = \frac{\int_{so}^{s} (R/\eta)\, ds}{\int_{so}^{s} R\, ds} \qquad (3.1.40)$$

The average Nusselt number, up to the point s, is defined as $\bar{Nu}_s = \bar{h}s/k$

and $\bar{Nu}_s \cdot \left[\omega^{-\frac{1}{2}}A^{\frac{1}{4}}\right] = \frac{s \int_{so}^{s} (R/\eta)\, ds}{\int_{so}^{s} R\, ds} \qquad (3.1.41)$

It will be observed that equation (3.1.40) is non-dimensional but equation (3.1.41) is not and has the dimensions of length. The equations (3.1.36) - (3.1.41), as will be appreciated, enable the behaviour of both the condensate film thickness and the heat transfer coefficients to be predicted for a given body without reference to any experimental evidence. In practice, however, some experimental evidence might be necessary in order to evaluate "A" correctly since it involves θ, the temperature drop across the condensate.

3.2 Applications of equation (3.1.35)

As stated earlier, equation (3.1.35) is the non-dimensional form of the governing equation of condensation on any rotating exisymmetrical body. Its applications are unlimited as far as the choice of the generator is concerned but it is limited with regard to the speed of rotation. As $\xi = R\omega^2/g$, and both $\mathcal{F}$ and F have ξ as a multiplier, equation (3.1.35) become indeterminate when ω=o. This resulted from the non-dimensionalisa-

tion of equation (3.1.21). Therefore, for the condition that $\omega=o$ one has to go back to equation (3.1.23) and carry out the analysis from there. On the other hand, this is not necessary if ω is given some small starting value. This is the common procedure in a case of this kind, and the author has made use of the procedure. The applications of equation (3.1.35) to cones, discs and cylinders are given in Appendix C to show primarily its validity and the ease of its application. In the following section therefore, only the curved body with a generator which forms a circular arc of 90^{o} is considered.

3.2.1 Application of equation (3.1.35) to the circular curved body (experimental curved body)

The circular curved body with a generator which forms an arc of 90^{o} is of particular interest here because it represents the experimental curved body. The application of the general equation (3.1.35) in the form of equation (3.1.37) is illustrated using such a body.

Consider the generator with the constant radius of curvature R_c shown below.

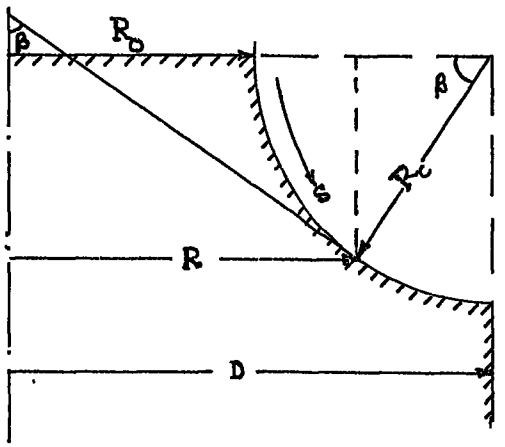

$$R = R_o + R_c\,(1-\cos\beta) = \boxed{D - R_c\cos\beta}$$

$$\xi = R\omega^2/g = \boxed{D - R_c\cos\beta}\;\omega^2/g$$

$$\beta = s/R_c = \psi(s)$$

$$\xi = \left[\bar{D} - R_c \cos(s/R_c)\right] \omega^2/g = \Phi(s)$$

Thus in equation (3.1.37)

$$\Phi = \left[\bar{D} - R_c \cos(s/R_c)\right] \omega^2/g \text{ and } \psi = s/R_c$$

Also equations (3.1.40) and (3.1.41) respectively become:

$$\bar{h}\left[\frac{\omega^{-\frac{1}{2}}A^{\frac{1}{4}}}{k}\right] = \frac{1}{\left[\bar{D}s - R_c^2 \sin(s/R_c)\right]} \int_o^s (R/\eta)\, ds \qquad (3.1.42)$$

$$\text{and, } \bar{Nu}_s\left[\omega^{-\frac{1}{2}}A^{\frac{1}{4}}\right] = \frac{s}{\left[\bar{D}s - R_c^2 \sin(s/R_c)\right]} \int_o^s (R/\eta)\, ds \qquad (3.1.43)$$

For the experimental curved body fig. (9), R_c = 0.1346m and D = 0.2745m and when these are substituted into the above equations the complete solutions of equations (3.1.37) - (3.1.43) are obtained. Figures 3, 4 and 5 show respectively, the complete solution of equation (3.1.37), (3.1.38) and (3.1.42) for the experimental curved body. The figures also show the solutions for the same body when the curvature term, as outlined in equation (3.1.23), is excluded in the solutions of the above mentioned equations. The graphs show the predicted non-dimensional film thickness, local and average heat transfer coefficients plotted against distance along the surface of the generator. However, before these results are discussed, an outline of the method of solution will be given.

3.2.2 The integration routine

The integration of the numerator of equation (3.1.35) can be straight forward depending on the complexity of the generator and whether curvature and gravity are neglected. In the study of the experimental curved body, a straight forward integration was not possible and numerical integration had to be employed.

A computer programme was developed for use on an IBM 360/67 digital computer to carry out the numerical integration. The integration routine

utilized the Simpson's $1/3$ rule, as outlined by McCormick and Salvadori (80). In the above mentioned computer programme, which was written in FORTRAN IV, the term $\mathcal{F}F^{1/3}$ in equation (3.1.35) was represented by a single function $f(x) = \mathcal{F}F^{1/3}$. A FUNCTION SUBPROGRAMME evaluated the function $f(x)$ and a DO LOOP carried out the "Simpson" summation.

The programme was simple but powerful and was capable of integrating many mathematical functions. If n is the even number of strips and H the width of a strip, then the error in the Simpson's $1/3$ rule applied to multiples of n=2 strips as in this case, is of the order H^4. Hence, the smaller the width of the strips, the more accurate the final result. For many known mathematical functions which were used as a test for the programme, strip width of the order 10^{-2} of one unit (of the dimensions of the limits of the integration) was sufficient to produce a very high degree of accuracy. However, for the results presented in this work, strip width of the order 10^{-4} was used.

3.2.3 Discussion of the predicted results

After the computer programme had been carefully tested and the confidence in its use established, the programme was applied to equations (3.1.37), (3.1.38) and (3.1.42), using the data from the experimental curved body. Fig. 3 shows the predicted behaviour of the film of condensate as given by equation (3.1.37). The figure also shows the solution for the same body when the curvature term in the equation is neglected. This implies that the generator is made up of a series of cones. For the results presented here, the experimental curved body was assumed to be made up of 450 truncated cones. This corresponds to a β value of 0.2° which approaches the smallest starting value when equation (3.1.36) is used. The need to use equation (3.1.36) instead of equation (3.1.37)

in such a case has been given. Different numbers of truncated cones were considered and the choice of the 450 cones was a compromise between accuracy and the use of computer time. The improvement in the value of η at 1000 rev/min when 450 cones are used instead of 18 cones is only 3.5 percent but the computer time required is now 25 times greater.

A range of speeds, varying from 0.1 rev/min to one million rev/min were considered in the analysis. The solutions at some of these speeds are presented in fig. 3. The speed of 0.1 rev/min was used instead of zero rev/min for reasons stated earlier, namely that equation (3.1.36) or (3.1.37) becomes indeterminate when the speed of rotation is zero.

Looking at the solution that includes the curvature term, it will be observed that for speeds up to 100 rev/min, the film of condensate starts at the leading edge of the generator and grows in thickness with distance. For speeds between 100 rev/min and 1000 rev/min, the film grows to some maximum thickness and then thins out. The higher the speed of rotation, the shorter the distance required for the film to grow to the maximum thickness. At speeds above 3000 rev/min, the maximum thickness is attained almost instantaneously at the leading edge of the generator and the thinning takes place all the way down.

To understand the behaviour, one has to go back to equation (3.1.23) which is reproduced here for convenience

$$\frac{3}{4}\frac{d\delta^4}{ds} = \frac{A - \{\delta^4 \mathrm{Sin}\beta(2R\omega^2\mathrm{Sin}\beta + g\mathrm{Cos}\beta)/R + \delta^4(R\omega^2\mathrm{Cos}\beta - g\mathrm{Sin}\beta)/R_c\}}{(R\omega^2\mathrm{Sin}\beta + g\mathrm{Cos}\beta)} \quad (3.1.23)$$

The numerator of equation (3.1.23) was shown (section 3.1.4) to be:

$A - \delta^4(a_1 + b_1)$ when $\omega = o$ and $\beta \leq 90^o$

and $A - \delta^4(a_2 + b_2)$ when $\omega >> o$ and $\beta \leq 90^o$

where "a" and "b" are as defined in equations (3.1.25) and (3.1.26).

From equation (3.1.25)

$$a_1 = [g\mathrm{Sin}(2\beta)] / 2R$$

and $b_1 = -(g\mathrm{Sin}\beta)/R_c$

Now since $\mathrm{Sin}\beta \geq \frac{1}{2}\mathrm{Sin}(2\beta)$ and the geometry of the experimental curved body is such that $R > R_c$ at any point on the generator, it follows that at very low speeds, $|b_1| > |a_1|$. Hence, $A - \delta^4(a_1 + b_1)$ will always be positive under such circumstances and the slope $d\delta^4/ds$ will always be positive as observed. Also in equation (3.1.23) the denominator is given by $g\mathrm{Cos}\beta$ when $\omega = o$. Thus when $\beta \to 90^o$, $\frac{d\delta^4}{ds} \to \infty$. This behaviour is exhibited by the curve for the 0.1 rev/min in addition to the positive slope outlined above.

Considering the case where $\omega >> o$ and the effects of gravity are negligible, the numerator becomes:

$$A = \delta^4 (a_2 + b_2)$$

where $a_2 = \omega^2 [1 - \mathrm{Cos}(2\beta)]$

and $b_2 = (R\omega^2 \mathrm{Cos}\beta)/R_c$

As β lies between 0^o and 90^o, both a_2 and b_2 will be positive in such a case, and for large values of ω, $A - \delta^4 (a_2 + b_2)$ will be negative and hence the slope $d\delta^4/ds$ will be negative. Such a behaviour is exhibited by the curve labelled "limiting case". The term "limiting case" as used here implies the solution of equation (3.1.35) for which the non-dimensional film thickness η is not affected by further increases in the rotational speed. The limiting case was attained at speeds of 3000 rev/min and over.

Thus between zero rev/min and 3000 rev/min, the slope changes from positive to negative. The family of curves in fig. 3 when the first 0.015m is neglected show that the slope remains positive up to 100 rev/min and thereafter begin to change. The effects of the centrifugal field can be said to begin to show prominence after 100 rev/min.

Without exception, the curves representing the solution with the curvature term start with a positive gradient, although this may be difficult to see in the case of the curve representing the limiting case. Depending on the speed of rotation, the gradient of some of the curves later change to negative. This is to be expected because the leading edge of the generator forms a vertical cylinder and for the first 0.003m it could be treated as such. It has been shown that for such a case,

$$\frac{3}{4}\frac{d\delta^4}{ds} = \frac{A}{g} \qquad (3.1.30)$$

and $\delta \sim s^{\frac{1}{4}}$ i.e. $\eta \sim s^{\frac{1}{4}}$

It can therefore be seen that at the leading edge, the slope $d\delta^4/ds$ will always be positive.

The relationship $\delta \sim s^{\frac{1}{4}}$ was further exploited as one of the methods by which the computer programme could be tested. A plot of log η against log s - not included - confirmed the relationship $\eta \sim s^{\frac{1}{4}}$ at the leading edge.

In equation (3.1.23) when $\omega > o > g$, the numerator, as before is:

$A - \delta^4 (a + b)$

and $a = Sin\beta(2R\omega^2 Sin\beta + gCos\beta)/R$

$b = (R\omega^2 Cos\beta - gSin\beta)/R_c$

$A - \delta^4(a + b)$ will either be positive or negative depending on "a" or "b", hence the change of slope by some of the curves.

It should be noted that the rate of change of the slope is governed by $\delta^4(a + b)$ which is a function of ω and β, hence the point at which the slope changes sign, and the rate at which the slope changes, will vary. This can be observed in fig. 3.

The family of curves representing the solution without the curvature term exhibit similar characteristics, in many ways, to those discussed above. Nevertheless, there are some outstanding differences when the two families of curves are compared.

It was shown earlier that at low speeds of rotation, the growth of the film is assisted by the curvature effect. The comparison of the curves at 50 rev/min ant 0.1 rev/min shows this very clearly. The growth of the film, on the otherhand, is retarded by the curvature effect at high speeds and this also can be observed when the rest of the curves are compared. It could be estimated from fig. 6 which shows the deviations in heat transfer coefficients when the two solutions are compared, that for the above experimental curved body, the transition from the assisting effect to the retarding effect takes place at 70 rev/min.

Turning to equation (3.1.23) once more, it should be noticed that the numerator $A - \delta^4(a + b)$ becomes $A - \delta^4(a)$ since $b \to o$ when $R_c \to \infty$ and the rate of change of the slope $d\delta^4/ds$ becomes less in comparison. It is evident that for speeds greater than 70 rev/min, the curves representing the solution with the curvature term will lie beneath the corresponding curves for the solution without the curvature term. In other words, the solution without the curvature term predicts a thicker film of condensate and hence lower heat transfer coefficients compared with the solution with the curvature term.

It should also be evident that the difference between $A - \delta^4(a + b)$ and $A - \delta^4(a)$ is $\delta^4(b)$ which represents the curvature effect. Thus the difference between the corresponding curves in fig. 3 represent the curvature effect at the given speed of rotation. The examination of fig. 3 shows that the importance of the curvature effects in the analysis

of the condensation on rotating bodies cannot be over stressed. Comparing the two limiting cases in fig. 3, it can be seen that the analysis without the curvature term can over-estimate the local film thickness by up to 71 percent. This is reflected in the local heat transfer coefficients, fig. 4 and hence in the average heat transfer coefficients shown in fig. 5.

Fig. 4 shows the solution of equation (3.1.38a). It shows the predicted behaviour of the local heat transfer coefficients for both cases of with and without curvature. These curves are the inverse of the curves shown in fig. 3 and no further comment is necessary.

Sparrow and Hartnett (69) have shown that for cones rotating at very high speeds, $\eta = 0.841/(\sin^{\frac{1}{2}}\beta)$. Equation (3.1.28) confirms this. Thus for a given cone η is constant and the heat transfer coefficient is independent of the distance s. This is not the case here and fig 4 shows that the local heat transfer coefficient h, is dependent on s even at high speeds.

The average heat transfer coefficients (fig. 5), tell a similar story. Fig. 5 represents the solution of equation (3.1.42). Both graphs show that at low rotational speeds, when gravity is the dominant field, the heat transfer coefficients decrease with s. The situation is reversed when gravity becomes less important and the centrifugal field more dominant.

The effect of curvature on the local and average heat transfer coefficients can easily be observed from fig. 4 and fig. 5 respectively. Fig. 6 illustrates the variation of the effects with respect to the rotational speed. Expressing the maximum percentage deviation as $\frac{(X1-X2)}{X1} \cdot 100$, where X1 is the predicted heat transfer coefficient when the curvature term is included and X2 the predicted heat transfer coefficient when the curvature term is excluded, fig. 6 shows that the

local heat transfer coefficients could be under-estimated by 43 percent for speeds of 3000 rev/min and over. The average heat transfer coefficients show a slightly lesser percentage. Nevertheless, the under-estimation of the average heat transfer coefficient by 37.5 percent is something that could be avoided. As pointed out earlier and illustrated by fig. 6, the curvature effects are speed dependent and the above percentages decrease with the speed. Fig. 6 shows that at 70 rev/min, the curvature effects are zero and below 70 rev/min, the solution with the curvature term tends to under-estimate the heat transfer coefficients. For speeds below 50 rev/min, fig. 6 becomes less meaningful because the solution with the curvature term implies no drainage at the disc end of the generator, and the film should, therefore, grow to infinity. This, therefore, distorts the percentage deviation as presented here, particularly the local values.

4.0 APPARATUS

4.0 INTRODUCTION

The present work is the final stage of the research started by Hoyle and his colleagues at the Imperial College of Science and Technology and later continued at Durham. This means that the basic equipment was available at the start of the present work and any experimental studies had to take this into consideration.

The basic rig at Durham (fig. 7), was designed and built jointly by Robson (75) and Howe (71). Robson was interested in the fluid mechanics of the film of condensate while Howe was concerned with the heat transfer properties. Each designer paid particular attention to the overall design from his own point of view and their combined effort produced a large and versatile apparatus. Both Robson and Howe have given a comprehensive account of the design, manufacture and installation of the equipment in their work.

4.1 Specification of the basic rig

After a careful study, Robson and Howe drew up the following specification in 1966 to form the basic requirements of the apparatus:

1) Steam pressure; variable up to 13.8 bar.
2) Steam condition; dry saturated.
3) Base diameter of the experimental body; 0.61m. (2 ft.).
4) Speed of rotation; variable and up to 2000 rev/min.
5) The outside surface temperature of the experimental body should be capable of controlled variation.
6) The condensate forming on the interior surface of the pressure vessel should not drip onto the condensing surface.
7) The condensing surface should be capable of being viewed both tangentially and normally while under test.
8) Windows in the pressure vessel should be capable of withstanding the working steam pressure and temperature, and allow the condensing surface to be photographed,.

9) The polar axis of the experimental body should be vertical.

10) The experimental body should be capable of being rotated with the minimum vibration.

11) The steam supply should be free from non-condensable gases.

The condensing elements were made as large as possible to reduce scale effects. This was necessary if the test results were to be used to calculate the thermal stresses in turbine rotors. A base diameter of 0.61m. gave a large condensing surface even when cones of largeapex angle are used.

4.2 General arrangement and operation of the basic rig.

Fig. 7., modified from Howe (71), shows the main features and the general view of the complete assembly of the apparatus. Item numbers are assigned to the important parts of the apparatus and these will be referred to in the following section.

The experimental body (iterm 7) which comprises a cover, the curved body and a cylindrical base is mounted on the 0.58m. diameter base plate which is coupled to the main shaft (item 19) by the screw on flange. The main shaft had to be hollow to create a passage for cooling water flowing into and out of the experimental body. A pair of high precision tapered roller-bearings (item 13), mounted back to back, supported the main shaft. The thrust from the bearings was equally distributed to brackets welded to the four legs supporting the pressure vessel. A double-row spherical seating ball-bearings (item 11), mounted in a sliding housing, acted as a locating bearing at the upper position.

Rotation to the main shaft, and hence the base plate and the experimental body, was applied through the timing belt and the driving pulley (item 12). Power was supplied by a 11.5 kW. d.c. motor with

a 200 per cent overload starting torque. The power to the motor was provided by a control unit, comprising a 400 - 440V, 3 phase, 50 Hz. thyristor bridge.rectifier for armature supply, together with a single phase bridge rectifier for field supply.

The upper part of the main shaft with the attached base plate and the experimental body was enclosed in a pressure vessel. The pressure vessel had provisions for a pressure gauge, a thermometer pocket (item 16), a blow-off valve (item 17) and a stuffing box gland (item 5) to accommodate the hollow steel shaft (item 18) which carried the thermocouple wires to the slip-ring unit (item 6). A total of 7 ports of two different sizes were provided. Five of these ports had a diameter of 0.3m. (item 3) and the rest 0.24m. diameter (item 4). The ports were covered with armour-plate glass. The armour-plate glass was strong enough to stand the design temperature and pressure, and also clear enough to allow viewing and the photographing of the condensing surface.

The steam to the condensing surface was supplied by an English Electric automatically regulating oil fired package boiler unit. The boiler was capable of 1400 kg/hr of steam with dryness fraction 0.99 at 15 bar. The steam supply to the pressure vessel was controlled by a reducing valve which could produce reduced pressures over the range 0.05 to 0.8 of the supply pressure. Throttling the steam down to the desired pressure caused a certain degree of superheat. The steam was therefore passed through a de-superheater before entry into the pressure vessel.

The steam entered the pressure vessel via the steam inlet (item 25) and the steam distributor (item 9). The condensate was removed through a drain in the base of the pressure vessel via the condensate drain (item 26) to a condenser.

The cooling water to the inside of the condensing surface was supplied via an inlet manifold which divided the water into five independent supplies (item 15). The five water supplies were connected to separate passages inside a 0.05m. diameter stationary pipe which conducted them to the experimental body along the central hole in the main shaft (item 19). Each of the water supplies terminated in one of the four (originally five in Howe's work) water-tight chambers of the sprayer head (item 8). Water was carried from these chambers to the inner surface of the body by a number of 0.005m. bore tubes. The five independent supplies allowed the flow in each chamber to be adjusted during operation so that the inside surface temperature of the condensing body could be maintained as constant as possible.

At the base of the experimental body, the cooling water was collected by four stationary 0.025m. diameter scoops and carried into the annular passage between the stationary central inlet pipe and the bore of the rotating shaft. A sealed perspex box (item 14), mounted over two 0.064m diameter holes in the shaft, collected the cooling water discharged from the annular passage.

A good sealing arrangement was required if the leaking of steam was to be avoided. A mechanical seal (item 10), which ran in a housing and could be pressurized by water to pressures in excess of the vessel pressure, offered the best solution. Dry asbestos packing and P.T.F.E. tape were used to pack the gland (item 5), which sealed the small shaft.

4.3 The experimental body

The experimental body (fig. 8) comprised a cover, the curved body and a cylindrical base. It is a manganese bronze and manufactured to B.S. 1400 H.T.B.1 specification.

Fig. 9 shows the details of the curved body.

The cover which had a base diameter of 0.2794m. was conical in shape. It had a cone angle of 174^{o} and a wall thickness of 0.0178m. The conical shape was essential to ensure that any condensate on the cover drained off. Condensation on the cover was inevitable at the beginning of a test. The cover performed three main functions:

(i) coupled the hollow shaft (item 18), which carried the thermocouples to the slip-ring unit (item 6), to the curved body.

(ii) ensured that no steam leaked into the inside of the experimental body or water out of the experimental body to contaminate the steam.

(iii) carried thermocouples to measure the steam temperature inside the pressure vessel. This was essential in order to correct for the effects of rotation on the slip-ring unit.

A diaphragm made of 0.0032m. thick brass plate and 0.2794m. diameter with 0.0064m. thick asbestos joint on one side (the water side) separated the curved body and the cover. The diaphragm prevented cooling water from reaching the cover. It was essential that the cover did not condense any steam after the warm through period since this would affect the results. The diaphragm was very effective in this respect.

The cylindrical base had an outside diameter of 0.6096m., a wall thickness of 0.0254m. and an overall height of 0.1905m. Its function was to extend the base plate in such a way that the curved body would clear the scoops. It also enabled the author to estimate without difficulty, the approximate maximum stresses in the experimental body. The author assumed that the maximum stresses would occur in the cylindrical base and this allowed the use of standard equations for

the stresses in rotating cylinders. The approximate calculations, which neglect thermal stresses, gave a minimum safety factor of over 2.0 at 3000 rev/min and this safety margin gave a measure of confidence in the design.

Two small pieces, 0.007m. square by 0.12m. long, were removed from opposite sides of the cylindrical base and used to determine the thermal conductivity of the body material. The strength and the general appearance of the cylindrical base were not affected by the removal of the material.

Dividing the experimental body into the three main parts as above facilitated the manufacture. Of the three main parts, the one of interest here is the curved body. It is the body under study and will be examined more closely.

4.3.1 The rotating curved body

The experimental curved body, fig. 9, represents a generator with a constant radius of curvature. It has a radius of curvature of 0.1346m. and a thickness of 0.0178m. It has an external leading edge (cylindrical) diameter of 0.2794m. and a base or disc diameter of 0.6096m. with a working length of 0.2115m. The material is a high tensile brass B.S. 1400 H.T.B.1.

The choice of the manganese bronze H.T.B.1 as the working material was mainly for its cheapness compared with aluminium bronze. The use of steel, other than stainless steel, could not be contemplated because of corrosion. Stainless steel on the otherhand was too expensive to be considered. Manganese bronze has corrosion resistance and strength characteristics comparable with aluminium bronze, but has a higher thermal conductivity.

The choice of the generator was influenced by both practical and theoretical considerations. From the theoretical point of view, any generator other than the one with a 90^{o} arc of a circle could have

been chosen. However, the circular arc offered the ease of manufacture. In addition, the circular arc was easier to check dimensionally. Such checks were carried out by mounting the body on a lathe and the surfaces traversed with a clock guage. In all cases, the measurements were within the specified limits of $\pm 5 \times 10^{-5}$m.

The choice of the radius of curvature was governed by:

(i) The existing apparatus, particularly the base plate

(ii) A reasonable working length.

(iii) The theory which suggests a high value of the ratio of radii R/Rc

The base plate diameter of 0.58m. was intended to give the base diameter of the experimental body a value of 0.6096m. and this fixed the disc diameter of the experimental curved body.

To eliminate scale effects and the errors associated with small measurements, a working length of about 0.2m. was considered appropriate.

One of the objectives of the present work is to examine the importance of curvature on the condensation of vapours on a rotating body. In section 3.1.4, it was shown that the magnitude of the curvature effects is governed by the ratio of the radii R/Rc. A small value of Rc would have been desirable but this would have given a smaller working length. The choice of Rc = 0.1346m. was a compromise between the theory, the working length and the restriction on size set by the existing apparatus. The Rc of 0.1346m. gave a working length of 0.2115m. and a working R/Rc ratio of 1.075 : 1 to 2.08 : 1. These were considered adequate to meet the requirements.

4.3.2 Thermocouples

Copper-constantan thermocouples were used. The conductors had a diameter of 0.000315m. each. Each conductor was insulated with paper glass and varnished before being braided together with a

twin flat glass paper between them and further varnished.

The junctions of the thermocouples were made by first removing the unwanted insulation. The conductors were then twisted together such that the finished product resembled a closed helical spring. The junction so formed was dipped in a molten high melting point solder. This ensured a complete eletrical contact between conductors. This method of construction was preferred to spot welding because one could make the junction longer than required and then cut off the excess when the couple was bonded onto place. This was necessary in order to ensure that the junctions were not buried far beneath or protruded above the surface of the body.

The number of thermocouples that could be used was dictated by the capacity of the slip-ring units available. Two slip-ring units were available. The two could handle a total of 23 thermocouples. One of the slip-ring units handled 17 thermocouples and the other, the remaining six.

A total of 21 out of the 23 thermocouples allowed by the slip-ring units were used on the experimental curved body. The remaining two were used to measure the steam temperature in the pressure vessel. A total of 24 thermocouples were required, the 24th thermocouple being used to measure the steam temperature in the pressure vessel directly, without passing through any of the slip-ring units. By measuring the steam temperature through each of the slip-ring units and comparing with the direct reading, the effects of rotation on the slip-ring units could be estimated and corrected for.

After manufacture, the junctions of the thermocouples were insulated by immersing them in Bostik 1160, dried for an hour at $27^{o}C$ and finally cured for 20 minutes at $141^{o}C$ in an oven. The same

bonding agent, Bostik 1160, was used to bond the thermocouples onto the experimental curved body. To read local temperatures, it was necessary that the thermocouple junctions did not make electrical contact with one another through the experimental body. Insulating the junctions before being bonded onto the experimental body ensured that.

It is shown later (Section 7) that the overall accuracy and reliability of the experimental results depend on the accurate measurement of the fluid film and the body interfacial temperatures. In view of this each thermocouple had to be calibrated. The calibration rig consisted of:

(i) A range of N.P.L. standard thermometers which covered the range 0° - 200°C in steps of 0.1°C.

(ii) A thermostatically controlled calibrating oil bath with a range of 0° - 200°C and fitted with stirrer assembly and contact thermometer

(iii) A ZEREF type 136 thermocouple ice point reference

(iv) CROPICO type SP2/P/B/CT, 24 positions, double pole thermocouple selector switch

(v) SOLARTRON type LM 1420 - 2 digital voltmeter

The sketch below shows the diagramatic arrangement of the calibrating rig.

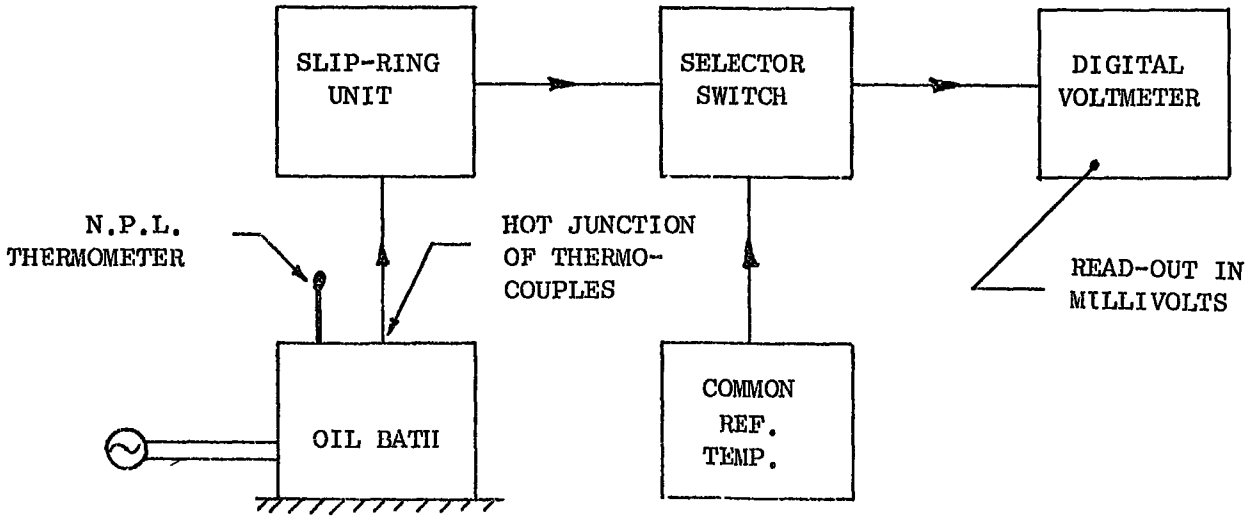

On the experimental rig, the curved body fig. 9, replaced the oil bath, otherwise there was no change in the above set up. It could be said that the calibration was not for the thermocouples alone but the instrumentation as a whole. The calibration covered the range 0^{o} - 200^{o}C. By the use of the X4 scale of the Digital voltmeter, variations in temperature of 0.05^{o}C could be measured. This order of accuracy was considered more than adequate to meet the experimental requirements. The hot ends of the thermocouples were soaked in 10 per cent solution of Decon 90 for several hours to remove the oil before use.

4.3.3 Instrumentation and Dynamic balancing of the rotating body

Of the 21 thermocouples used on the curved body, 14 were used on the condensing surface to measure the condensate and the body wall interfacial temperatures. The remaining 7 were used to measure the cooling water and the body wall interfacial temperatures. Grooves of 0.0013m. deep, 0.001m. wide and 0.051m. long were run on both surfaces to house the thermocouples. Fig. 10(a) shows the distribution of the grooves and fig. 10(b) the details of a groove with a thermocouple in position.

The grooves were equi-spaced circumferentially but at different distances from the leading edge of the body. For identification purposes, the body was divided into two diametrically opposite halves, front and back. The letter F refers to the front while B refers to the back. The letter I refers to the inside. The 7 inside thermocouples were also equi-spaced but covered only one half of the circumference. They covered the front part of the body such that 1F and 1I had the same angular position when observed from the centre of curvature of the generator. The same was true for 2F and 2I and

so on. The grooves on the inside however, faced the opposite direction to those at the front outer surface. This was necessary in order to avoid two grooves (one inside and one outside) facing each other and hence reduce the thickness of the body wall considerably at that point.

From the theory, a knowledge was gained as to the general behaviour of the film of condensate. The angular positions of the grooves, with respect to the centre of curvature of the generator, were chosen such that enough information could be obtained where it was needed, namely, at the start of the film.

It can be observed in fig. 10(b) that, the thermocouples were bonded into place with the manufacturer's insulation still on the conductors except at the junctions. This provided a complete electrical insulation of the thermocouples against the generator body; and also the insulation of each conductor against the other so that the junctions could not be short circuited. The leads of the thermocouples were carried through 0.0014m. diameter holes to the inside of the body. All the leads were twisted together and bonded onto the inside wall to secure them against the cooling water spray tubes, fig. 7.

Before the thermocouples could be bonded onto the curved body, the grooves had to be prepared to receive the bonding cement. By the use of a broken hacksaw blade, the grooves were dovetailed at the base to offer a greater resistance to any centrifugal force acting to dislodge the cement from the grooves. A preparation of 1 part Ammonium Persulphate to 4 parts of water by weight was used to etch the grooves and the surrounding areas. The solution at $20^{o}C$ was applied. for 30 seconds and then washed off with clean cold water. The grooves were finally rinsed with distilled water and dried in air stream at $20^{o}C$.

The thermocouples were bonded onto the curved body as shown in fig. 10(b). The cement (Bostik 1160) was cured by drying for one hour at 27°C, followed by 20 minutes at 141°C. Surplus cement and the excess thermocouple junctions were removed after the curing. The surface of the curved body was rubbed down with different grades of wet and dry carborundum paper, down to the finest grade, to restore the contour of the curved body. The experimental body was then assembled as shown in fig. 8 before being dynamically balanced.

The base plate, the shaft flange and the driving pulley were attached to the main shaft, fig. 7, to make a sub-assembly of the rotating parts. This sub-assembly was dynamically balanced by the designers of the basic rig, Howe and Robson. The dynamic balancing mentioned above therefore applied to the experimental body only.

For balancing purposes only, the loose ends of the thermocouple leads were coiled and secured between the cover plate and the diaphragm. Existing special jigs were adapted to support the experimental body between the two bearings of the balancing machine. The balancing was carried out for speeds up to 1500 rev/min by British Electrical Repairs Ltd. of Killingworth. The balanced experimental body was finally rubbed down with a very fine wet and dry carborundum paper before being coupled to the balanced sub-assembly to form the complete assembly of the rotating parts.

4.3.4 The general instrumentation

The measurement of an analytically useful condensate flow rate was ruled out because under the experimental set up, such measurements would have required no condensation to take place on the cylindrical base of the experimental body and also no condensation by the pressure vessel. This was practically impossible. However, this was not an obstacle because the only measurements required for

the experimental analysis were those of the speed of rotation, the saturation temperature of the steam, the cooling water-body and condensate-body interfacial temperatures.

The steam pressure in the pressure vessel was measured with a Budenberg standard test guage. It had a range of 0 - 5 bar gauge in steps of 0.01 bar. The gauge was connected to the end of an extension pipe from the pressure vessel to help keep the gauge at the calibration temperature of 20°C.

The speed of rotation was measured with a hand tachometer applied to the end of the motor shaft. The high precision hand tachometer used, recorded an average value speed over a period of several seconds.

The temperature measurements were recorded with the same instruments and the same set up as described for the calibration. Although each of the instruments in the set up was highly accurate for the normal operations for which it was designed, the accuracy of the individual instrument was unimportant as long as it was consistent. The calibration of the thermocouples, and hence the instruments, eliminated any inaccuracy of the individual instrument.

The steam temperature inside the pressure vessel was measured with one stationary thermocouple and two rotating ones. The two rotating thermocouples were attached to the cover of the experimental body such that the hot junctions were about 0.025m. above the cover. This meant that the two rotating thermocouples measured the stagnation temperature. However, a simple calculation indicated that the contribution to the actual steam temperature, as a result of the rotation, was negligible. The leads of the two thermocouples were passed through the hollow shaft to the slip-ring units. As stated before, it was necessary to measure the steam temperature through the slip-ring units so that the effects of rotation on the slip-rings

could be determined.

Finally, no attempt was made to measure the dryness fraction of the steam and the concentration of non-condensable gases. Howe (71) had shown that if the operating procedure for the boiler was adhered to, dryness fraction of 0.96 to 0.99 and the concentration of non-condensables of less than 0.06 per cent were always achieved. Furthermore, if the pressure vessel was adequately vented during the starting procedure, the non-condensables did not attain significant levels during the test period of 30 minutes. These procedures were strictly adherred to.

4.4 Photography

The formation and drainage of the film of condensate on the condensing surface of the curved body was studied with the aid of still photographs taken through a window in the pressure vessel.

A large format (0.1016m. x 0.127m.) plate camera was used to take the still photographs. Illumination was provided by a Hadland 2μs flash unit which could provide a 50J flash every 30 seconds.

A special (0.1016m. x 0.127m.) POLAROID plate holder was adapted for use with the camera. This enabled instant photographs to be taken to determine the correct focus and exposure before photographs for the detail study were taken.

5.0 COMMISSIONING TESTS

6.0 TEST PROCEDURE

5.0 COMMISSIONING TESTS

Preliminary test runs were carried out after the apparatus had been assembled. The experimental body was rotated at 50 rev/min and steam was admitted into the pressure vessel at 1.5 bar absolute. The thermocouples were checked for functioning. The failure of a thermocouple to function correctly was usually the result of "dry joint" and this was immediately corrected. The cooling water flow rate was adjusted such that the cooling water-body interfacial termperatures were as uniform as possible. The running time was increased from 30 minutes to 2 hours over one week. The apparatus was checked for leaks and any form of failure during these runs. Apart from few leaks which were observed at the beginning of the tests, and which were put right immediately, the apparatus functioned as expected.

5.1 The production of filmwise condensation

Dropwise condensation was observed during the first week of tests. It was presumed that the condensing surface was contaminated and that the action of the steam would clean the surface after a few more runs. This however, did not happen. After 20 hours of running, the condensing surface was soaked with a solution of 5 percent LIQUINOX and 95 percent water by volume for a period of 24 hours. LIQUINOX is the trade name of a soap concentrate widely used for cleaning and degreasing commercially. Access to the condensing surface was gained by removing one of the 0.3m. diameter glass windows. The soaking did not have any significant effect and the dropwise condensation persisted.

Pitting of the cement bonding the thermocouples onto the condensing surface was observed. It was assumed at the time that the LIQUINOX had attacked the cement. The LIQUINOX was replaced with DECON 75, another detergent.

The pitted surface of the cement was repaired by applying more Bostik 1160 and curing as described before while the experimental body was still in the pressure vessel. The excess cement was removed after curing and the condensing surface cleaned with Grit 600 wet and dry paper and 5 percent solution of Decon 75 in distilled water.

Signs of a stable film of condensate were observed after 35 hours of running. It was also observed, that the area covered by the stable film of condensate increased when the steam pressure was increased to about 9.0 bar absolute and the test sustained at that pressure for at least one hour. The belief was that the comparatively high temperatures - associated with the higher pressures - coupled with the cleansing action of the steam, eliminated to some extent, the impurities in the casting which promoted the dropwise condensation. In addition, the high temperature steam favoured the formation of a stable film of oxide on the condensing surface which improved the wettability of the surface considerably.

Further pitting of the cement was observed. This disproved the assumption that the Liquinox had attacked the cement. The manufacturers attributed this failure of the cement to the strain at the cement-metal interface on the grooves and not to erosion by either the steam or the condensate. Re-cementing was carried out while the body remained in the pressure vessel. The excess cement was not removed however until after several hours of running and a stable film of condensate had been obtained for over 90 percent of the condensing surface. Subjecting the cement to the heating and the cooling in this way, had a pre-stressing effect on the cement and further pitting was not observed after the body had been finally cleaned.

Complete filmwise condensation was achieved after 50 hours of running. A run usually lasted between 2 and 3 hours. The condensing surface was gently rubbed down with a very fine wet and dry paper and 5 - 10 percent solution of Decon 75 in distilled water after each run.

5.2 Performance of slip-ring units

The smaller slip-ring unit, capable of carrying 6 thermocouples, was mounted on the bigger slip-ring unit and the assembly was then coupled to the hollow shaft (item 18). The drive for the slip-ring units was supplied by the hollow shaft through two "pin and flange" arrangement.

Friction between the silver graphite brushes and the silver rings of the slip-ring units generated heat when the units were rotated. Since copper-silver and constantan - silver connections were used at the input and output terminals of the slip-ring units, it followed from the "Law of Intermediate Metals" that a secondary e.m.f. would be induced as a consequence of the temperature difference across the corresponding input and output terminals resulting from the heating by friction.

To eliminate the secondary e.m.f., provision was made by the manufacturer of the slip-ring units to remove the heat generated by the friction. This comprised air cooling of the slip-ring units.

Compressed air from the laboratory air line was filtered and used for the cooling. The provision for the cooling on the small slip-ring unit was adequate and the test runs showed that the effect of rotation on the small slip-ring unit was negligible. Thus the comparison of the steam temperature as measured:

(i) directly, and

(ii) through the small slip-ring unit at varying speeds of rotation showed no significant difference.

The cooling on the bigger slip-ring unit however was inadequate. An appreciable secondary e.m.f. was observed. To improve the cooling, the outer casing of the unit was removed and the cleaned compressed air blown at the unit. This improved the circulation of the air but not enough to eliminate the secondary e.m.f. A maximum difference of $3.5^{o}C$ was recorded for a rotational speed of 1000 rev/min when the comparison of steam termperatures was made. It was observed that the effect of rotation on the bigger slip-ring unit was insignificant for speeds up to 200 rev/min. Thereafter, the effect was a function of the speed of rotation.

5.3 Performance of thermocouples

The consistency of the e.m.f. readings from the thermocouples on the curved body was checked several times. The check usually took place when the apparatus had been standing for several hours and had attained the ambient temperatures of the laboratory. The readings of e.m.f. were found to be consistent to within $\pm$ $0.1^{o}C$. This consistency was maintained even at rotational speeds of 1000 rev/min when the effects of rotation on the slip-ring units had been corrected for.

Of the 23 thermocouples that passed through the slip-ring units, two suffered damage. These were 1B and 5B (fig. 10(a)), both of which were on the condensing surface. The thermocouple 1B was damaged during the dynamic balancing operation. The thermocouple 5B was observed, during these tests, to read excessively higher than the rest. There was no explanation for this and the thermocouple 5B was rejected. The loss of these two thermocouples did not make any

serious difference to the experimental results since the remaining 12 thermocouples functioned as expected. In addition, both came from the same group (the "B" group) and this meant that the entire condensing surface was still covered by the thermocouples of the "F" group.

The failure of another two thermocouples occurred after 30 hours of operation. The cause of this failure was traced to be mechanical vibrations acting on the soldered contacts of the input into the slip-ring unit. Re-soldering restored the thermocouples. No further failures have since been observed.

6.0 TEST PROCEDURE

A standard test procedure evolved during the commissioning tests and this was followed throughout the experimental tests. The procedure is briefly outlined below.

6.1 Condensing surface preparation

Experience from the commissioning tests indicated that filmwise condensation on the entire condensing surface was possible if the surface was prepared immediately before a test.

The condensing surface was very gently rubbed down with a Gritt 600 wet and dry paper and a solution of Decon 75 in distilled water. The solution of 15 - 20 percent by volume of Decon 75 was much stronger than recommended by the manufacturers. of the detergent. After rubbing down, the surface was rinsed with distilled water while the wettability of the surface was critically examined. If the entire surface was wettable, the surface was finally rinsed with some of the solution before the glass window, which was removed to allow access to the body, was replaced. It was observed that if a break occurred in the film of condensate, the area occupied by the break increased with time. It was necessary therefore to obtain a film without a break at the start of a test. Rinsing the condensing surface with the solution maintained the wettability of the surface and promoted the film formation on the entire surface.

6.2 Starting procedure

The procedure adopted for starting the rig is outlined below. The sequence evolved as a consequence of the commissioning tests. It assumes that instruments such as the Digital voltmeter and the Zeref ice point reference which required at least 3 hours warming up have attained their working temperatures.

(i) The boiler was flashed to raise steam at 15 bar.

(ii) The experimental body cooling water stop and drain valves were opened.

(iii) The mechanical seal was pressurised to 2 bar above the intended operating pressure after starting the water pump. The flow of water was then adjusted to 0.5 m^3/h.

(iv) A supply of cooling air was delivered to the slip-ring units from the Aerox filter.

(v) The steam blow-off valve was opened.

(vi) Steam was admitted to the pressure vessel at a pressure slightly above 1.0 bar absolute, using the pressure reducing valve. The steam pressure was increased to 1.2 bar absolute.

(vii) Cooling water was supplied to the inner surface of the experimental body by opening the main valve at the distribution manifold.

(viii) The experimental body was rotated at 50 rev/min after the motor-control unit had been switched on.

(ix) The cooling water to the experimental body was adjusted such that the cooling water-body interfacial temperatures were as uniform as possible.

(x) Examination of the pressure chamber through one of the windows showed a misty atmosphere. The blow-off valve was closed when the mist cleared. This usually took 5 - 10 minutes.

(xi) The steam pressure in the pressure vessel was adjusted to the desired value.

(xii) The condensate so far produced was drained before the system was connected to the condenser.

(xiii) The rotational speed was gradually brought up to the required value.

(xiv) The thermocouple readings was constantly checked for the steady state running conditions.

(xv) The steam blow-off valve was opened for 30 seconds while observing the e.m.f. readings from the thermocouples to check for the presence of non-condensables.

(xvi) Five minutes was allowed after operation (xv) before readings were taken.

The starting and warming through procedure outlined above usually occupied 15 to 20 minutes. If the apparatus had been standing for more than 48 hours, this period was exceeded.

6.3 Test runs

A test run usually lasted 10 - 15 minutes. The parameters that constituted the test conditions were:

(a) steam pressure and temperature

(b) speed of rotation

(c) the temperature reading from the inner and outer surfaces of the curved body and from the pressure chamber.

For each pressure and speed setting, at least 3 complete results were taken. The average of the results was used for the experimental analysis. In practice it was found that the results were consistent once a steady state had been reached and the averaging of results proved largely unnecessary.

The condensing surface of the body was illuminated with stroboscopic light to check that the condensate remained filmwise. The test was abandoned if the areas supporting dropwise condensation occupied more than 5 percent of the condensing surface.

7.0 EXPERIMENTAL RESULTS

7.0 EXPERIMENTAL RESULTS

Over 300 results were recorded. These results were divided into two sets so that their repeatability could be checked. A further set of results was planned but as the first two sets were in close agreement, this was not considered necessary.

In this section, the results are analysed and compared with the theoretical predictions. A photographic study of the mode of drainage of the film of condensate is also presented. Finally, the end effects - the effects of bolt holes at the leading edge - on the heat transfer rate are discussed.

The experimental analysis is based on a thin wall theory. The justification for this is outlined in Appendix B.

In the theoretical analysis (section 3.2.1), both local and average heat transfer coefficients were considered. In this section, only local values are considered. It will be shown that the end effects influenced the experimental results, particularly at the leading edge, and the average heat transfer coefficients which required the numerical integration of the local values would have been grossly in error.

7.1 Mathematical analysis of the experimental results

Let the sketch below represent a working section of the experimental curved body.

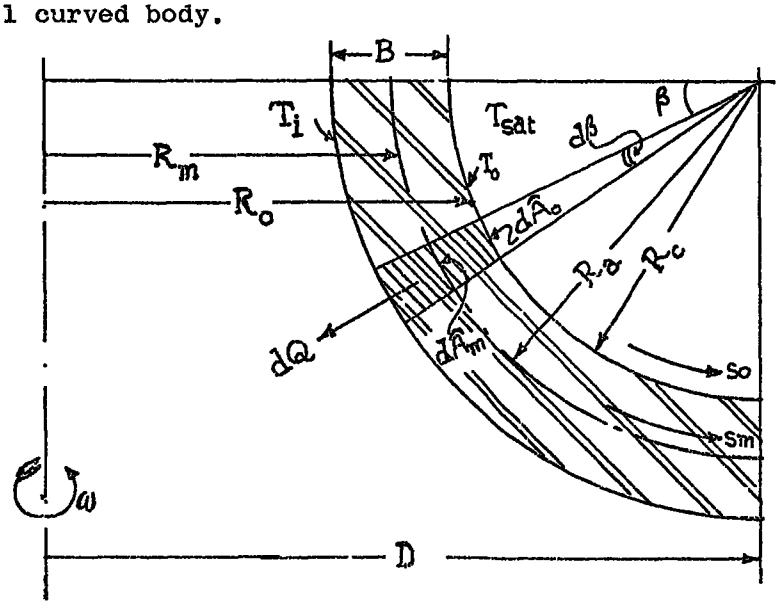

Consider the element of area $d\hat{A}_o$ at the outer face (condensing surface) and $d\hat{A}_m$ at the mean radius R_m. Let dQ be the energy crossing the boundaries per unit time and q the heat flux (energy transfer per unit area per unit time). The other symbols are as defined in the sketch or in the numenclature.

From the "thin-wall theory",

$$dQ = d\hat{A}_o \cdot q_o = d\hat{A}_m \cdot q_m = k_w \cdot d\hat{A}_m \cdot (T_o - T_1)/B \qquad (7.1.1)$$

Also $dQ = h \cdot d\hat{A}_o \cdot (T_{sat} - T_o) = h \cdot d\hat{A}_o \cdot \theta$ (7.1.2)

From equations (7.1.1) and (7.1.2)

$$h \cdot d\hat{A}_o \cdot \theta = k_w \cdot d\hat{A}_m \cdot \theta_w / B$$

and $$h = \frac{k_w}{B} \cdot \frac{\theta_w}{\theta} \cdot \frac{d\hat{A}_m}{d\hat{A}_o} \qquad (7.1.3)$$

From previous analysis (or appendix B),

$$\hat{A}_o = 2\pi \left[DR_c\beta - R_c^2 \operatorname{Sin} \beta\right] \qquad (7.1.4)$$

Similarly, $$\hat{A}_m = 2\pi \left[DR_a\beta - R_a^2 \operatorname{Sin} \beta\right] \qquad (7.1.5)$$

From (7.1.4) $$d\hat{A}_o/d\beta = 2\pi \left[DR_c - R_c^2 \operatorname{Cos} \beta\right] \qquad (7.1.6)$$

From (7.1.5) $$d\hat{A}_m/d\beta = 2\pi \left[DR_a - R_a^2 \operatorname{Cos} \beta\right] \qquad (7.1.7)$$

From (7.1.6) and (7.1.7),,

$$\frac{d\hat{A}_m}{d\hat{A}_o} = \frac{R_a (D - R_a \operatorname{Cos} \beta)}{R_c (D - R_c \operatorname{Cos} \beta)}$$

$$\frac{d\hat{A}_m}{d\hat{A}_o} = \frac{R_a R_m}{R_c R_o} \qquad (7.1.8)$$

Substituting equation (7.1.8) into (7.1.3)

$$h = \frac{k_w}{B} \cdot \frac{\theta_w}{\theta} \cdot \frac{R_a R_m}{R_c R_o} \qquad (7.1.9)$$

For the experimental curved body, B, R_c and R_a are constant and $R_a/BR_c = 59.957$. Hence the local heat transfer coefficient h, is given by:

$$h = 59.957\, k_w \cdot \frac{\theta_w}{\theta} \cdot \frac{R_m}{R_o} \qquad (7.1.9)$$

Multiplying both sides of equation (7.1.9) by $[\omega^{-\frac{1}{2}}A^{\frac{1}{4}}/k]$, equation (7.1.9) becomes:

$$h\left[\frac{\omega^{-\frac{1}{2}}A^{\frac{1}{4}}}{k}\right] = 59.957\, \frac{k_w}{k} \cdot \frac{\theta_w}{\theta} \cdot \frac{R_m}{R_o} \cdot \omega^{-\frac{1}{2}}A^{\frac{1}{4}} \qquad (7.1.10)$$

The comparison of equations (3.1.38a) and (7.1.10) show that the L.H.S. are identical. Thus the comparison of the R.H.S. of equations (7.1.10 and 3.1.38) is a direct comparison of the experimental results and the results predicted by the laminar theory.

Looking at the R.H.S. of equation (7.1.10), the unknowns are: k_w/k, θ_w/θ, R_m/R_o and $\omega^{-\frac{1}{2}}A^{\frac{1}{4}}$. The thermal conductivity of the body material k_w, was experimentally determined. The procedure is outlined in Appendix A. The thermal conductivity of the material was expressed by the equation,

$$k_w = 190.4\left[\frac{T_w + 273}{T_w + 776.6}\right] + 7.5\ \frac{W}{mK}$$

where $T_w = (T_o + T_i)/2$, the arithmetic mean temperature of the body walls.

The thermal conductivity and the other properties of the condensate were determined from the "U.K. Steam Tables in S.I. Units 1970" published by Edward Arnold. The ratio of thermal conductivities k_w/k was thus determined.

The ratio of the temperature differences was determined from the experimental measurements. Fig. 11 shows typical temperature distributions at the condensate-wall interface and wall-cooling water interface from which the ratio of temperature differences was determined.

The ratio of the radii R_m/R_a was determined from the geometry

of the body and the speed of rotation ω, was measured experimentally. The constant A, was determined from the fluid properties of the condensate once the Drew reference temperature $T = T_{sat} - 0.75\theta$ was known. The Drew reference temperature was determined from the experimental temperature distribution. The R.H.S. of equation (7.1.10) was thus completely determined.

From equation (7.1.10), the experimental local Nusselt number was obtained in the form

$$Nu_s = \frac{hs}{k} = 59.957 \frac{k_w}{k} \cdot \frac{\theta_w}{\theta} \cdot \frac{R_m}{R_o} \cdot s \qquad (7.1.11)$$

or $$Nu_s[\omega^{-\frac{1}{2}}A^{\frac{1}{4}}] = 59.957 \frac{k_w}{k} \cdot \frac{\theta_w}{\theta} \cdot \frac{R_m}{R_o} \cdot \omega^{-\frac{1}{2}}A^{\frac{1}{4}} \cdot S \qquad (7.1.11a)$$

The reader may compare equations (7.1.11a) and (3.1.39a).

7.1.1 Computer programme for experimental analysis.

A computer programme was developed to carry out the experimental analysis. The programme provided solutions for equations (7.1.9), (7.1.10), (7.1.11), (7.1.11a), (3.1.38), (3.1.38a), (3.1.39) and (3.1.39a). The fluid properties of the condensate, namely thermal conductivity, kinematic viscosity, specific heat at constant pressure and Prandtl number, together with the specific enthalpy of condensation and their corresponding temperatures were stored in the computer. Each fluid property was evaluated by a separate sub-programme for a given temperature. A quadratic interpolation procedure, employing the Aitken-Neville interpolation subroutine, was employed in the evaluations. Each sub-programme was checked for the accurate reproduction of the stored data before being incorporated in the main programme.

Experimental data of the temperature distributions and their corresponding positions on the body were similarly stored before use.

From the other input to the computer, namely pressure, speed of rotation and saturation temperature, the programme first evaluated the Drew reference temperature before proceeding to evaluate the fluid properties. The arithmetic mean temperature of the body wall, T_w, was evaluated and the thermal conductivity of the wall material determined. The solutions of the above equations were then carried out.

7.2 Typical temperature distribution

It could be observed from equation (7.1.10) that the accuracy and reliability of the experimental results depend on the accurate measurement of the thermal conductivity of the body material and the ratio of the temperature differences.

Fig. 11 shows a typical temperature distribution for both the outside and inside faces of the curved body. They represent the condensate-wall and wall-cooling water interfacial temperatures. The results represent the two extreme cases of pressure considered, and also rotational speeds of 50 and 1000 rev/min. With the exception of the results for no rotation, any other result presented here lies within these bands of extremities.

It can be observed from Fig. 11 that no information was obtained at the leading edge. The thermocouple 1B (Section 5.3), which should have provided the information was damaged during the dynamic balancing.

However, it is not difficult to observe that on the condensate side, the interfacial temperature was highest at the leading edge, and gradually decreased away from the leading edge. For rotational speeds of 100 rev/min and over, the pattern of distribution was similar. The temperature decreased for about 0.05m. of the distance from the leading edge and then remained constant. For speeds 50 rev/min and below, the temperature rapidly decreased for the first quarter of the distance from the leading edge and then more gradually for the rest of the working distance. It can be said therefore that at low speeds of rotation, axial conduction existed along the entire working length, and along the first 0.05m. at higher speeds of rotation.

The above behaviour can be explained by the fact that the water spray and collector unit - fig. 7 (item 8) - did not rotate with the experimental body. The effect of the higher speeds of rotation of the body was equivalent to increased flow rate and better distribution of the cooling water. The existence of the temperature gradient promoting the axial conduction, before and after the first 0.05m. of the working length, can be attributed to the inadequate supply and distribution of the cooling water.

A comparison of the temperature gradients, 0.05m. after the leading edge, for 50 rev/min at 6.0 bar and 1.5 bar indicate that the temperature gradient at 6.0 bar is 3 times greater than that at 1.5 bar. This confirms the assertion that inadequate cooling promoted the axial conduction because, a greater amount of energy had to be transferred at 6.0 bar than at 1.5 bar and the inability to do so resulted in the greater axial conduction rate.

The corresponding inner surface temperatures on the other hand were approximately constant. It was observed however, that for rotational speeds 500 rev/min and over, the cooling water-wall interfacial temperature increased with distance from the leading edge. The increase in temperature continued for the first 0.04m. of the working length and remained constant. This suggested some interference in the energy transfer process at the leading edge. It will be shown later that this was due to the end effects.

The assumption of one dimensional flow of energy in both the theoretical and experimental analysis is still justified although it is not exactly true. Consider the temperature distribution for the 50 rev/min at 6.0 bar, which is the worst case. If the first 0.05m. from the leading edge is neglected for this analysis, then as the film thickness is of the order of 5×10^{-5} m., it will be appreciated from fig. 11 that $dT/dy >> dT/ds$. The overall effect however is a slight under-estimation of the heat flux in the Y-direction.

7.3 Comparison of experimental and theoretical results

The aim of the experimental work was to test the theory outlined in section 3. The discussion which follows compares the theoretical and experimental results and points out where any discrepancies occur and the possible cause of the discrepancies.

Fig. 12(a-g) show the solution of equation (7.1.10) compared with the solution of equation (3.1.38a). It should be remembered that the solution of equation (3.1.38a) was obtained purely from the geometry of the body while that of equation (7.1.10) was obtained from the experimental measurements. Hence the solution of equation (7.1.10) is referred to as "EXPERIMENTAL" in the above presentations. The theoretical solution without curvature term is also included for comparison. However, unless otherwise stated, the words "theory" or

"theoretical" will imply the solution with the curvature term included in this section.

The presentation covers the range 1.5 to 6.0 bar absolute and 50 to 1000 rev/min. The experimental results show a considerable deviation from the mean at 50 and 100 rev/min and again at 500 and 1000 rev/min. The worst case of the deviation occurred at 50 rev/min and 1000 rev/min. At 50 rev/min, the deviation is $\pm$5 per cent of the mean. At 1000 rev/min the deviation is $\pm$ 6.7 per cent of the mean if the results up to 0.05m. from the loading edge are neglected. Some degree of deviation from the mean was expected particularly at rotational speeds below 100 rev/min due to the inadequate and poor distribution of the cooling water. The deviation at higher speeds of rotation was not expected. However, it can be observed from Fig. 11 that at 1000 rev/min, the temperature difference across the film of condensate was 7^{o} - 9^{o}C. Thus a deviation of $\pm$ 1^{o}C from the true value could result in a deviation up to $\pm$ 14.2 per cent, which is far in excess of the maximum deviation of $\pm$ 6.7 per cent measured. As the results outlined by Fig. 12 (a-g) represent 300 individual results recorded over a period of 6 weeks, the author can claim the repeatability of the overall results to within $\pm$ 7 per cent.

The comparison of the overall experimental results and the theoretical results show a remarkable agreement particularly at high rotational speeds. Fig. 12(g) shows the comparison at 1000 rev/min. Here it can be observed that for the first 0.05m. from the leading edge, the experimental results deviate considerably from the predicted results. Thereafter, the remarkable agreement cannot be over-stressed.

Fig. 12 (a-g) show the variation of local heat transfer coefficient with distance along the surface of the curved body at the indicated rotational speed. The increase in the local heat transfer coefficient at the leading edge was believed to be the consequence of the detachment

of drops as predicted by Howe (71). Examination of all the results showed that higher local heat transfer coefficients were obtained at the leading edge even at speeds where the detachment of drops was not possible. It was concluded that the end effects were responsible for the behaviour. This was later shown to be the case (section 7.5).

It is noticeable in fig. 12 (a-g) that the degree of agreement between the theoretical and experimental results diminish as the speed of rotation is decreased. In addition, the degree of agreement vary with distance along the surface for a given rotational speed. However, a pattern of behaviour can be established if the analysis is confined to a fixed point along the surface of the generator. The author has chosen to examine the pattern of behaviour at a point 0.130m. from the leading edge. This point is chosen because it can be assumed to be free of the end effects.

Fig..15 curve (A) shows the percentage deviation of the experimental (non-dimensional heat transfer coefficient) results from the laminar theory. It shows how the experimental results deviate from the theory with speed. It shows also that in all cases considered, the laminar theory under-estimated the heat transfer coefficient. At 50 rev/min, the theory under-estimated the local heat transfer coefficient by 42 per cent and 5.5 per cent at 1000 rev/min. Curve (B) shows the comparison when curvature is neglected. The comparison shows that the solution without the curvature term under-estimated the local heat transfer coefficient by 58 per cent at 1000 rev/min compared with 5.5 per cent when curvature was included.

Fig. 13 (a-h) represent the solutions of equations (3.1.38) and (7.1.9), and show the comparison between the actual experimental and theoretical local heat transfer coefficients. These results are different from those of fig. 12 (a-g) in the sense that they are actual values $W/m^2\ ^oC$, and that local values of the experimental temperature distribution were used to evaluate the theoretical as well as the experimental results. Thus, the theoretical values shown in fig. 13 (a-h) take into account the axial conduction which was neglected in the previous case. The agreement here is even better and both theoretical and experimental curves show similar profiles. Fig. 15 curve (c) shows that the percentage deviation of experimental results from the laminar theory is 39 per cent at 50 rev/min and 5.5 per cent at 1000 rev/min.

The comparison of curve (A) and curve (B) indicate that the assumption of no axial conduction was justified because at 50 rev/min where the effect was considered very high, the difference between the two results is only 3 per cent. This difference reduced to zero at 800 rev/min.

Fig. 13 shows the theoretical heat transfer coefficient for the indicated rotational speeds. These curves are extracted from Fig. 13 (a-h) and allow the comparison of the heat transfer coefficients at the various speeds. Fig. 13 shows that the heat transfer coefficient is a function of the rotational speed as well as distance from the leading edge. It shows that the heat transfer coefficient increases with the speed of rotation and that there is a unique curve for each rotational speed. For speeds of 100 rev/min and below, the heat transfer coefficient is larger at the starting point of condensation and decreases with distance s. At 150 rev/min, the decrease continues

until 0.08m. from the leading edge and then remain constant. For the higher speeds of rotation, the decrease continues to about 0.05m. and then increase very gradually again. This form of behaviour is characteristic of the growth of the film as predicted theoretically.

Fig. 14 (a-h) show the comparison between the theoretical and experimental local Nusselt numbers. They represent the solutions of equations (3.1.39) and (7.1.11). Fig. 14 shows the theoretical Nusselt number against distance for the various rotational speeds. It can be observed here that the energy transfer rate near the leading edge was comparatively low. The axial conduction and poor cooling rate at the leading edge tended to increase the wall temperature and thereby reduced the Nusselt number. For the zero rotational speed, the energy transfer rate increased with the distance s, from the leading edge to a maximum value and then rapidly decreased. This is in agreement with the predicted film growth which showed that the curvature effect assisted the growth of the film at low rotational speeds. Thus as the film thickness increases rapidly at the disc end of the generator, the resistance to the energy flow increases and the energy transfer rate consequently decreases.

The general trend of the comparison between experimental and theoretical results shows that the laminar theory under-estimates the heat transfer coefficients. This implies that the experimental film thickness was less than predicted by the laminar theory. As it was not possible to measure the experimental film thickness, this could not be proved. Fig. 15 curve (c) shows that the deviation is 44 per cent at zero rotational speed while it is only 5.5 per cent at 1000 rev/min. Before any explanation is attempted, the attention of the reader will be drawn to the photographs plate (1-8). The photographs which show the behaviour of the film of condensate at 5.0 bar and rotational speeds of 0.0 to 1000 rev/min are discussed in detail in section 7.4.

The reader should observe the roll-waves on plate (1-5) which represent the rotational speed range of 0.0 to 200 rev/min. On plate 6, which shows the behaviour of the film of condensate at 300 rev/min, the roll waves could be observed to disappear and give way to ridges. On plate (7-8), which represent rotational speeds of 500 and 1000 rev/min, the roll-waves have given way to the ridges. The ridges can be observed to be thicker at 500 rev/min than at 1000 rev/min.

Kapitza (24) has shown that the heat transfer in a fluid under undulatory conditions differs from that under laminar ones. He showed analytically that if no turbulent heat transfer is assumed, then the heat transfer under the undulatory conditions will be under-estimated by 21 per cent by the laminar theory. Leonard and Estrin (25) and Frisk and Davis (81) have published work on heat transfer through wavy films and have shown that waves enhance the heat transfer rate. Leonard and Estrin (25) found that the wave shape significantly influenced the heat transfer rate, and that for low Reynolds numbers where wave amplitudes were small, predictions corresponded to the Nusselt smooth laminar film model. Frisk and Davis (81) carried out an experimental investigation into the enhancement of heat transfer by waves. They studied four regimes of flow:

(i) smooth liquid film flow

(ii) two-dimensional wavy flow

(iii) three-dimensional wavy flow

(iv) roll-wave flow.

Their findings show that roll-waves appear to be quite turbulent and that three-dimensional and roll-waves can increase the Nusselt numbers by more than 100 per cent compared with smooth film flow. Of the four cases studied, roll-waves produced the highest enhancement effect.

In the theoretical analysis (section 3), the Nusselt smooth laminar

film model was assumed. The photographic evidence of the behaviour of the film of condensate shows that the laminar model was not achieved. Between zero and 300 rev/min where the roll-waves persisted, the heat transfer coefficient was under-estimated by between 44 per cent and 20 per cent as indicated by curve (c) of fig. 15. This value of 20 to 44 per cent agrees with the findings of Kapitza (24) and Frisk and Davis (81). The fact that the greatest deviation from the laminar theory occurred at the zero rotational speed is not surprising since from the above photographs and the temperature distributions curves it could be recognised that the film was thickest at zero rotational speed. The thicker the film the greater the deviation from the laminar model and the greater the turbulent effects associated with the roll-waves which enhance the heat transfer.

At speeds above 300 rev/min, the roll-waves were observed to give way to ridges. From the photographic observations and the temperature distribution curves, it can be observed that not only had the roll-waves disappeared and given way to the ridges, but also the film thickness was decreasing with the higher rotational speeds. Between 300 and 1000 rev/min, the laminar theory under-estimated the heat transfer coefficient by between 20 per cent and 5.5 per cent. It can be said that as the roll-waves disappeared and the film became thinner with increasing speed, conditions approximated more to the laminar state and a better agreement between laminar theory and experimental results was possible.

The comparison of plate (7) and plate (8) which are of the same scale shows that the amplitude of the ridges at 500 rev/min were greater than those at 1000 rev/min. At 1000 rev/min, the amplitudes are relatively small and the film could approximate to a smooth one. From the findings of Leonard and Estrin (25), the under-estimation of the heat transfer coefficient by only 5.5 per cent should not be surprising.

In section (2.5.3), it was reported that Howe (71) measured heat transfer coefficients of 1.2 to 1.9 times the value predicted by the laminar model. Both theoretical and experimental evidence, including photographic studies, show that Howe dealt with comparatively thicker films of condensate than the author. Thus, the measurement of heat transfer coefficients of 1.2 to 1.9 times the laminar value by Howe, and 1.055 to 1.44 times the laminar value as reported here, goes to confirm what has been said so far, namely that roll-waves enhance heat tranfer and that the degree of enhancement depends on the thickness of the film.

It can therefore be concluded that the experimental results have confirmed the theoretical predictions and that the under-estimation of the heat transfer coefficient of up to 44 per cent by the laminar theory was to be expected. The comparison of curves (A) and (B) of fig. 15 confirm the theoretical findings, that for the condensation on a rotating body the curvature term is important.

7.3.1 Heat transfer coefficient

The main aim in this section is to provide an equation for the experimental results after the comparison with the theory. It has been explained however, that the theory is in very good agreement with the experimental results. It is therefore unnecessary to provide new equations. The designer whose interest lies in the heat transfer coefficient should use the laminar theory in conjunction with a correction factor. The "laminar equations" such as equation (3.1.38a) can be used in the form:

$$h\left[\frac{\omega^{-\frac{1}{2}}A^{\frac{1}{4}}}{k}\right] = M \cdot \frac{1}{\eta} \qquad (7.3.1)$$

where M is a correction factor. For the curved body used in THIS work, M is given by curve (c) of fig. 15.

The error in such an analysis is governed by the errors associated with the experimental determination of the heat transfer coefficient h, given by equation (7.1.9)

$$h = \frac{k_w}{B} \cdot \frac{\theta_w}{\theta} \cdot \frac{R_m R_a}{R_o R_c} \qquad (7.1.9)$$

From the measurements made of the experimental curved body after manufacture, it was established that all the dimensions were within $\pm$ 5 x 10^{-5}m. For such high accuracies, the errors associated with the geometric part of equation (7.1.9) can be neglected.

By differentiating equation (7.1.9) and taking the modulus of the errors,

$$\frac{\Delta h}{h} = \frac{\Delta k_w}{k_w} + \frac{\Delta \theta_w}{\theta_w} + \frac{\Delta \theta}{\theta}$$

From appendix A, $\Delta k_w / k_w = \pm 0.03$

As stated before, the thermocouples were calibrated such that temperature differences of 0.05°C could be detected. For this analysis however, it will be assumed that the temperatures could be read to $\pm$ 0.1°C. From fig. 11, the minimum temperature difference across the film occurred at 1000 rev/min and 1.5 bar. For the temperature difference of $\theta = 7^{\circ}$, $\Delta\theta/\theta = \pm 0.029$

Similarly, $\Delta\theta_w/\theta_w = \pm 0{,}004$

Hence $\Delta h/h = \pm$ 6.3 per cent.

Thus, there is a possible inherent error of 6.3 per cent associated with the heat transfer coefficient measurements. It will be pointed out that the drawing of a graph reduces the effects of random errors in individual readings but not consistent systematic error such as above. This method of analysis gives very pessimistic assessments of the experimental errors.

If both sides of equation (7.1.9) are multiplied by $[\omega^{-\frac{1}{2}}A^{\frac{1}{4}}/k]$, then as A contains θ, the error will increase.

From above, $\Delta\theta/4\theta = \pm 0.007$

The hand tachometer could be read to 0.2 per cent. Hence $2\Delta\omega/\omega = \pm 0.004$

Thus in the expression,

$$h\left[\frac{\omega^{-\frac{1}{2}}A^{\frac{1}{4}}}{k}\right] = 59.957 \frac{k_w}{k} \cdot \frac{\theta_w}{\theta} \cdot \frac{R_m}{R_o} \cdot \omega^{-\frac{1}{2}}A^{\frac{1}{4}} \qquad (7.1.10)$$

there is a possible inherent error of 7.4 per cent. The designer can use equation (7.3.1) in the light of this pessimistic error assessment.

7.4 Photographic study

The photographic study was carried out with two main objectives:

(i) to study the behaviour of the condensate.

(ii) to observe the mode of drainage of the condensate.

The photographs, plate (1-8), show in full size the behaviour of the film of condensate as it drained along the condensing surface at the indicated rotational speed.

All the photographs were taken under the same conditions and at a pressure of 5.0 bar absolute. To avoid the misting of the glass window through which the photographs were taken, and hence avoid the blurring of the photographs, the steam pressure inside the pressure vessel was raised above 5.0 bar absolute, sustained for about 5 minutes, before being reduced to the 5.0 bar absolute. This procedure was repeated for all the photographs.

It must be pointed out that no attempt was made, when these photographs were taken, to prepare the condensing surface so as to achieve a complete filmwise condensation as the test procedure indicates. The belief was that the breaks in the film of condensate would give detail to the photographs. Plate 3 offers a good example of this. Even under this adverse conditions, the total area occupied by dropwise condensation is less than 1.1 per cent of the entire condensing surface area.

On plates (1-6), patterns of roll-waves are visible on the film over the lower two-thirds of the working surface. On plates (1-2), which represent zero and 50 rev/min it can be observed that the waves do not have a regular pattern and no meaningful measurements could be made of them. Plates (3-5) reveal a lot more information and it can be observed from these photographs that the main waves appear to be preceded by up to six smaller ripples. The separation of the main waves is irregular but have an approximate wave length of 0.010m. to 0.020m. For rotational speeds below 100 rev/min, the photographs indicate that the drainage of the film of condensate was along the path of the generator. For rotational speeds above 100 rev/min, the drainage path changed and became inclined to the path of the generator. Measurements of the inclinations indicate that they do not follow a definite pattern. At 100 rev/min, the inclination was 7^{o} while at 150 and 200 rev/min, it was 18^{o}. At 300 rev/min (plate 6), where the roll-waves were giving way to the ridges, the angle of inclination was 11^{o}. This angle of inclination was maintained at 500 and 1000 rev/min. Plate (7-8) show that at 500 and 1000 rev/min the roll-waves have given way completely to the ridges. At 1000 rev/min, the amplitude of the ridges are comparatively smaller and it can be observed that the ridges become slightly irregular in shape and tend to join up with neighbouring ridges. The comparison of the break in the film of condensate at 100 rev/min (plate 3) and at 1000 rev/min (plate 8), gives some idea of the relative thicknesses of the film. The distance between ridges was also irregular and vary between 0.002m. and 0.003m.

It is interesting to note that these observations are in agreement with those of Howe (71), Robson (75) and Holgate (76). In addition to the similar observations as above, Howe (71) observed the formation and the detachment of drops from his 10^{o} and 20^{o} cones. Howe did not however, observe any drop detachment on his 60^{o} cone. Howe related his observations of the drop detachment to the ratio of centrifugal to gravitational accelerations and predicted that drop detachment should occur at the shaft end of a body with a curved generator, as reported in section (2.5.4).

The photographic study so far has not indicated the detachment of drops. Plate 9 shows the experimental body rotating at 100 rev/min. The film of condensate with its associated roll-waves can be seen to drain along the generator and down the cylindrical base. There was no detachment of drops oven where the film had broken and given way to the dropwise condensation. Plate 10 shows the body rotating at 150 rev/min. The film of condensate could be seen to drain along the generator still but drops had began to be thrown off the disc end. A careful examination also shows that drops were beginning to be detached from the cylindrical base. Plate 11 shows the body rotating at 1000 rev/min. Here again the detachment of drops was confined to the disc end and the cylindrical base. It is evidently clear that the drainage of the condensate was along the generator, and that the growth of the film was not influenced by the detachment of drops at any point on the body or at any rotational speed. The above evidence did not only take away the substance from Howe's (71) prediction, but also dostroyed the idea that the high heat transfer coefficients observed at the leading edge could be the effects of the detachment of drops at the leading edge.

While the above findings confirmed the belief that the end effects were responsible for the high heat transfer coefficients at the leading edge, it also called for an explanation of the behaviour. For such an explanation, a careful re-examination of the question of drop detachment and of Howe's criterion were necessary.

Howe's (71) predictions were based purely on the ratio of centrifugal to gravitational accelerations and did not involve the film thickness. A careful study of the problem indicated that the criterion to predict the onset of the detachment of drops should not only involve the ratio of the centrifugal to gravitational accelerations but must also be a function of the film thickness. The use of the non-dimensional film thickness η, whose solution involves the ratio of centrifugal to gravitational accelerations as well as the geometry of the condensing surfaces, for such a criterion was considered one step better and more satisfactory.

Fig. 16 shows the solution of equation (3.1.35) in the form of equation (3.1.37) for the 10^{o} and 20^{o} cones used by Howe and later by Smith (77). It also shows the limiting values of η for the 10^{o}, 20^{o}, 25^{o} and 60^{o} cones and the limiting value for the experimental curved body. The limiting case for a given body is of course the asymptote to which the film of condensate grows. For cones the asymptote is given by $\eta^{4} = 1/(2\ \mathrm{Sin}^{2}\ \alpha)$. The position along the surface of the generator of a given body at which the growing film is close to the asymptote is a function of the rotational speed. In fig. 16, the film at 800 rev/min on the 10^{o} cone will almost reach the asymptote before the one at 600 rev/min. If it is assumed that some minimum force is required to overcome molecular and surface

tension forces before the detachment of drops is possible, then the onset of the detachment of drops will vary with rotational speed and the distance from the leading edge. Thus, experimental evidence of the detachment of drops from a body or bodies at different speeds should enable a criterion to be established. The experimental evidence of drop detachment obtained from Howe (71) and Smith (77) and presented on fig. 16, point to $\eta = 1.8$ as the critical value. Thus η should be equal to or greater than 1.8 for the onset of drop detachment.

In terms of cones, $\eta = 1.8$ represent the limiting case for the 25^{o} cone. This is in a remarkable agreement with the findings of Gerstmann and Griffith (38) whose work on the stationary inclined plate showed that drop detachment from the underside of an inclined plate ceased when the angle of inclination was greater than 13^{o} (i.e. 26^{o}cone), and all the condensate ran off the end of the test surface. Thus, there is a strong independent experimental evidence to support the assertion, that drops are detached when η is equal to or greater than 1.8.

From fig. 16, it can be observed that as the limiting case value for a 60^{o} cone is $\eta = 1.19$, and that for the experimental curved body is less than unity and decreasing, the formation and the detachment of drops from the 60^{o} cone and the experimental curved body could not be expected. Howe's (71) observations of the 60^{o} cone and the experimental evidence presented by the author confirms this.

Finally, it is shown in appendix C that $\eta^{4} = 4\omega^{2}s/3g$ for a rotating cylinder, and $\eta \sim \omega^{\frac{1}{2}} s^{\frac{1}{4}}$. The value of η will be governed by ω and s. If ω is small, s will have to be large to yield $\eta = 1.8$ and vice versa. For a cylinder, the limiting value of $\eta = \infty$, i.e. the film will grow to an infinite thickness. It can be appreciated that drop detachment is inevitable on a rotating cylinder

but how far down the cylinder it occurs is governed by the speed of rotation.

7.5 End effects

It became apparent after the photographic study that the higher heat transfer coefficient obtained at the leading edge was the result of the end effects.

Fig. 9 shows that the cover of the experimental body was bolted onto the curved body. The cover was located in place by two dowels 0.013m. diameter and then bolted down with ten 5/16" B.S.F. bolts. The tapped holes on the curved body to receive the above bolts had a minimum threaded depth of 0.013m. To achieve this, the manufacturer drilled to a depth of about 0.030m. before tapping to the right depth. As the bolts could not travel the full length of the holes when the body was assembled, air was trapped inside these holes. The first 0.030m. from the leading edge of the curved body was therefore not homogenous and behaved differently from the rest of the body. It behaved similarly to a very porous casting with the effective thermal conductivity considerably reduced. The experimental analysis used the expression for the thermal conductivity obtained for the homogenous body and this was bound to introduce errors in the solution at the leading edge.

To confirm the above assertion experimentally, the ten bolts were removed while the experimental curved body was still in place inside the pressure vessel, and the excess holes filled with lead pellets. Fig. 17 shows the comparison of results at 200 rev/min and 1000 rev/min of the cases with and without the lead pellets. As shown in fig. 17, improvements in the condensate-wall interfacial temperatures of 1.5^{o}C to 2^{o}C were observed at the leading edge.

This confirmed what was expected. The decrease in the thermal conductivity of the body material at the leading edge meant a greater resistance to the energy flow at the leading edge. The effect of this was that the condensate-wall interfacial temperature increased at the leading edge. At 1000 rev/min, the cooling water flow rate, as far as the curved body was concerned, was at the maximum and the distribution was better, hence the drop in the cooling water-wall interfacial temperature at the leading edge indicate that a comparatively lower energy was crossing the boundary at the leading edge.

Apart from the reduced thermal conductivity of the body material at the leading edge, there was the question of axial conduction by the bolts. This would have the effect of raising the wall temperature at the leading edge and producing similar effects.

The complete eradication of the end effects would have been difficult in a case like this, though its magnitude could have been reduced. Nevertheless, the overall effect is small.

8.0 CONCLUSIONS

8.0 CONCLUSIONS

The following is a summary of the main points of this report.

The condensation of a vapour onto a general curved body rotating with the axis of symmetry vertical was analysed. The theory developed for the process used the laminar film model. Many other assumptions were made and these are listed in section 3. The theory assumed that the film drainage was along the surface of the generator under the influence of both gravitational and centrifugal accelerations resolved along the surface.

The general equation (3.1.21), which governed the rate of growth of the condensate film, was developed and analysed. The analysis showed that the equation represented a more general case than those derived by Nusselt (9), Sparrow and Gregg (55), Sparrow and Hartnett(69) and Howe (71), all of whose results could be obtained as special examples of the general result. Above all, the analysis outlines the importance of the curvature term when dealing with the condensation on rotating bodies. It was shown that the curvature effect assisted the growth of the film at low rotational speeds but the reverse was the case at higher speeds.

Equation (3.1.21) was non-dimensionalised and solved to yield

$$\eta^4 = \frac{4}{3} \frac{\int_0^{\xi} \mathcal{F} F^{1/3} \, d\xi}{F^{4/3}} \qquad (3.1.35)$$

which applies to any axisymmetric body and requires only one itegration for any given case. Equation (3.1.35) was applied to the experimental curved body by:

(i) considering the generator as a smooth continous curve

(ii) considering the generator as made up of 450 truncated cones.

The results showed that the analysis without the curvature term could over-estimate the film thickness by up to 71 per cent. This was reflected in the local heat transfer coefficient. It was shown that without the curvature term, the local heat transfer coefficient could be under-estimated by 43 per cent for speeds of 3000 rev/min and over. The effect on the average heat transfer coefficient was slightly less at 37.5 per cent. The theoretical heat transfer coefficient was expressed in the form:

$$h\left[\frac{\omega^{-\frac{1}{2}}A^{\frac{1}{4}}}{k}\right] = \frac{1}{\eta} \qquad (3.1.38a)$$

and the Nusselt number based on distance as: $Nu_s\,[\omega^{-\frac{1}{2}}A^{\frac{1}{4}}] = s/\eta$ (3.1.39a)

The experimental results have shown that some of the assumptions made were far from expected. Due to unsatisfactory cooling at rotational speeds below 100 rev/min, axial conduction could not be avoided. In addition, due to the inhomogeneity of the body material at the leading edge, and also the use of bolts to secure the cover plate to the curved body, axial conduction at the leading edge was inevitable at all speeds of rotation. The assumption of no axial conduction could not fully be realized.

The photographic evidence has shown that the assumption of plane laminar flow along the generator was never found during the experiments. The flow was dominated by roll-waves and ridges. The comparison of the theoretical and the experimental results have shown that the laminar theory under-estimated the heat transfer coefficients in all the tests carried out. It was explained that this was to be expected because roll-waves have been shown by Kapitza (24), Frisk and Davis (81) and Leonard and Estrin (25) to enhance heat transfer. It became clear from the discussion that there is no definite rule governing the degree

of enhancement. Kapitza (24) predicted 21 per cent while Frisk and Davis (81) observed over 100 per cent increases in the heat transfer rate. Howe (71) also observed 20 to 90 per cent increases in heat transfer rate on his cones and the author 20 to 44 per cent in the roll-waves region but 5.5 to 44 per cent over the entire range covered by the experiment. It is the author's belief that the degree of enhancement is linked to the turbulence associated with the roll-waves and will therefore be a function of the film thickness. This is something that could be looked into in the future.

Despite the fact that the assumptions about the laminar model and axial conduction were not fully realized, the comparison of the theoretical and experimental curves leave one in no doubt that the agreement between the theory and the experimental work is good. The author therefore strongly recommends the theoretical predictions presented in this report for the analysis of the condensation on rotating bodies. It should however be borne in mind that because of surface waves and the departure from the simple laminar flow, the theory will always under-estimate the heat transfer coefficient. The degree of the under-estimation will depend on the film thickness and hence the geometry and the speed of rotation. The knowledge available at the moment makes it difficult to lay down any rules that will correct for the deviations. The experimentalist is advised to determine the order and the magnitude of the deviation for a given case. The theoretical predictions presented here should offer the basis or platform from which to work.

For the experimental curved body studied here, the local heat transfer coefficient is expressed by:

$$h\left[\frac{\omega^{-\frac{1}{2}}A^{\frac{1}{4}}}{k}\right] = M \cdot \frac{1}{\eta} \qquad (7.3.1)$$

where M is a correction factor and has no dimensions or units. M has the value of 1.055 to 1.440 for the above case depending on the rotational speed, and it is obtained from curve (c) of fig. 15. The fluid properties of the condensate in the constant A namely, ν, C, k and Pr, are evaluated at the Drew reference temperature of $T = T_{sat} - 0.75\theta$, and the enthalpy of condensation h_{fg} at the saturation temperature T_{sat}.

It should be clear that the task of the experimentalist is simply to determine the correct value of M for a given case in order to use the theoretical relationships presented here. Where this cannot be done, the M. values presented here should offer a guide line.

The assumption of film drainage along the generator, together with the rest of the assumptions were justified. The photographic evidence has shown that contrary to Howe's (71) predictions, drop detachment was not observed and that the drainage was along the generator. In the light of the experimental evidence, the criterion for the onset of the detachment of drops were re-appraised. A new criterion based on the non-dimensional condensate film thickness has been proposed. The criterion states that the non-dimensional condensate film thickness η, must be equal to or greater than 1.8 for the detachment of drops to be possible. The criterion is based on the experimental evidence of Howe (71), Smith (77), Gerstmann and Griffith (38) and that of the author. However, it can only be a proposition until further experimental evidence, preferrably from other experimentalists, become available to establish or disprove it.

9.0 REFERENCES

(1) Tanner, D.W., Potter, C.J., Pope, D. and West, D.
'Heat transfer in dropwise condensation - Part i'
1965, Int. J. Heat Mass Transfer, 8, 419-426

(2) Tanner, D.W., Potter, C.J., Pope, D. and West, D.
'Heat transfer in dropwise condensation- Part II'
1965, Int. J. Heat Mass Transfer, 8, 427-436

(3) Osment, B.D.J., Tudor, D., Speirs, R.R.M. and Rugman, W.
'Promoters for the dropwise condensation of steam'
1962, Trans. Instn. Chem. Engrs., 40, 152-160

(4) Poll, A., Potter, C.J. and Powell, A.W.
'Effect of dropwise condensation on the thermal efficiency of a triple effect water distillation plant'
1966-67, Inst. Mech. Engrs., Proc., 181, 707-715

(5) McCormick, J.L. and Westwater, J.W.
'Drop dynamics and heat transfer during dropwise condensation of water vapour on a horizontal surface'
1966, Chem. Eng. Prog. Symp. Series No. 62, 120-134

(6) McCormick, J.L. and Westwater, J.W.
'Drop dynamics and heat transfer during dropwise condensation of water vapour on a horizontal surface'
-966, Chem. Eng. Prog. Symp. Series No. 62, 120-134

(7) Le Fevre, E.J. and Rose, J.W.
'Heat transfer measurements during the dropwise condensation of steam'
1966, Proc. 3rd. Int. Heat Transfer conf.,
Am. Inst. Chem. Engrs., 2, 362

(8) Rose, J. W.
'On the mechanism of dropwise condensation'
1967, Int. J. Heat Mass Transfer, 10, 755-762

(9) Nusselt, W.
'Die oberflachenkondensation des wasser damfs'
1916, Zeit. Ver Deut. Ing., 60, 541

(10) Bromley, L.A.
'Effect of heat capacity of condensate'
1952, Ind. and Engng. Chem., 44, 2966-2969

(11) Rohsenow, W.M.
'Heat transfer and temperature distribution in laminar-film condensation'
1956, Trans. ASME, 78, 1645-1648

(12) Hampson, H. and Ozisik, N.
'An investigation into the condensation of steam'
1952, Proc. I. Mech. E., 1, Series B, 282-293

(13) Sparrow, E.M. and Gregg, J.L.
'The effect of vapour drag on rotating condensation'
1960, Trans. ASME. Series C, 82, 71-72

(14) Chen, M.M.
'An analytical study of laminar film condensation' Parts I and II
1961, Trans. ASME. Series C, 83, 48-66

(15) Koh, J.C.Y., Sparrow, E.M., Hartnett, J.P.
'The two phase boundary layer in laminar film condensation'
1961, Int. J. Heat Mass transfer, 2, 69-82

(16) Shekriladze, I.G. and Gomelauri, V.I.
'Theoretical study of laminar condensation of flowing vapour'
1966, Int. J. Heat Mass Transfer, 9, 581

(17) Sugawara, S., Michigoshi, I. and Minamiama, T.
1956, Proc. 6th. Jap. Mat. Contr. for Appl. Mech. III-4

(18) Sparrow, E.M. and Gregg, J.L.
'A boundary-layer treatment of laminar-film condensation'
1959, Trans. ASME. Series C, 81, 13-18

(19) Zozula, M.V. In: Mikheer, M.A. (Editor)
Heat transfer and thermal modelling, 287-289
1959, Moscow: Akad. Nauk. SSSR, (DSIR Trans No. 668)

(20) Kirkbride, C.G.
'Heat transfer by condensing vapour on vertical tubes'
1934, Am. Inst. Chem. Eng., 30, 170

(21) Friedman, S.J. and Miller, C.O.
'Liquid films in the viscous flow region'
1941, Ind. Eng. Chem., 33, 885

(22) Dukler, A.E. and Bergelen, O.P.
'Characteristics of flow in falling liquid films'
1952, Chem. Eng. Prog., 48, No. 11, 557

(23) Ginabit, A.
1924, Wärme, 47, 5, 588

(24) Kapitza, P.L.
1948, Zh. Eksparim 1. Teor Fiz. 18, 3
" " " " 18,19
Translated in "Collected works of Kapitza"
Pergamon 1965

(25) Leonard, W.K. and Estrin, J.
'Heat transfer through a wavy film on a vertical surface'
1972, AIChE. Journal, vol. 18, No. 2, 439-442

(26) Colburn, A.P.
'The calculation of condensation where a portion of the condensate layer is in turbulent motion'
1934, Trans. Am. Inst. Chem. Engrs., 30, 187-193

(27) Labuntsov, D.A.
1960, Inzh - Fiz. Zhur., 3, 3

(28) National Engineering Laboratory
'The condensation of superheated steam'
Edinburgh: H.M.S.O. 1962

(29) Othmer, D.F.
'Manometer for determination of gases in vapours'
1929, Ind. Eng. Chem, Vol. 1, 46

(30) Hampson, H.
'The condensation of steam on a metal surface'
1951, Proc. Gen. Disc. on Heat Transfer, 50, 58-61

(31) Sparrow, E.M. and Eckert, E.R.G.
'Effects of superheated vapour and non-condensible gases on laminar-film condensation'
1961, Amer. Inst. Chem. Engr. J, 7, 473-477

(32) Baasel, W.D. and Smith, J.C.
'A mathematical solution for the condensation of vapours from noncondensing gases in laminar flow inside vertical cylinders'
1963, Amer. Inst. Chem. Engrs. J., 9, 826-830

(33) Sparrow, E.M. and Lin, S.H.
'Condensation heat transfer in the presence of a non-condensable gas'
1964, J. Heat transfer, 86, 430-436

(34) Sparrow, E.M., Minkowycz, W.J. and Saddy, M.
'Forced convection condensation in the presence of noncondensables and interfacial resistance'
1967, Int. J. Heat Mass Transfer, 10, 1829-1845

(35) Tamir, A. and Taitel, Y.
'Direct contact condensation with a multicomponent mixture of noncondensable gases'
1970, Int. J. Heat Mass Transfer, 13, 1501-1503

(36) Denny, V.E., Mills, A.F. and Jusionis, V.J.
'Laminar film condensation from a steam-air mixture undergoing forced flow down a vertical surface'
1971, J. Heat Transfer, 93, 297-304

(37) Dhir, V. and Leinhard, J.
'Laminar film condensation on plane and axisymmetric bodies in non-uniform gravity'
1971, Trans. ASME. Series C, 93, 97-100

(38) Gerstmann, J. and Griffith, P.
'Laminar film condensation on the underside of horizontal and inclined surfaces'
1967, Int. J. Heat Mass Transfer, 10, 567-579

(39) Labunstov, D.A.
1957, Teploenergetika, 4, 72-80
English Trans: CTS 454. Nat. Lending Library

(40) McAdams, W.H.
Heat Transmission, 1st. edition, McGraw-Hill, New York, 1933

(41) Poots, G. and Miles R.G.
'Effects of variable physical properties on laminar film condensation of saturated steam on a vertical flat plate'
1967, Int. J. Heat Mass Transfer, 10, 1677-1692

(42) Poll, A., Potter, C.J. and Powell, A.W.
'Effect of dropwise condensation on the thermal efficiency of a triple effect water distillation plant'
1966-67, Inst. Mech. Engrs., Proc., 181, 707-715

(43) Osment, B.D.J. and Tanner, D.W.
'Promoters for the dropwise condensation of steam'
1962, NEL Report No. 34

(44) Brown, A.R. and Thomas, M.A.
'Filmwise and dropwise condensation of steam at low pressures'
1966, Proc. 3rd. Int. Heat Transfer conf.
(Am. Inst. Chem. Engrs.)

(45) Erb, R.B. and Theilen, E.
'Promoting permanent dropwise condensation'
1965, Ind. Engng. Chem., 57, 49-52

(46) Gregorig, V.R.
'Hautkondensation an feingewellten Oberflächen bei Berucksichtigung der Oberflächenspannungen'
1954, Z. Anggew. Math. Phys., 5, 36-49

(47) Hawes, R.I.
'Development of the vertical tube multi 'effect process'
1970, 3rd, Int. Symp. on fresh water from the sea, 1, 275-289

(48) Thomas, D.G. and Alexander, L.G.
'Improved high-performance fluted tube for thin-film evaporation and condensation'
1970, Desalination, 8, 13-19

(49) Katz, D.C., Hope, St. C. II and Robinson, D.B.
'Condensation of Freon-12 with finned tubes'
1947, Refrigerating Engineering, 45, 211-217

(50) Henrici, H.
'Condensation of Refrigerants 12 and 22 on horizontal plain and finned tubes'
1961, Annexe Bull. Int. Ind. Refrig., 255-266

(51) Henrici, H.
'The condensation of R11, R12 and R22 on plain finned tubes'
1963, Kaltetechnik, 8, 251-256

(52) Ashraf, M.
'Forced Convection in corrugated tubes'
1969, M.Sc. Thesis, Univ. of Manchester

(53) Velkoff, H.R. and Miller, J.H.
'Condensation of vapour on a vertical plate with a traverse electrostatic field'
1965, Trans. ASME Series C, 87, 197-207

(54) Holmes, R.E. and Chapman, A.J.
'Condensation of freon 114 in the presence of a strong non-uniform alternating electric field'
1970, Trans. ASME. Series C, 92, 616-620

(55) Sparrow, E.M. and Gregg, J.L.
'A theory of rotating condensation'
1959, Trans. ASME. Series C, 81, 113-120

(56) Nandapurkar, S.S. and Beatty, K.O.
'Condensation on a horizontal rotating disc'
1959, Chem. Engng. Prog. Symp. No. 30, Vol. 56, 129-137

(57) Espig, H. and Hoyle, R.
'The transfer of heat from condensing steam to a cooled rotating disc'
1968, Proc. I. Mech. E., 182, part 3H, 406-412

(58) Espig, H. and Hoyle, R.
'Waves in a thin liquid on a rotating disc'
1965, J. Fluid Mech., Vol. 22, part 4, 671-677

(59) Yeh, L.
1953, Ph.D. Thesis, Imperial College of Science and Technology, London.

(60) Singer, R.M. and Preckshot, G.W.
1963, Proc. of the Heat transfer and fluid mechanics institute, No. 14, 205-221

(61) Hoyle, R. and Matthews, D.H.
'The effect of diameter size and speed of rotation on the heat transfer from steam to cooled cylinders'
1964, Int. J. Heat Mass Transfer, 7, 1223-1234

(62) Nichol, A.A. and Gacesa, M.
'Condensation of steam on a rotating vertical cylinder'
1970, Trans. ASME Series C, 92, 144-152

(63) Williams, A.G., Nandapurkar, S.S. and Holland, F.A.
'Condensation on a vertical rotating finned tube'
1971, Canadian J. Chem. Engng., 49, 51-55

(64) Hickman, K.C.D.
'Centrifugal boiler compression still'
1957, Ind. Engng. Chem., 49, 786-800

(65) Bromley, L.A.
'Prediction of performance characteristics of Hickman-Badger centrifugal boiler compression still'
1958, Ind. Engng. Chem., 50, No. 2, 233-236

(66) Bruin, S.
'Velocity distributions in a liquid film flowing over a rotating conical surace'
1969, Chem. Engng. Science, 24, 1647-1654

(67) Wu, C.S.
'Three dimensional incompressable laminar boundary layer on a spinning cone'
1959, App. Sci. Res., Section A, 8, 140-146

(68) Tien, C.L.
'Heat transfer by laminar flow from a rotating cone'
1960, Trans. ASME. Series C, 82, 252-253

(69) Sparrow, E.M. and Hartnett, J.P.
'Condensation on a rotating cone'
Feb. 1961, Trans. ASME. Series C, 101-102

(70) Howe, M. and Hoyle, R.
'Heat transfer from condensing steam to a cooled cone rotating about a vertical axis'
1970, Proc. I. Mech. E., 184, (3G), 37-44

(71) Howe, M.
'Heat transfer by steam condensing onto rotating cones'
1972, Ph.D. Thesis, Dept. Eng. Sci. Univ. of Durham

(72) Terrel, B.J.
'The influence of thermal effects on manoeuvrability of marine steam turbines'
1953, Trans. N.E. Coast Inst. Engrs. and Shipbuilders, 70, 93-101

(73) Hall, J.S. and Britten, A.F.
'Rapid starting technique: some significant tests at Poole power station'
1954, Proc. I. Mech. E., 168, No. 27, 717-741

(74) Moore, J.T.
'Engineering planning and design of large steam power plant for maximum availability'
1965, Proc. I. Mech. E., 179, Pt. (31)

(75) Robson, B.T.
'The formation and drainage of a film of condensate on the surface of a rotating cone'
1970, M.Sc. Thesis, Dept. Eng. Sci. Univ. of Durham

(76) Holgate, M.J.
'Stability of a fluid film on the surface of a cone'
1971, Ph.D. Thesis, Dept. of Eng. Sci., Univ. of Durham

(77) Smith, D.B.
'Condensate film flow on the surface of rotating cones'
- Ph.D. Thesis, Dept. Eng. Sci., Univ. of Durham

(78) Spiegel, M.R.
'Vector Analysis', Schaum's outline series
McGraw-Hill book company, 1959

(79) Lamb, H.
'Hydrodynamics', Camb. Univ. Press, 1932

(80) McCormick, J.M. and Salvadori, M.G.
'Numerical methods in Fortran',
Prentice-Hall Inc., New Jersey, 1964

(81) Frisk, D.P. and Davis, E.J.
'The enhancement of heat transfer by waves in stratified gas-liquid flow'
1972, Int. J. Heat Mass Transfer, 15, 1537-1552

(82) Hanson, D. and Rodgers, C.E.
'The thermal conductivity of some non-ferrous alloys'
1932, J. Inst. Met., 48, 37-45

(83) Smith, C.S. and Palmer, E.W.
'Thermal and electrical conductivities of copper alloys'
1935, Trans. Amer. Inst. Min. Met. Eng., 117, 225-243

(84) Koh, J.C.Y. and Fortrini, A.
'Prediction of thermal conductivity and electrical resistivity of porous metallic materials'
1973, Int. J. Heat Mass Transfer, 16, 2013-2021

(85) Powell, R.W.
'Correlation of metallic thermal and electrical conductivities for both solid and liquid phases'
1965, Int. J. Heat Mass Transfer, 8, 1033-1045

10.0 APPENDICES

APPENDIX A

Thermal conductivity of body material

The thermal conductivity of the body material was determined both directly and from the measurements of the electrical conductivity of the material.

In 1932, Hanson and Rodgers (82) gave a correlation between the thermal and electrical conductivities of several binary copper alloys. In 1935, Smith and Palmer (83) extended the study to include commercial copper alloys. More recently (1973), Koh and Fortini (84) further extended the study to cover porous metallic materials.

In 1965, Powell (85) reviewed the published data for the correlation of thermal and electrical conductivities for both solid and liquid phases of a wide range of materials. Powell gave the equation for the thermal conductivity of copper alloys as:

$$k_w = C_1 \sigma T + C_2 \qquad A1$$

where σ = electrical conductivity of the material with units $(1/\Omega m)$

T = absolute temperature K

$C_1 = 2.39 \times 10^{-8}$ W Ω/K^2

$C_2 = 7.5$ W/mK

By measuring the electrical resistance (r) of a conductor of length (ℓ), cross-sectional area (a) and at a temperature T, equation A1 can be solved by substituting $\sigma = \ell/ar$.

Fig. A1 shows the diagrammatic arrangement of the apparatus used to measure the electrical resistance of a specimen of the body material. The specimen was removed from the cylindrical base of the experimental body and machined to 0.0014m. diameter and 0.10m. long. The temperature of the specimen was varied by the oil bath. A current of 1.0 Amps. was passed through the specimen and the voltage drop across it measured. From the readings the resistance was estimated.

The by-pass circuit was necessary to eliminate drifting in the voltage readings due to the change in resistance of the circuitry as a result of electrical heating. Fig. A3 shows a plot of the thermal conductivity against temperature as obtained with the above apparatus.

To check the above results, an experiment was devised to measure the thermal conductivity directly. Fig. A2 shows the details of the main parts of the apparatus employed. A test specimen, also removed from the cylindrical base, was machined to 0.007m. diameter and 0.145m. long. It was heated electrically at one end and cooled at the other end by water. The temperature distribution across the specimen which was well insulated was determined. The thermal conductivity of the material was determined from the Fourier rate equation:

$$Q = -k_w a \, (dT/dx)$$

where "Q" is the energy flow rate, "a" the cross-sectional area of the specimen and dT/dx the temperature gradient. The results of these tests are also shown in fig. A3 and it can be observed that they confirm the results from the electrical method. A comparison between the thermal and electrical conductivities of copper alloys with composition close to that of the body material (H.T.B.1), showed that equation A1 predicted the thermal conductivity to within $\pm$3 per cent of the measured value.

From fig. A3, the thermal conductivity of the body material was derived as:

$$k_w = 190.4 \left[\frac{T_w + 273}{T_w + 776.6} \right] + 7.5 \qquad \frac{W}{m\,^{\circ}C}$$

where T_w is the material temperature in degrees centigrade ($^{\circ}C$).

APPENDIX B

Comparison of thin-wall and thick-wall theories

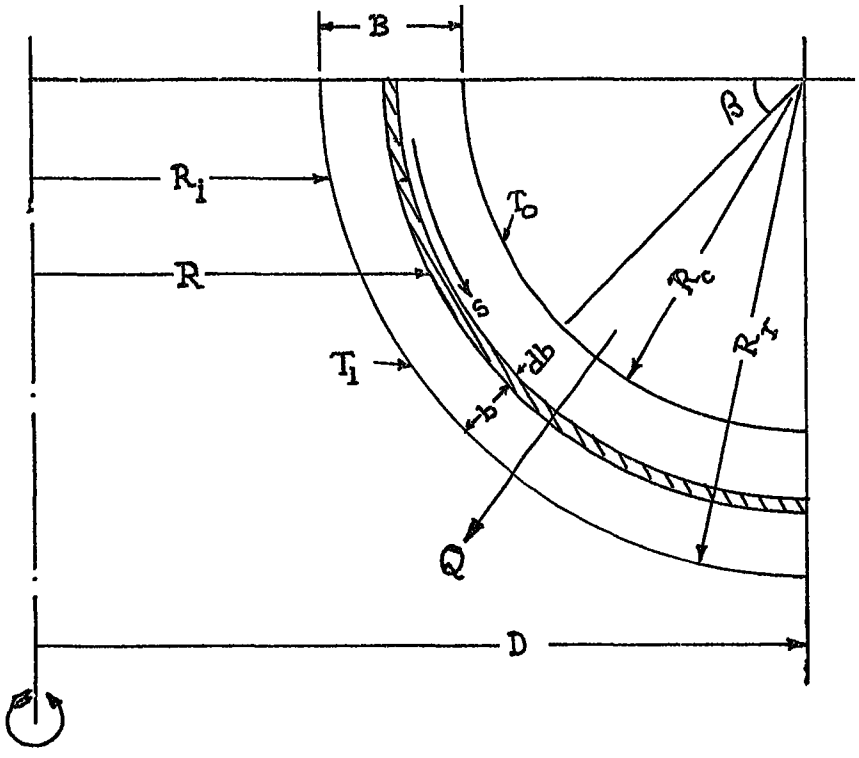

Consider the element db of the wall of the curved body at position b from the inner surface. The surface area of the element is given by:

$$\hat{A} = 2\pi \int_0^s R \, ds$$

$$R = D - [R_r - b] \cos (s/(R_r - b))$$

$$\text{and } \hat{A} = 2\pi \left\{ Ds - [R_r - b]^2 \sin (s/(R_r - b)) \right\}$$

Now consider the case when T_i and T_o are constant (i.e. no axial conduction). From Fourier's equation,

$$Q/\hat{A} = -k_w \, dT/db$$

$$\frac{Q}{2\pi \left\{ Ds - [R_r - b]^2 \sin (s/(R_r - b)) \right\}} = -k_w \frac{dT}{db}$$

$$\frac{Q}{2\pi k_w} \int_0^B \frac{db}{\left\{ Ds - [R_r - b]^2 \sin (s/(R_r - b)) \right\}} = \int_{T_i}^{T_o} dT$$

$$\therefore Q = \frac{2\pi k_w (T_o - T_i)}{\int_0^B \left\{ \frac{db}{Ds - [R_r - b]^2 \sin (s/(R_r - b))} \right\}} \qquad (B1)$$

Equation (B1) is the conduction equation for the curved body shown.

At the leading edge, the body approximates to a thick-wall cylinder.

$s/(R_r - b)$ is small and $\text{Sin}\ (s/(R_r - b)) = s/(R_r - b)$

If the substitution is made and equation (B1) is integrated the solution becomes

$$Q = \frac{2\pi s\, k_w\, (T_o - T_i)}{\ell n\ (R_o/R_i)} \qquad \text{where } R_o = R_i + B \tag{B2}$$

Equation (B2) is easily recognised as the conduction equation for a thick-wall cylinder. If $(s/(R_r - b)) = \pi/2$, equation (B1) yields the solution:

$$Q = \frac{\pi^2\, D\, k_w\, (T_o - T_i)}{\ln\left[\dfrac{R_r\,(2R_c - \pi D)}{R_c\,(2R_r - \pi D)}\right]} \tag{B3}$$

For the experimental curved body, $D = 0.2794$,m.

$R_c = 0.1346$m. and $R_r = 0.1524$m.

Substituting into equation (B3),

$$Q = 14.980\, k_w\, (T_o - T_i) \tag{B4}$$

If the thin-wall theory is assumed and the analysis is based on the area at the mean radius ($R_m = R_i + B/2$), then

$$Q = k_w \hat{A}_m\, (T_o - T_i)/B$$

$\hat{A}_m = 0.2666\ m^2$ and $1/B = 56.2$

Hence $$Q = 14.983\, k_w\, (T_o - T_i) \tag{B5}$$

The comparison of equation (B4) and equation (B5) show that the thin-wall theory could be used without any significant loss in accuracy.

Appendix C

Applications of equation (3.1.35)

To show the validity of equation (3.1.35) and the ease of its applications, the above equation is applied to the cylinder, the disc and the cone. The two forms of equation (3.1.35) namely, equation (3.1.36) and equation (3.1.37) are illustrated by applying equation (3.1.36) to the disc while equation (3.1.37) is applied to the cylinder and the cone.

The cylinder

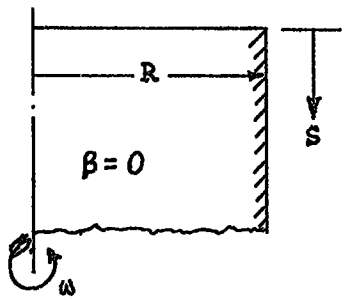

Equation (3.1.37) is given by

$$\eta^4 = \frac{4}{3\alpha} \frac{\int_{so}^{s} \Phi(\Phi^2 \mathrm{Sin}\psi + \Phi \mathrm{Cos}\psi)^{1/3}\, ds}{(\Phi^2 \mathrm{Sin}\psi + \Phi \mathrm{Cos}\psi)^{4/3}}$$

For the cylinder, $\beta = 0 = \psi$

$$\xi = R\omega^2/g = \Phi = \text{constant}$$

Hence $$\eta^4 = \frac{4}{3\alpha} \frac{\int_{o}^{s} \Phi^{4/3} ds}{\Phi^{4/3}}$$

$$\eta^4 = \frac{4}{3\alpha} s = \frac{4}{3} \frac{\omega^2 s}{g}$$

$$\delta^4 = \gamma^4 \eta^4 = 4As/3g \qquad \text{(C1)}$$

Equation (C1) should be recognised as equation (3.1.24a) which was shown to be the Nusselt (9) expression for the condensation on a vertical wall.

The disc

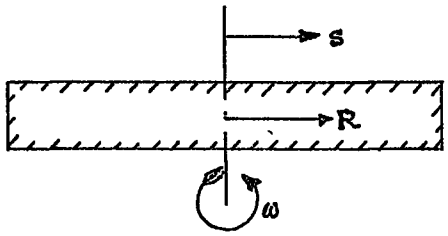

Equation (3.1.36) is given by:

$$\eta^4 = \frac{4}{3} \frac{\int_{\xi_o}^{\xi} (\xi/\mathrm{Sin}\lambda)(\xi^2\mathrm{Sin}\lambda + \xi\mathrm{Cos}\lambda)^{1/3}\, d\xi}{(\xi^2\mathrm{Sin}\lambda + \xi\mathrm{Cos}\lambda)^{4/3}}$$

For the solid disc, angle β is constant and $\xi_o = 0$

$$\beta = \pi/2 = \lambda; \quad \xi = R\omega^2/g$$

Hence $$\eta^4 = \frac{4}{3} \frac{\int_o^{\xi} \xi^{5/3}\, d\xi}{\xi^{8/3}}$$

$$\eta^4 = 1/2$$

and $$\delta^4 = \omega^{-2}A/2 \qquad \text{(C2)}$$

Equation (C2) compares with equation (3.1.27) which was shown to be the Sparrow and Gregg (55) solution for the condensation on a rotating disc.

The Cone

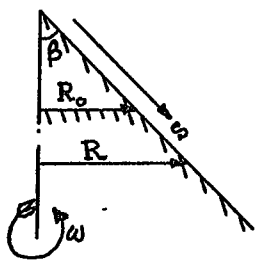

For the cone, the angle β is constant.

From equation (3.1.37)

$$\eta^4 = \frac{4}{3\alpha} \frac{\int_o^{s} \Phi(\Phi^2\mathrm{Sin}\psi + \Phi\mathrm{Cos}\psi)^{1/3}\, ds}{(\Phi^2\mathrm{Sin}\psi + \Phi\mathrm{Cos}\psi)^{4/3}}$$

Here $\beta = \psi$ = constant

For a truncated cone,

$$\xi = R\omega^2/g = (\omega^2/g)(R_o + s.Sin\psi) = \Phi$$

For a solid cone, R_o is zero.

It should be appreciated that even though ψ and Φ are known, equation (3.1.37) is best solved by numerical integration. However, if equation (3.1.37) is re-written as:

$$\eta^4 = \frac{4}{3\alpha} \frac{\int_o^s \Phi^{4/3} (\Phi Sin\psi + Cos\psi)^{1/3} ds}{\Phi^{4/3} (\Phi Sin\psi + Cos\psi)^{4/3}}$$

and Φ is assumed large, i.e. high rotational speeds, the solution becomes,

$$\eta^4 = \frac{4}{3Sin\beta} \frac{\int_o^s (R_o + s.Sin\beta)^{5/3} ds}{(R_o + s.Sin\beta)^{8/3}}$$

For a solid cone this becomes,

$$\eta^4 = 1/(2Sin^2\beta)$$

$$\text{and } \delta^4 = \omega^2 A/(2Sin^2\beta) \qquad \text{(C3)}$$

Equation (C3) is in agreement with equation (3.1.28) which is recognised as the Sparrow and Hartnett (69) solution for the condensation on rotating cones when gravity was neglected.

11.0 FIGURES AND PHOTOGRAPHS

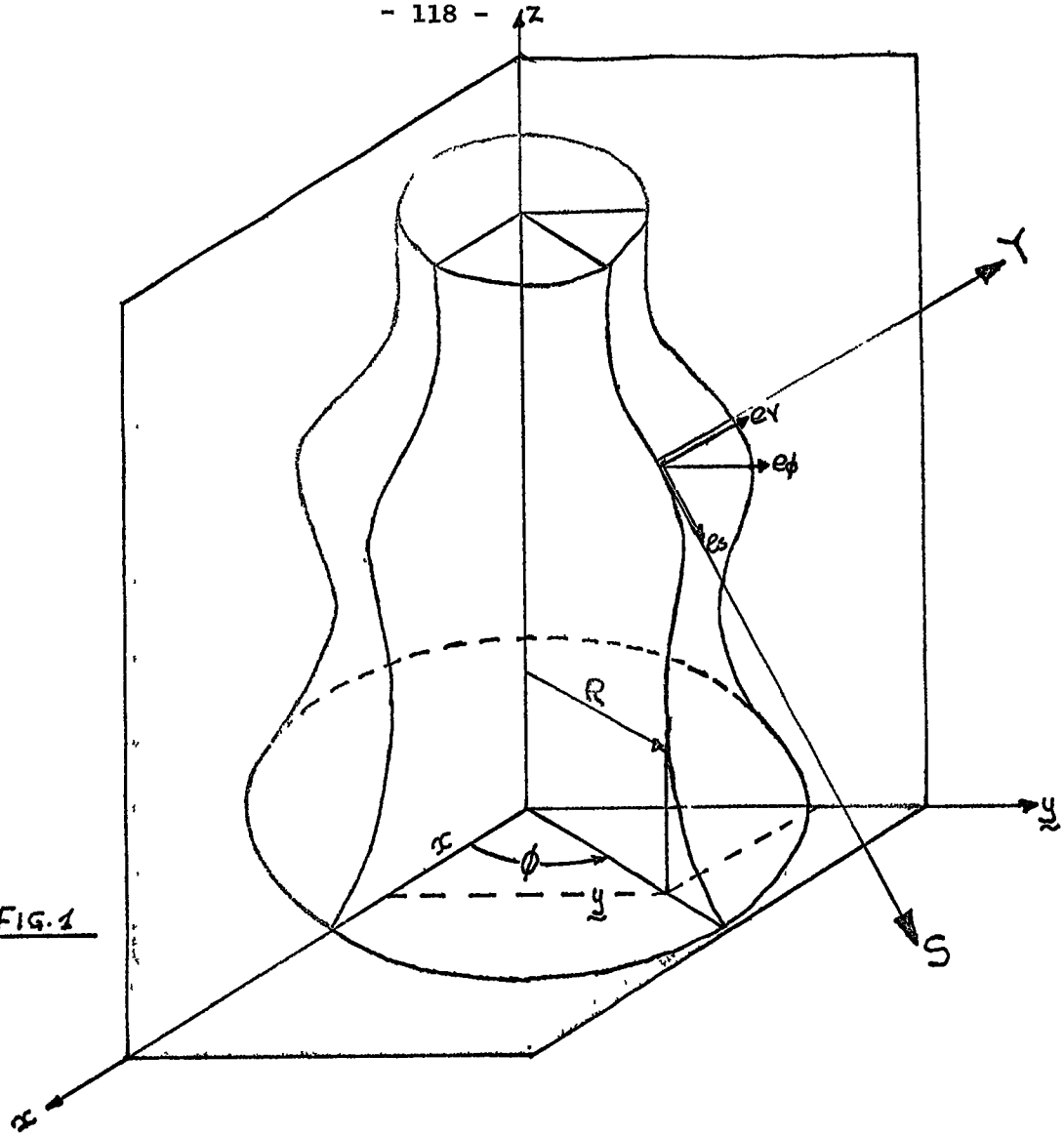

FIG. 1

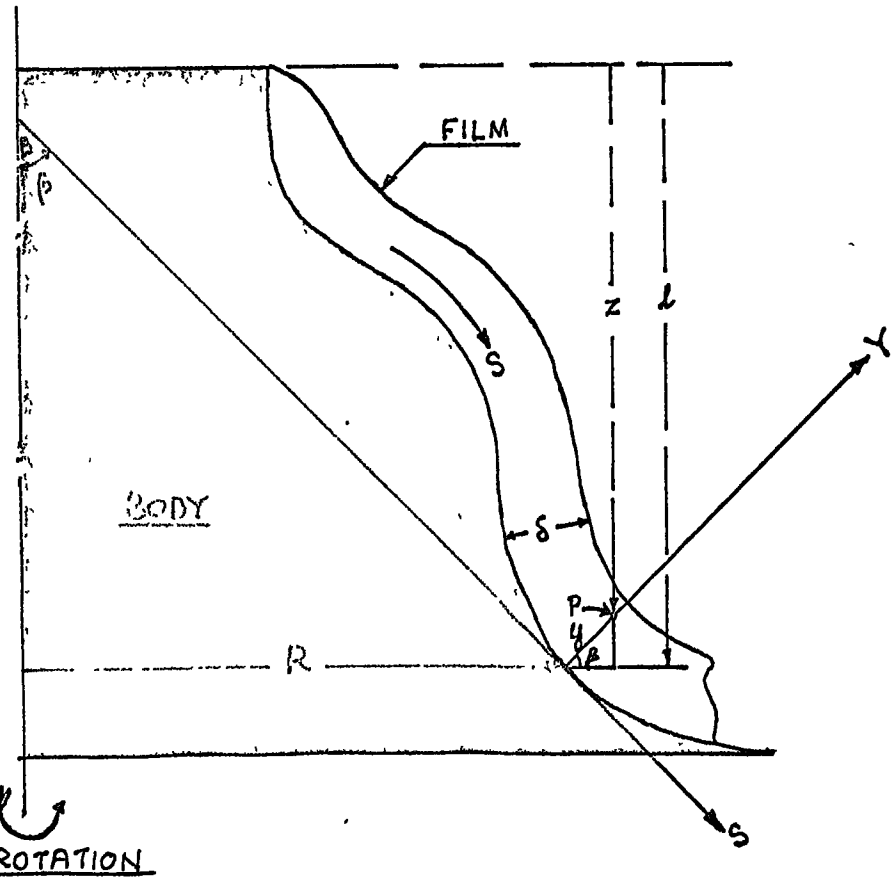

FIG. 2

AXIS OF ROTATION

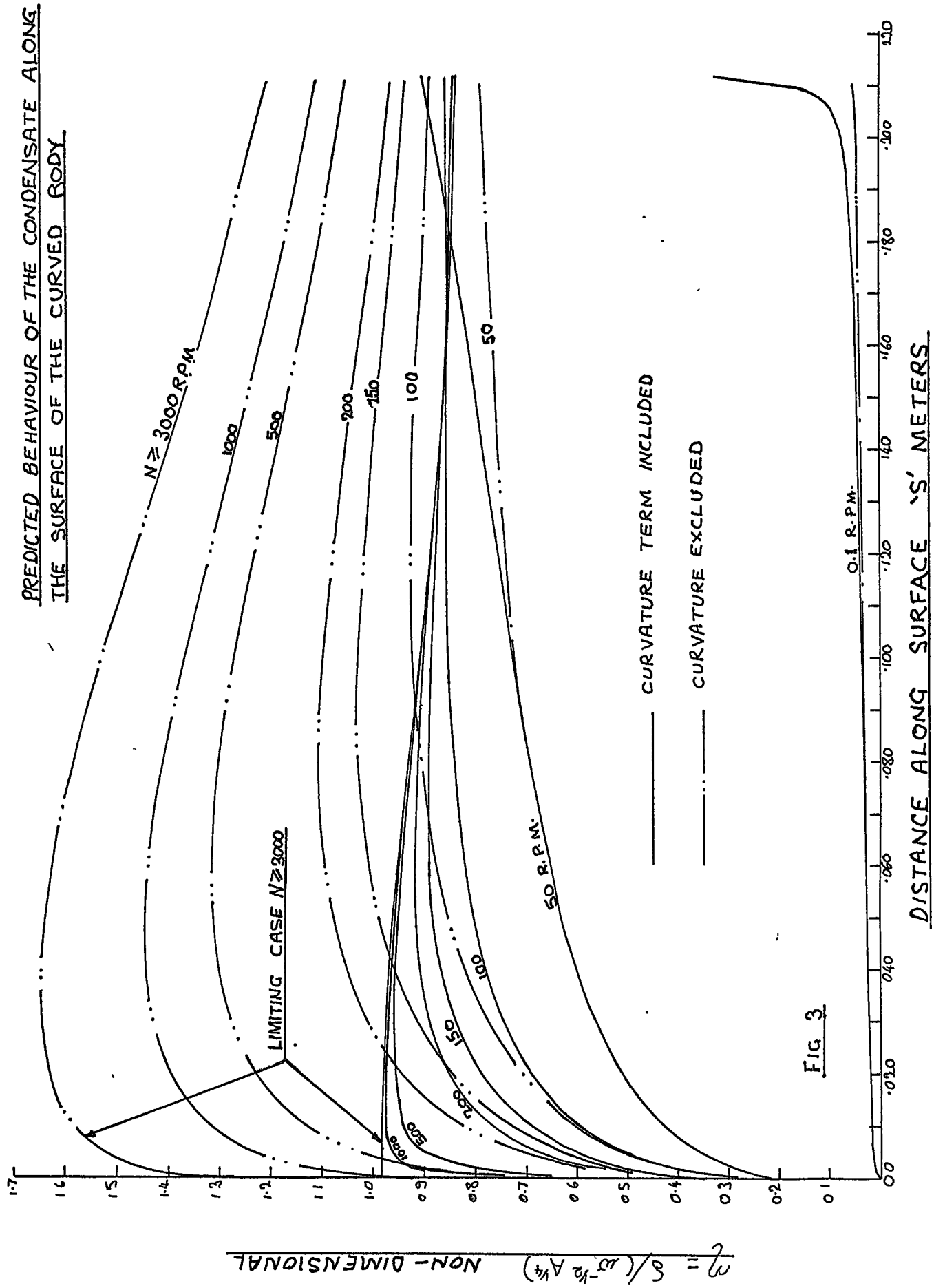
PREDICTED BEHAVIOUR OF THE CONDENSATE ALONG THE SURFACE OF THE CURVED BODY
N ≥ 3000 R.P.M
1000
500
200
150
100
50
LIMITING CASE N≥3000
50 R.P.M.
CURVATURE TERM INCLUDED
CURVATURE EXCLUDED
0.1 R.P.M.
DISTANCE ALONG SURFACE 'S' METERS
NON-DIMENSIONAL

FIG 3

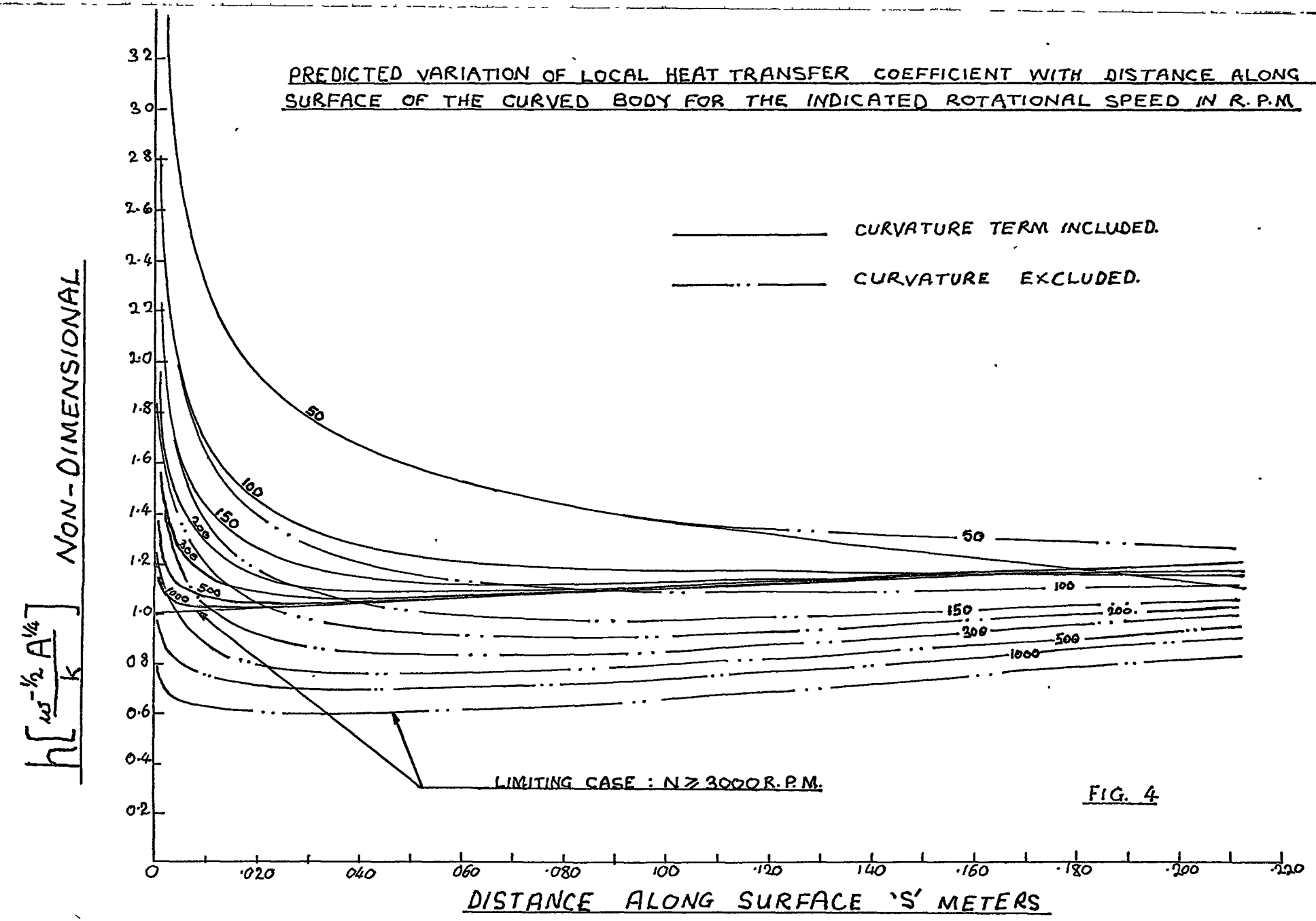
PREDICTED VARIATION OF LOCAL HEAT TRANSFER COEFFICIENT WITH DISTANCE ALONG THE SURFACE OF THE CURVED BODY FOR THE INDICATED ROTATIONAL SPEED IN R.P.M.
CURVATURE TERM INCLUDED.
CURVATURE EXCLUDED.
NON-DIMENSIONAL $\frac{h}{k}\left[\frac{L}{\omega^{-1/2} A^{1/4}}\right]$
DISTANCE ALONG SURFACE 'S' METERS
LIMITING CASE : N ≥ 3000 R.P.M.
50
100
150
200
300
500
1000
3.2
3.0
2.8
2.6
2.4
2.2
2.0
1.8
1.6
1.4
1.2
1.0
0.8
0.6
0.4
0.2
0
·020
·040
·060
·080
·100
·120
·140
·160
·180
·200
·220

FIG. 4

PREDICTED VARIATION OF AVERAGE HEAT TRANSFER COEFFICIENT WITH DISTANCE ALONG THE SURFACE OF THE CURVED BODY FOR THE INDICATED ROTATIONAL SPEED IN R.P.M.

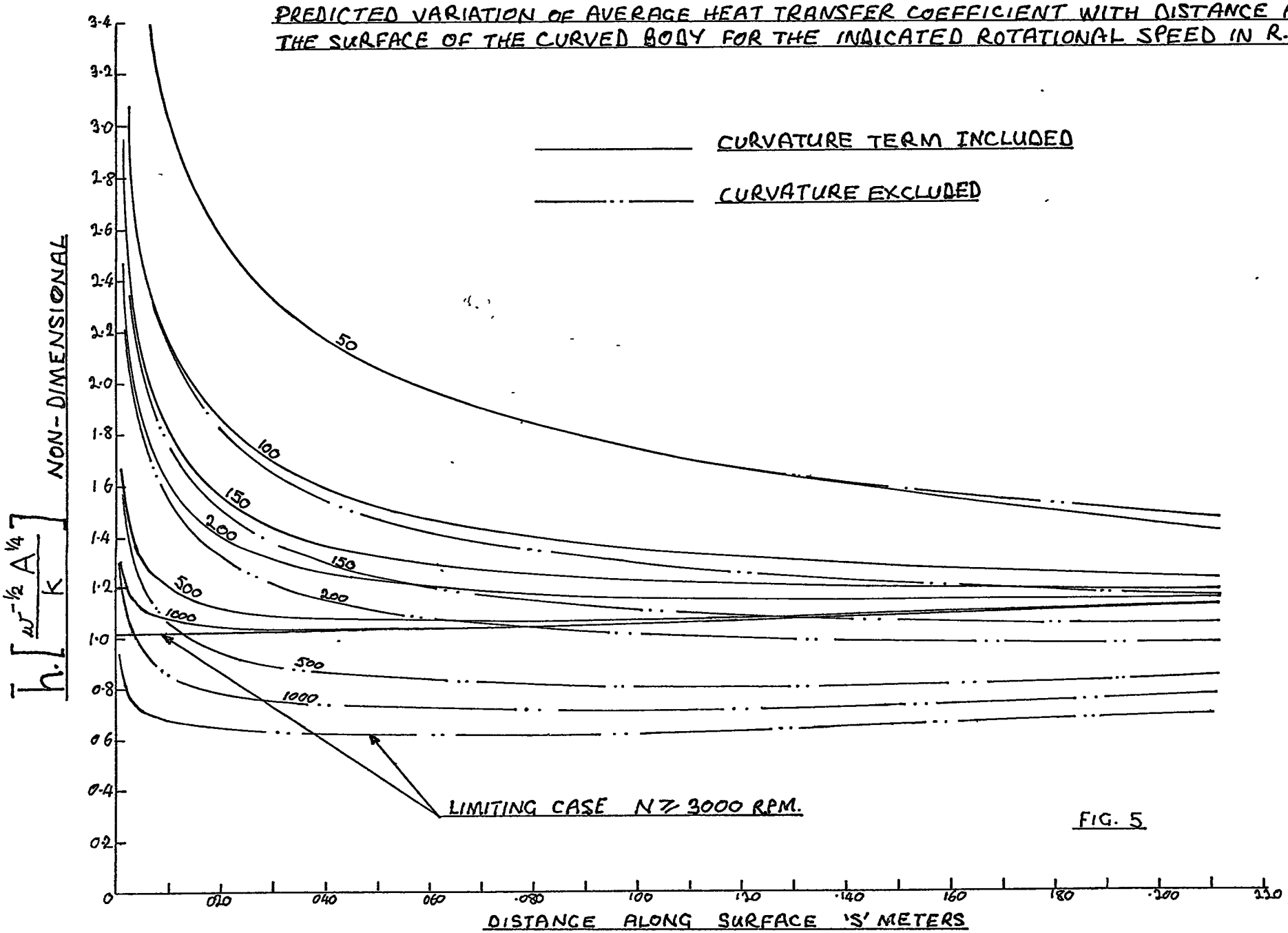

FIG. 5

MAX. % DEVIATION IN LOCAL AND AVERAGE HEAT TRANSFER COEFFICIENTS OF THE SOLUTION WITHOUT THE CURVATURE TERM FROM THE SOLUTION WITH THE CURVATURE TERM

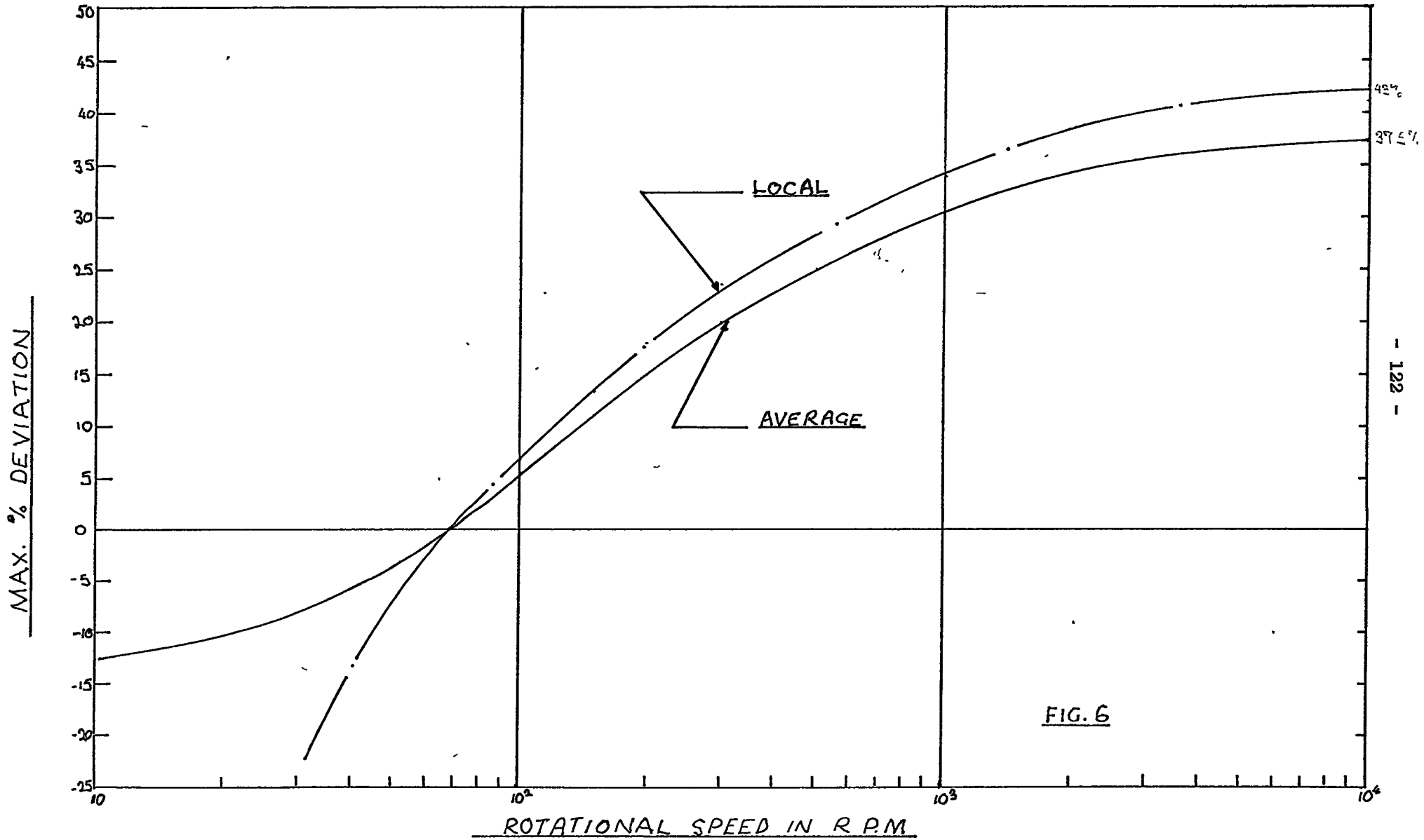

FIG. 6

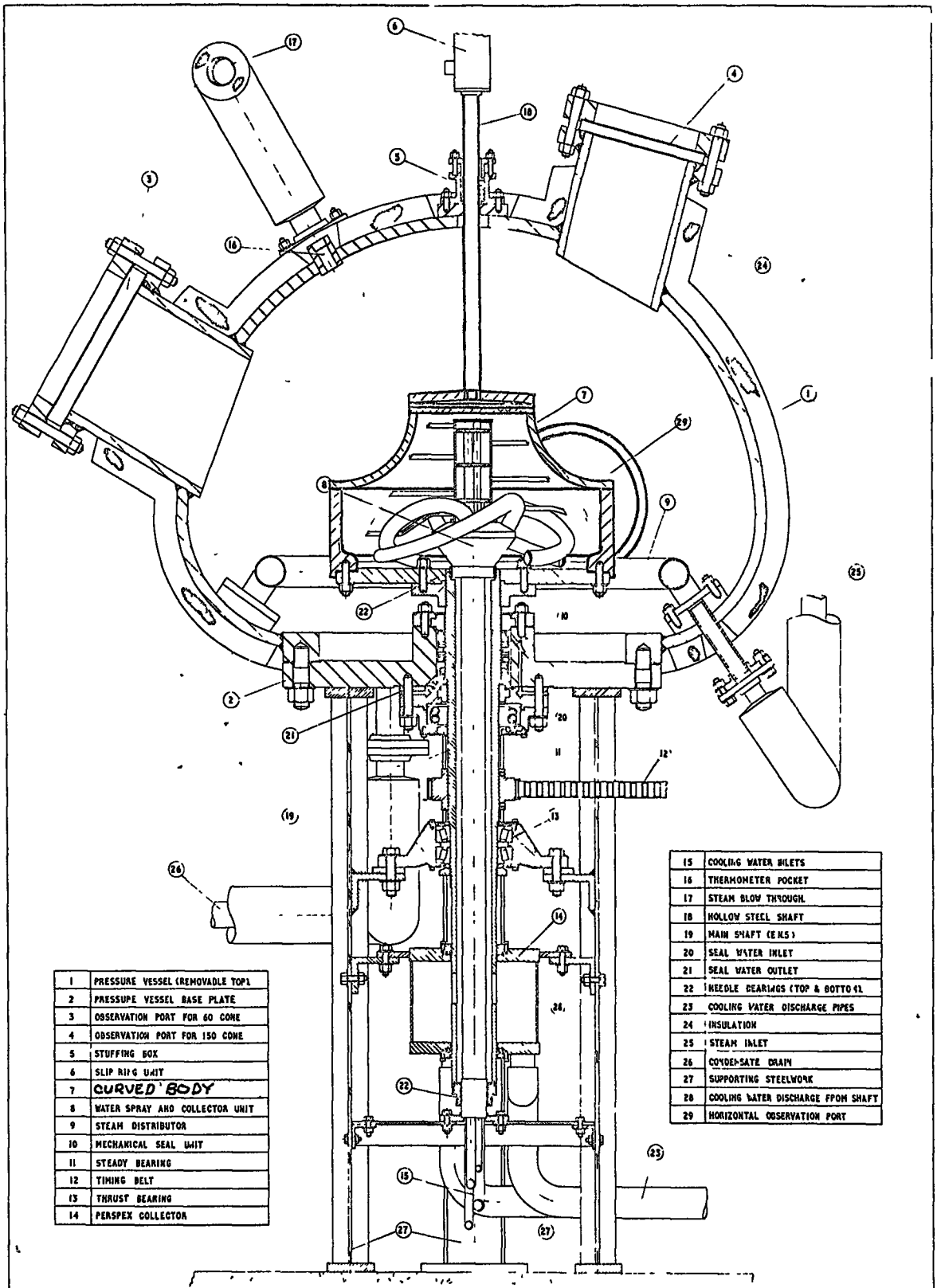
1 PRESSURE VESSEL (REMOVABLE TOP)
2 PRESSURE VESSEL BASE PLATE
3 OBSERVATION PORT FOR 60 CONE
4 OBSERVATION PORT FOR 150 CONE
5 STUFFING BOX
6 SLIP RING UNIT
7 CURVED BODY
8 WATER SPRAY AND COLLECTOR UNIT
9 STEAM DISTRIBUTOR
10 MECHANICAL SEAL UNIT
11 STEADY BEARING
12 TIMING BELT
13 THRUST BEARING
14 PERSPEX COLLECTOR
15 COOLING WATER INLETS
16 THERMOMETER POCKET
17 STEAM BLOW THROUGH
18 HOLLOW STEEL SHAFT
19 MAIN SHAFT (EN 8)
20 SEAL WATER INLET
21 SEAL WATER OUTLET
22 NEEDLE BEARINGS (TOP & BOTTOM)
23 COOLING WATER DISCHARGE PIPES
24 INSULATION
25 STEAM INLET
26 CONDENSATE DRAIN
27 SUPPORTING STEELWORK
28 COOLING WATER DISCHARGE FROM SHAFT
29 HORIZONTAL OBSERVATION PORT

FIG. 7

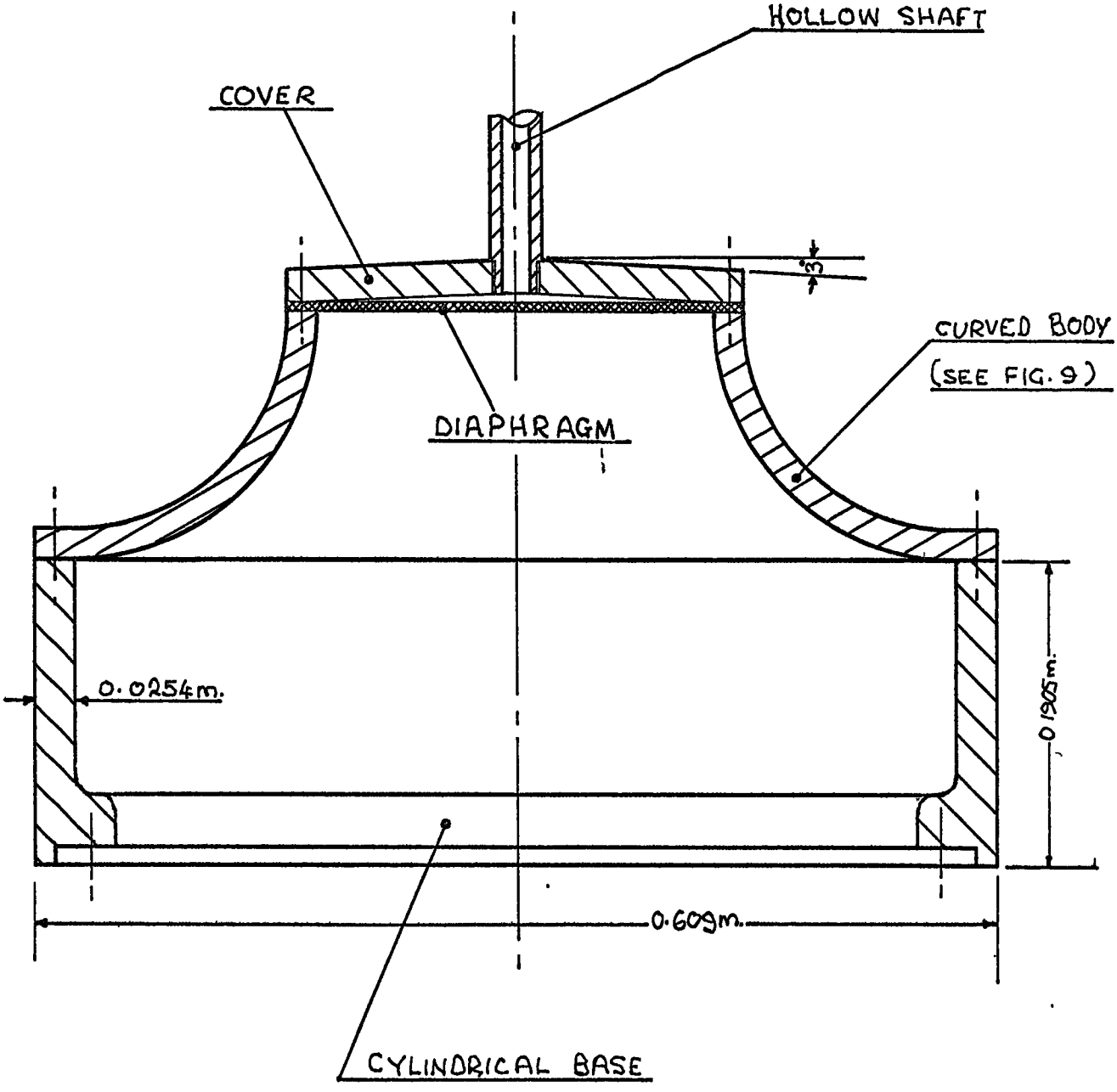

EXPERIMENTAL BODY FIG. 8

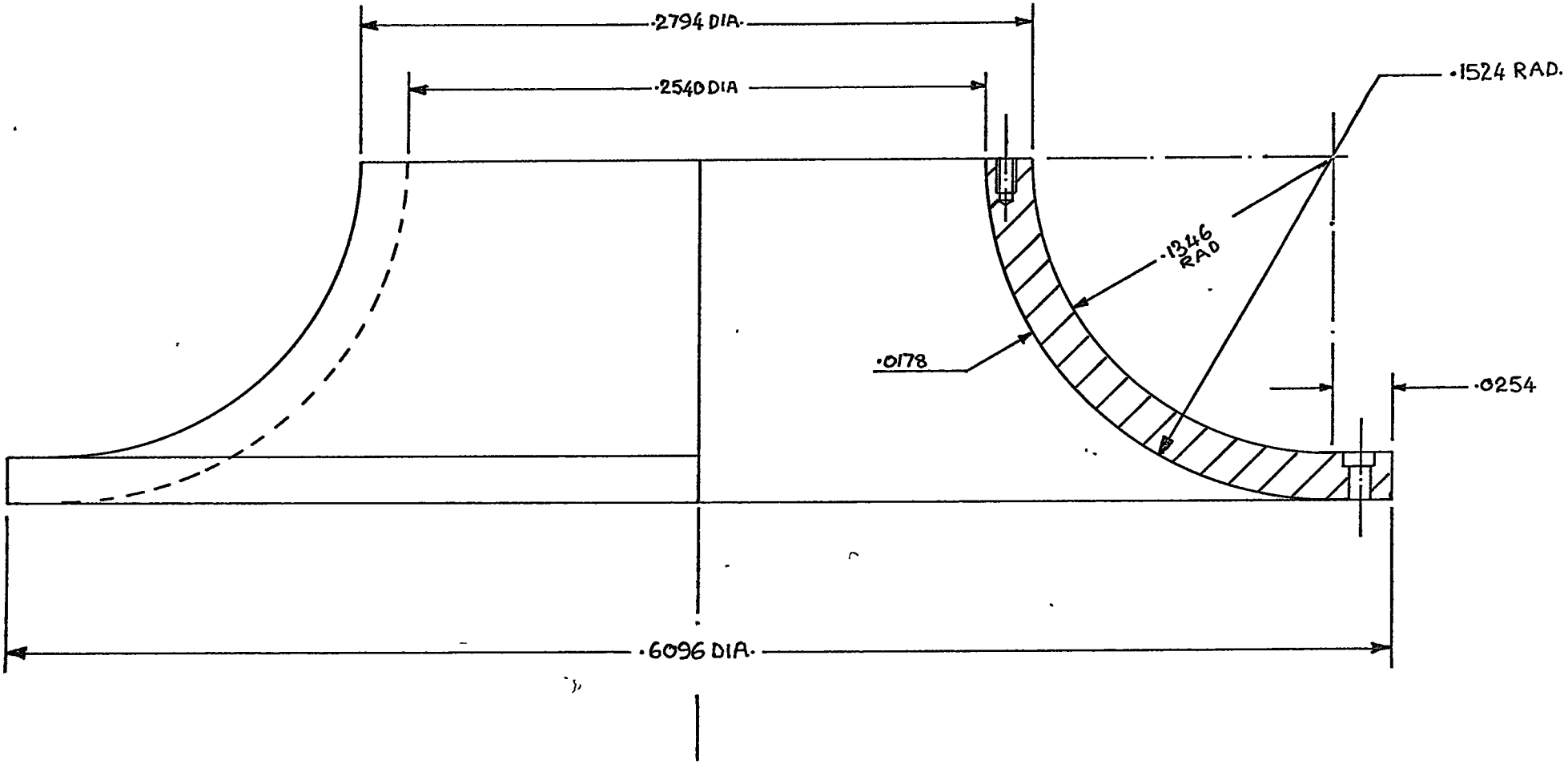

ALL DIMENSIONS IN METERS.

FIG. 9

SKETCH SHOWING CURVED BODY PARTIALLY SECTIONED.

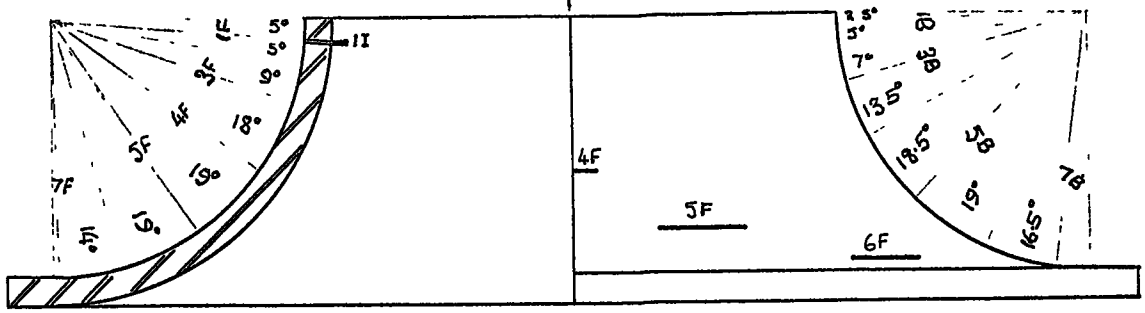

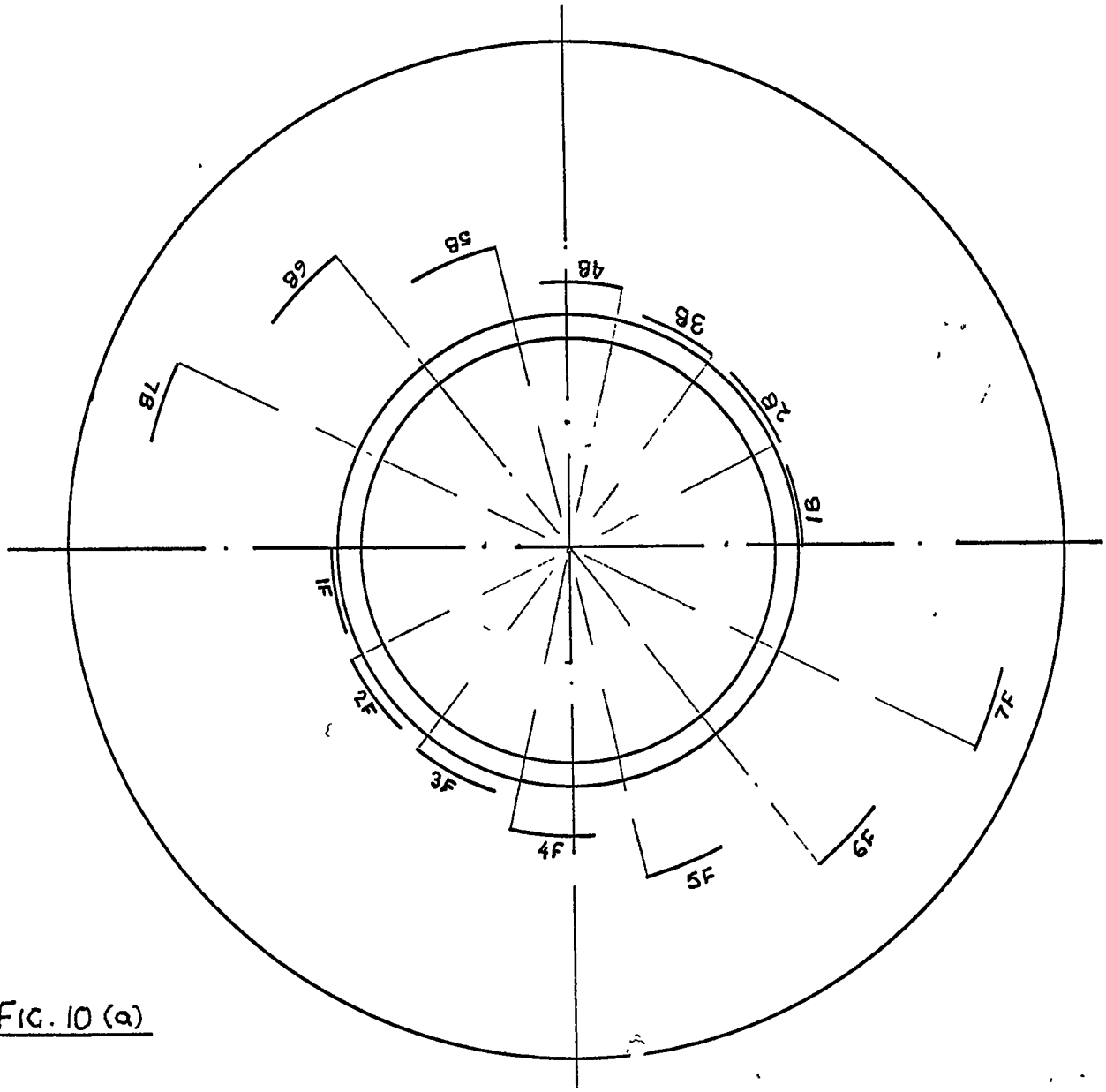

FIG. 10 (a)

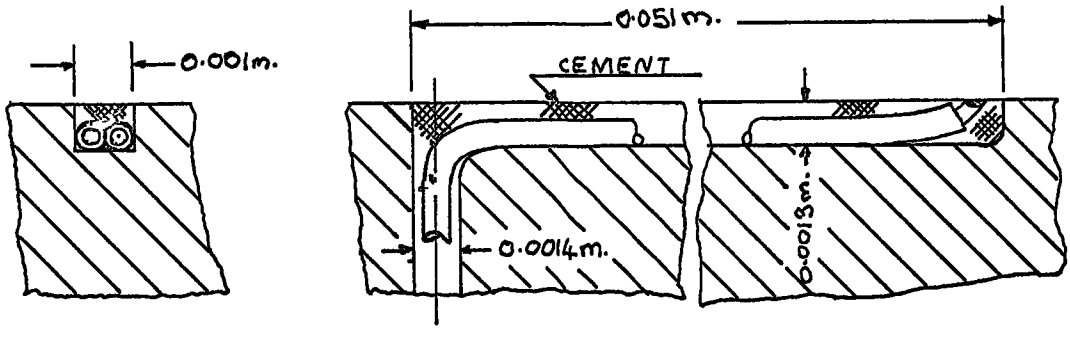

FIG 10 (b)

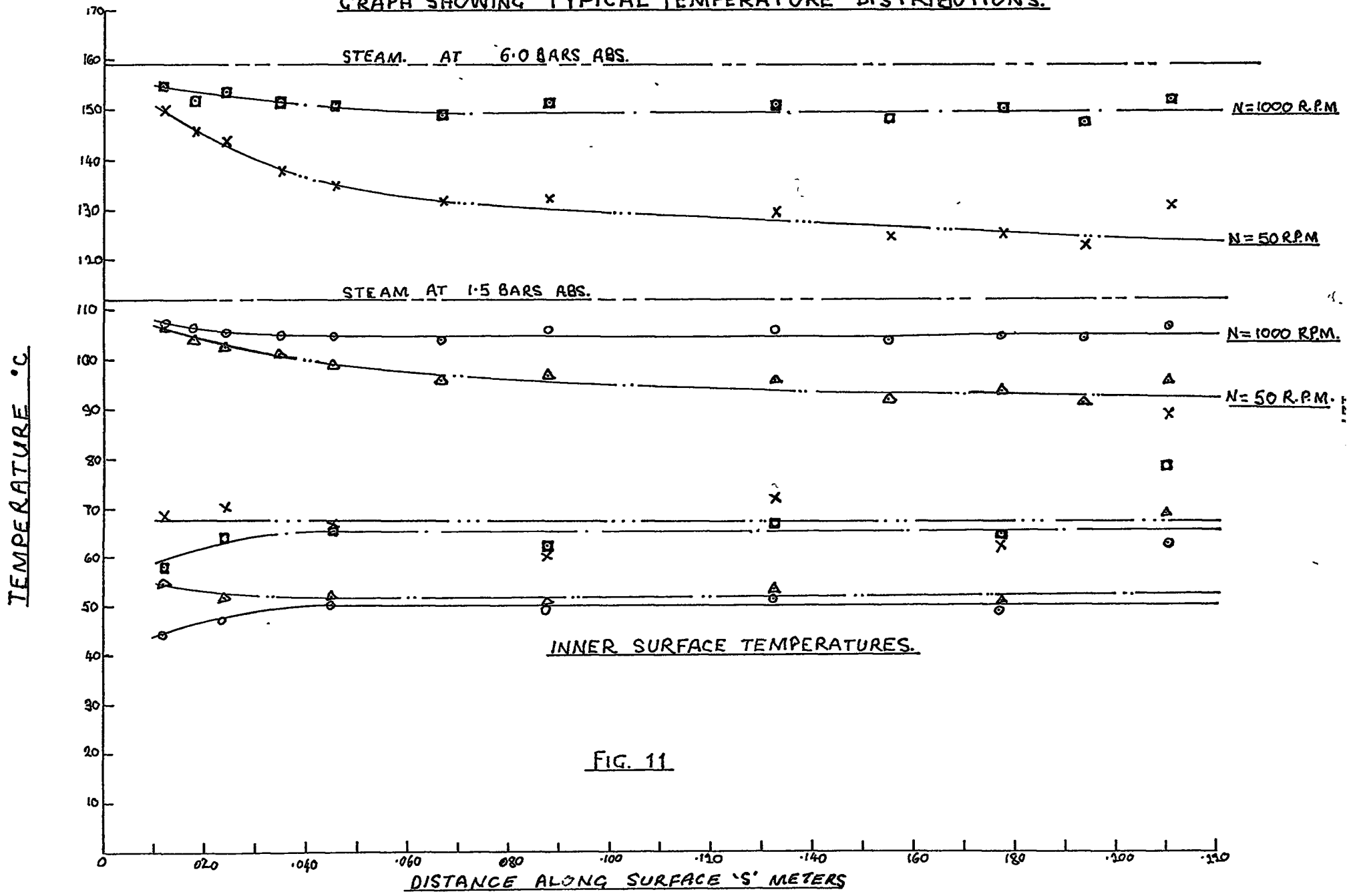
GRAPH SHOWING TYPICAL TEMPERATURE DISTRIBUTIONS.
STEAM AT 6·0 BARS ABS.
N=1000 R.P.M
N=50 R.P.M
STEAM AT 1·5 BARS ABS.
N=1000 R.P.M.
N=50 R.P.M.
INNER SURFACE TEMPERATURES.
TEMPERATURE °C.
DISTANCE ALONG SURFACE 'S' METERS
170
160
150
140
130
120
110
100
90
80
70
60
50
40
30
20
10
0
·020
·040
·060
·080
·100
·120
·140
·160
·180
·200
·220

FIG. 11

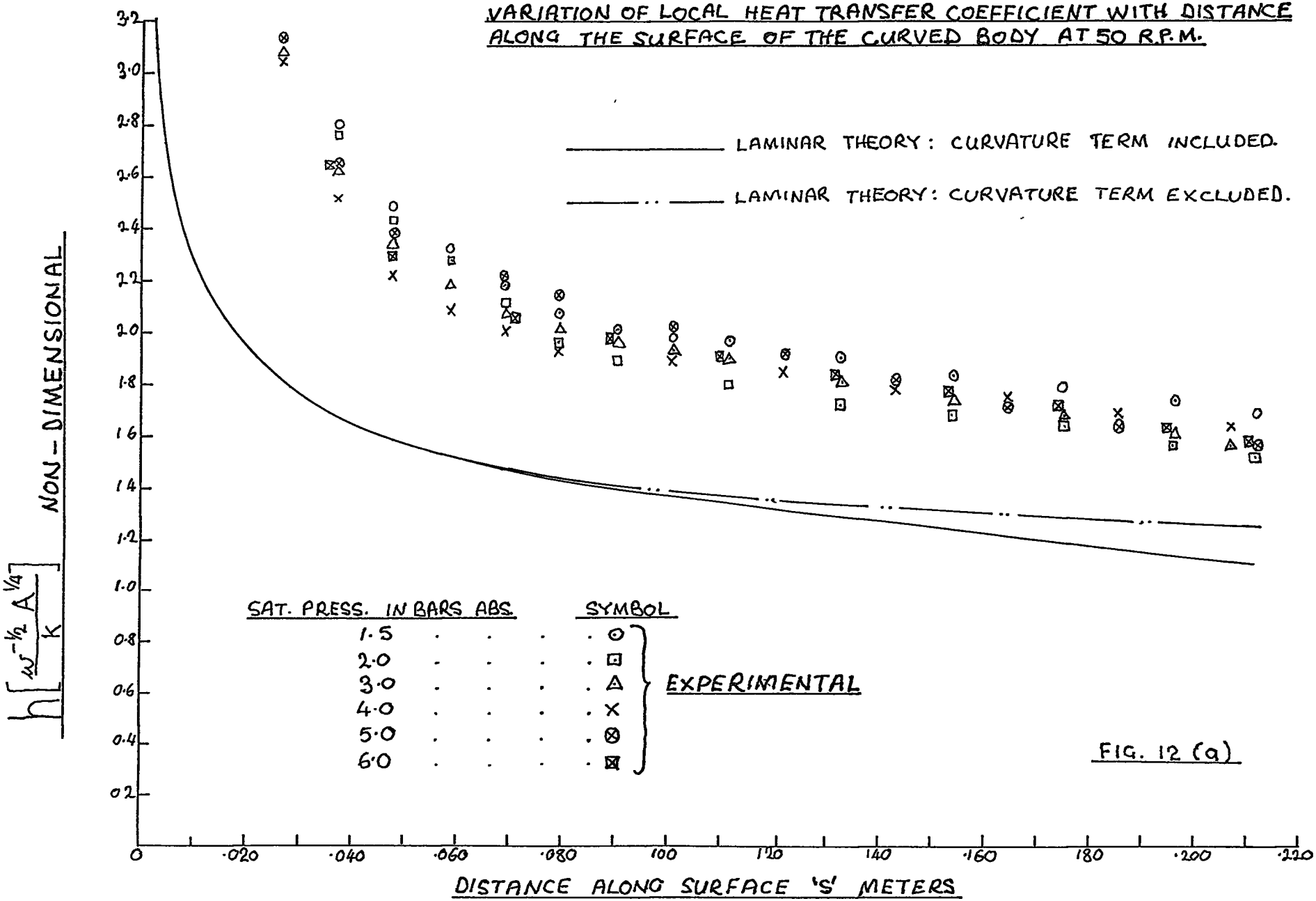
VARIATION OF LOCAL HEAT TRANSFER COEFFICIENT WITH DISTANCE ALONG THE SURFACE OF THE CURVED BODY AT 50 R.P.M.
LAMINAR THEORY: CURVATURE TERM INCLUDED.
LAMINAR THEORY: CURVATURE TERM EXCLUDED.
NON-DIMENSIONAL $h\left[\frac{\omega^{-1/2} A^{1/4}}{k}\right]$
SAT. PRESS. IN BARS ABS.
SYMBOL
1·5
2·0
3·0
4·0
5·0
6·0
EXPERIMENTAL
3·2
3·0
2·8
2·6
2·4
2·2
2·0
1·8
1·6
1·4
1·2
1·0
0·8
0·6
0·4
0·2
0
·020
·040
·060
·080
·100
·120
·140
·160
·180
·200
·220
DISTANCE ALONG SURFACE 'S' METERS

FIG. 12 (a)

VARIATION OF LOCAL HEAT TRANSFER COEFFICIENT WITH DISTANCE ALONG THE SURFACE OF THE CURVED BODY AT 100 R.P.M.

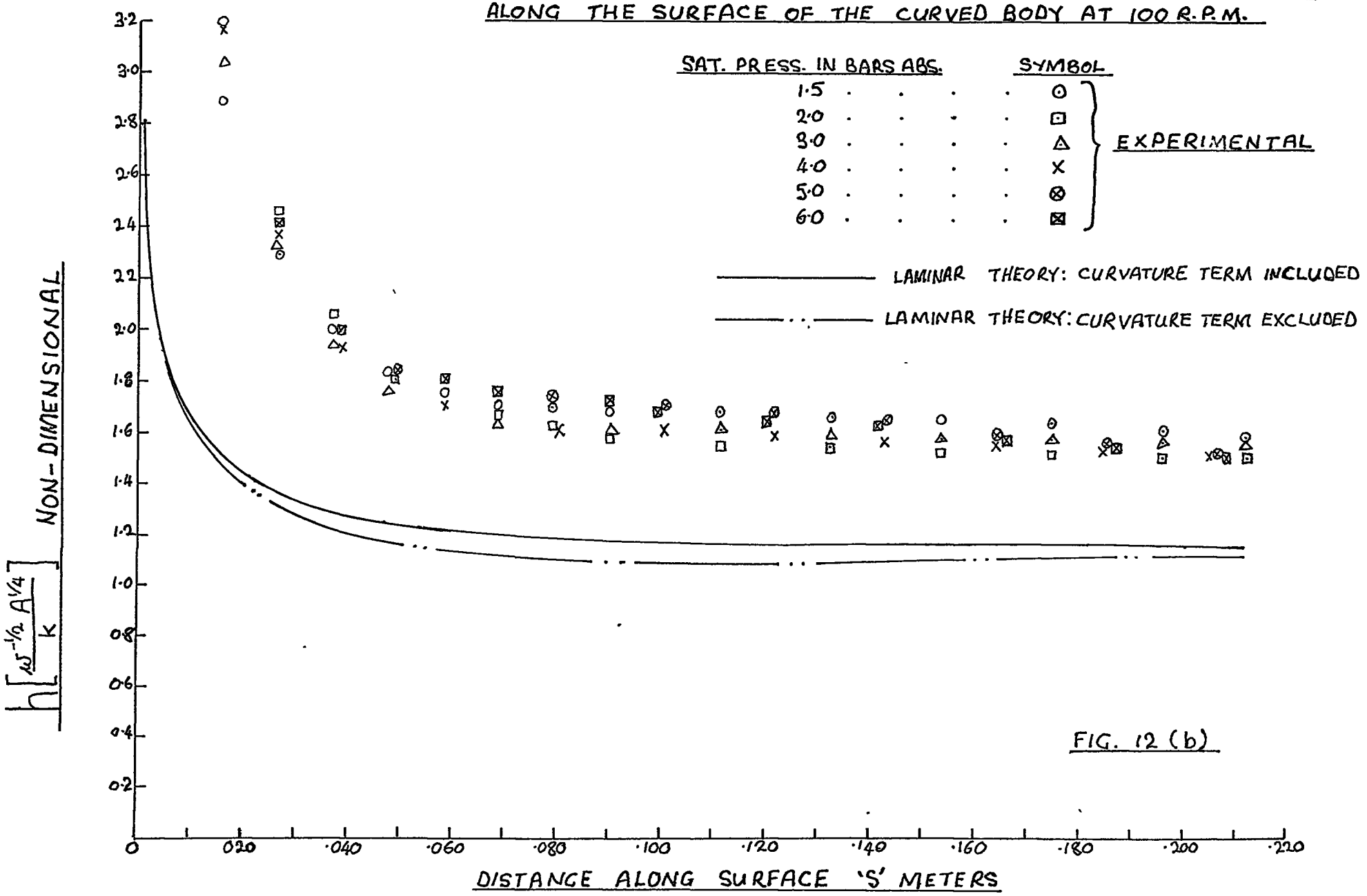

FIG. 12 (b)

VARIATION OF LOCAL HEAT TRANSFER COEFFICIENT WITH DISTANCE ALONG THE SURFACE OF THE CURVED BODY AT 150 R.P.M

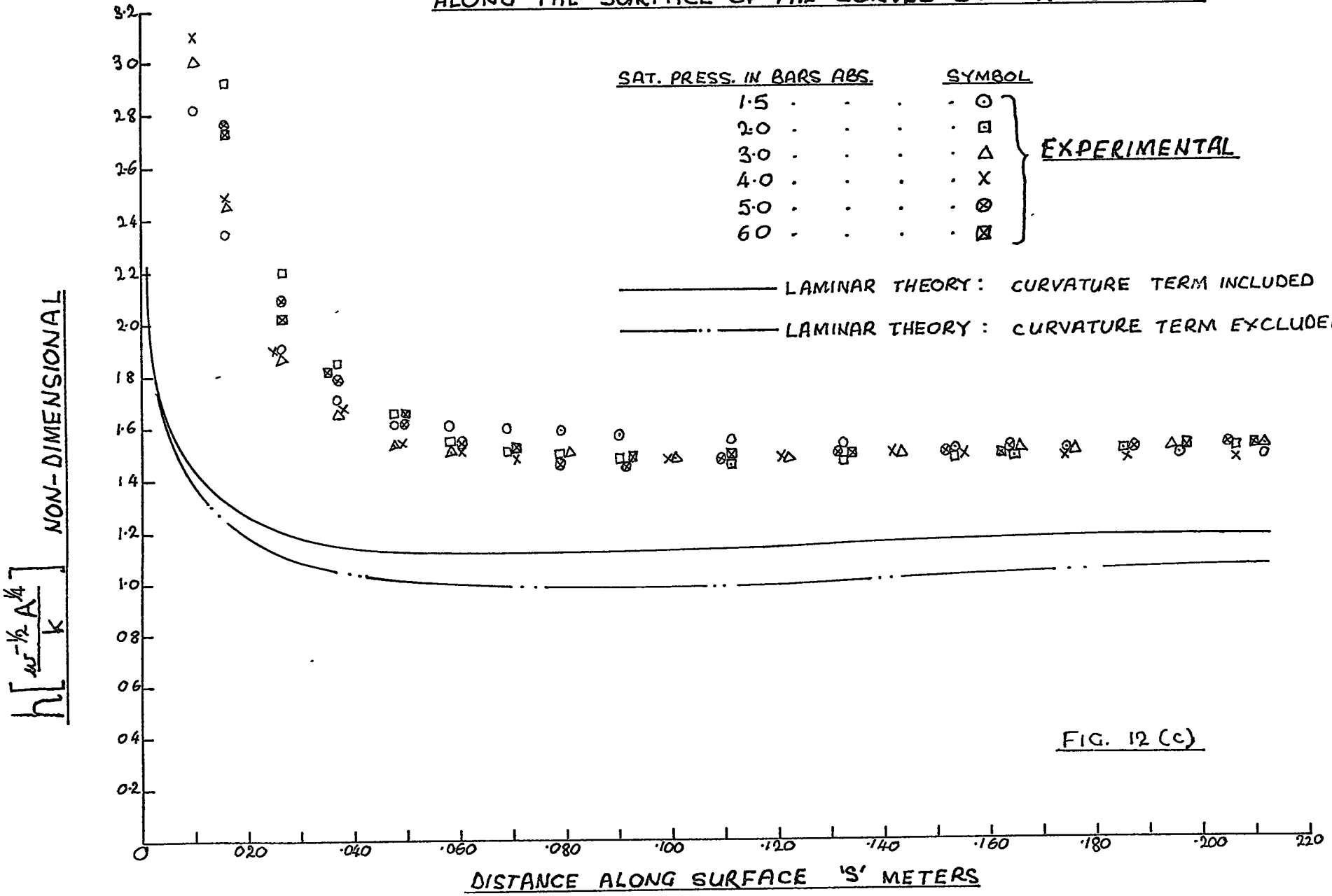

FIG. 12 (c)

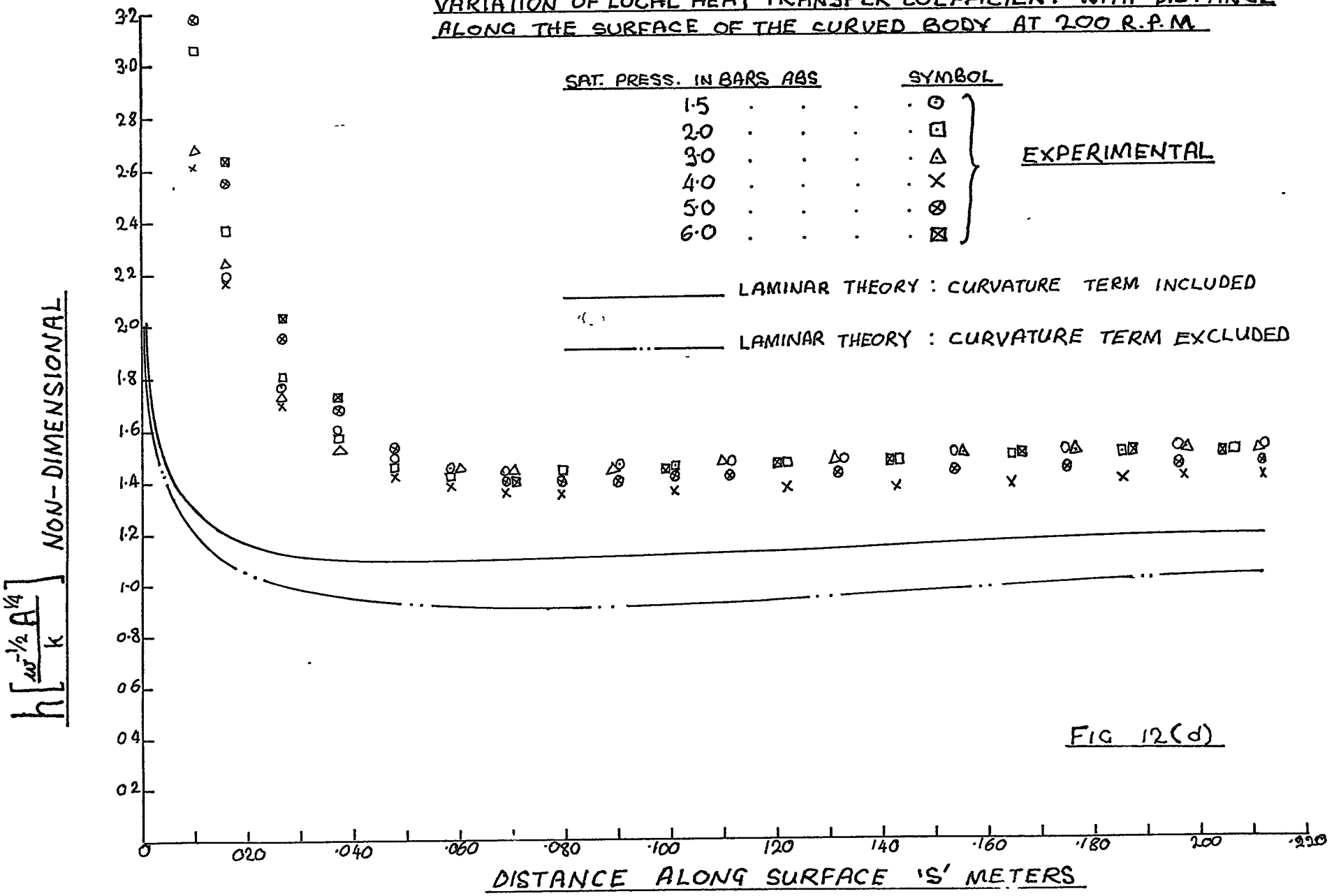
VARIATION OF LOCAL HEAT TRANSFER COEFFICIENT WITH DISTANCE ALONG THE SURFACE OF THE CURVED BODY AT 200 R.P.M.
SAT. PRESS. IN BARS ABS
SYMBOL
1·5
2·0
3·0
4·0
5·0
6·0
EXPERIMENTAL
LAMINAR THEORY : CURVATURE TERM INCLUDED
LAMINAR THEORY : CURVATURE TERM EXCLUDED
h [ω^-½ A^¼ / k] NON-DIMENSIONAL
3·2
3·0
2·8
2·6
2·4
2·2
2·0
1·8
1·6
1·4
1·2
1·0
0·8
0·6
0·4
0·2
0
·020
·040
·060
·080
·100
·120
·140
·160
·180
·200
·220
DISTANCE ALONG SURFACE 'S' METERS

FIG 12(d)

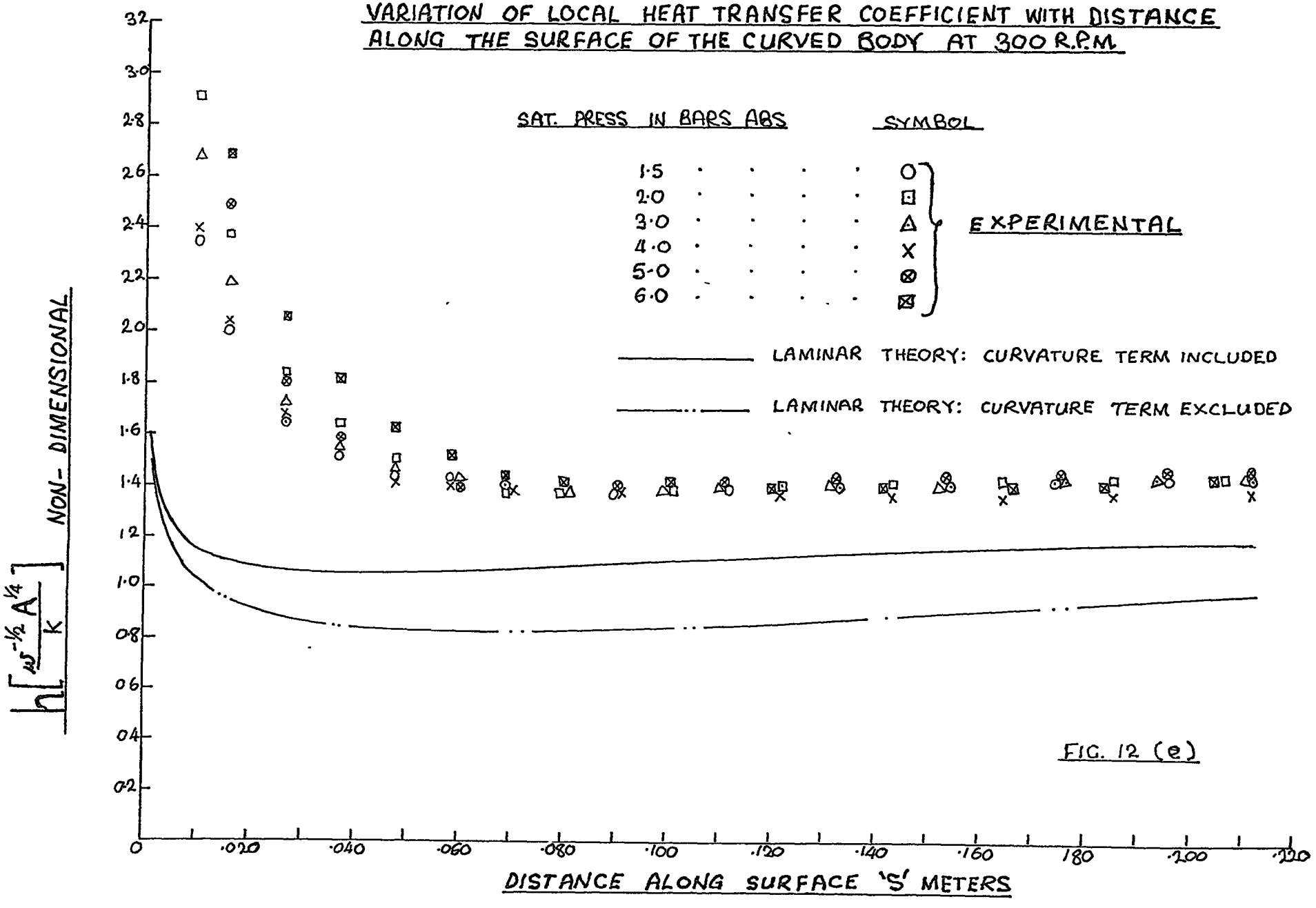
VARIATION OF LOCAL HEAT TRANSFER COEFFICIENT WITH DISTANCE ALONG THE SURFACE OF THE CURVED BODY AT 300 R.P.M.
SAT. PRESS IN BARS ABS
SYMBOL
1·5
2·0
3·0
4·0
5·0
6·0
EXPERIMENTAL
LAMINAR THEORY: CURVATURE TERM INCLUDED
LAMINAR THEORY: CURVATURE TERM EXCLUDED
NON-DIMENSIONAL
DISTANCE ALONG SURFACE 'S' METERS
32
30
28
26
24
22
20
18
16
14
12
10
08
06
04
02
0
·020
·040
·060
·080
·100
·120
·140
·160
180
·200
·220

FIG. 12 (e)

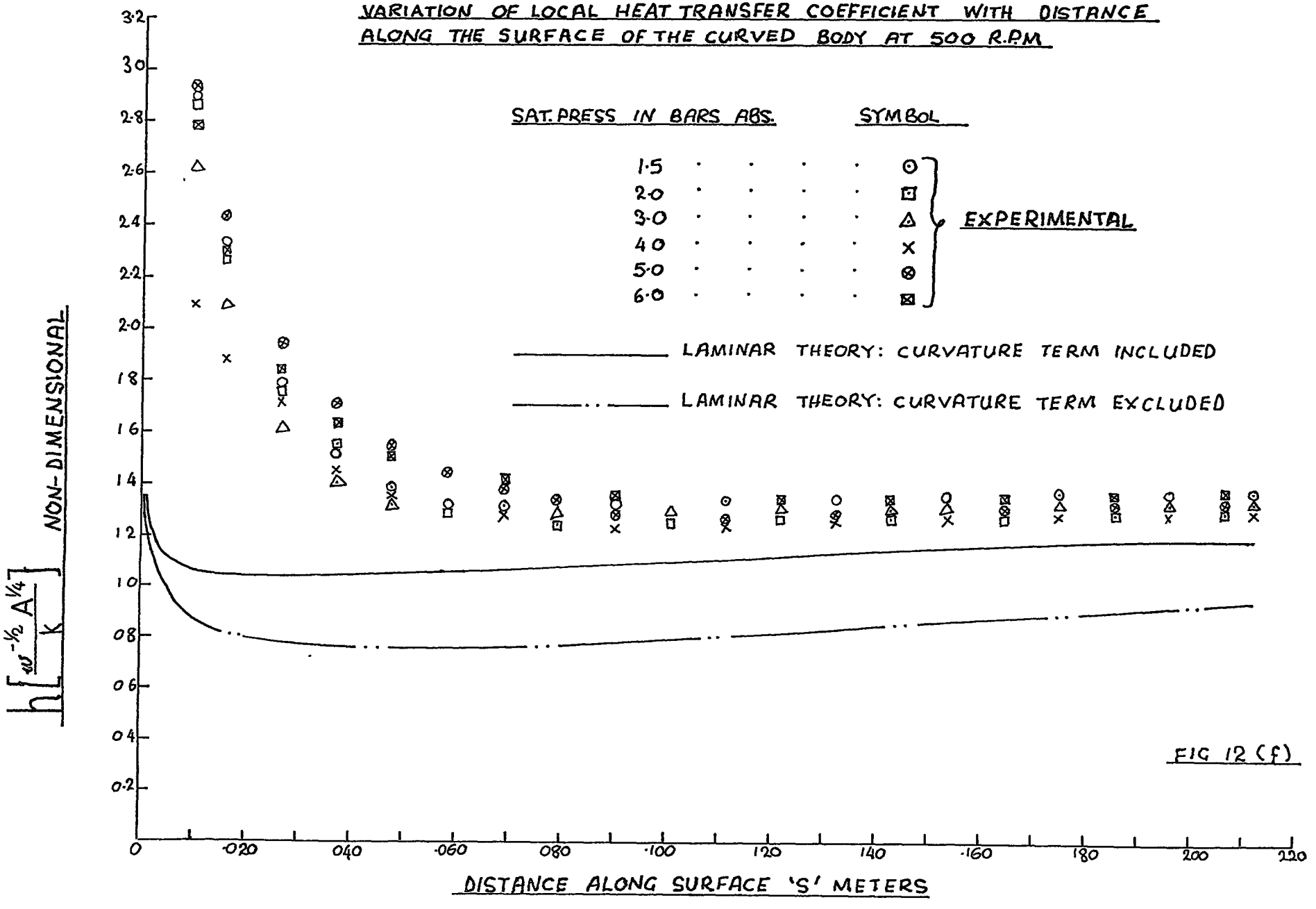
VARIATION OF LOCAL HEAT TRANSFER COEFFICIENT WITH DISTANCE ALONG THE SURFACE OF THE CURVED BODY AT 500 R.P.M
SAT. PRESS IN BARS ABS.
SYMBOL
1·5
2·0
3·0
4·0
5·0
6·0
EXPERIMENTAL
LAMINAR THEORY: CURVATURE TERM INCLUDED
LAMINAR THEORY: CURVATURE TERM EXCLUDED
NON-DIMENSIONAL
$\frac{h}{k}\left[\frac{\omega^{-1/2}}{L}A^{1/4}\right]$
3·2
3·0
2·8
2·6
2·4
2·2
2·0
1·8
1·6
1·4
1·2
1·0
0·8
0·6
0·4
0·2
0
·020
·040
·060
·080
·100
·120
·140
·160
·180
·200
·220
DISTANCE ALONG SURFACE 'S' METERS

FIG 12 (f)

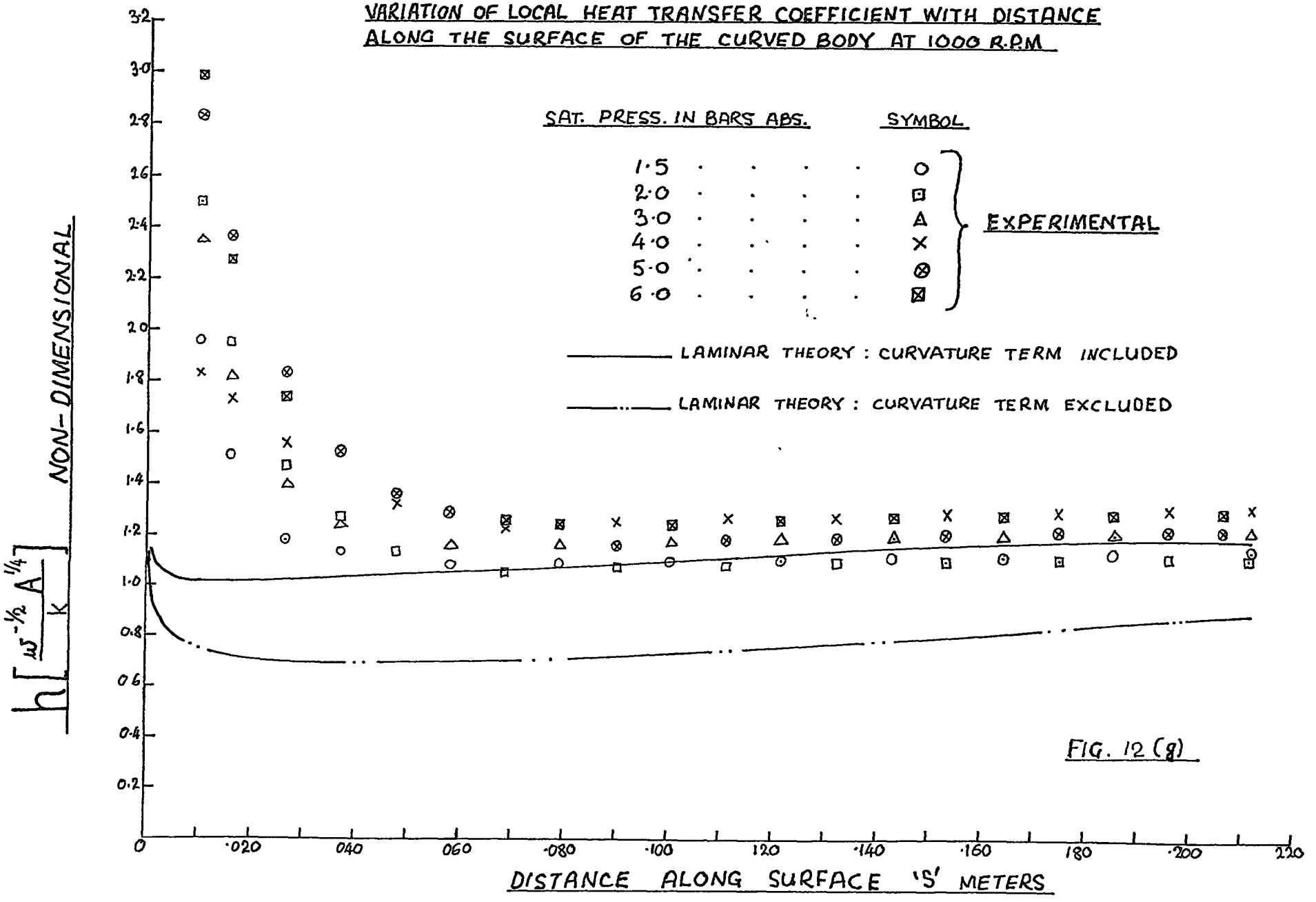
VARIATION OF LOCAL HEAT TRANSFER COEFFICIENT WITH DISTANCE ALONG THE SURFACE OF THE CURVED BODY AT 1000 R.P.M
SAT. PRESS. IN BARS ABS.
SYMBOL
1·5
2·0
3·0
4·0
5·0
6·0
EXPERIMENTAL
LAMINAR THEORY : CURVATURE TERM INCLUDED
LAMINAR THEORY : CURVATURE TERM EXCLUDED
NON-DIMENSIONAL
$\frac{h}{k}\left[\frac{\omega^{-1/2}}{A}\right]^{1/4}$
3·2
3·0
2·8
2·6
2·4
2·2
2·0
1·8
1·6
1·4
1·2
1·0
0·8
0·6
0·4
0·2
0
·020
040
060
·080
·100
120
·140
·160
180
·200
220
DISTANCE ALONG SURFACE 'S' METERS

FIG. 12 (g)

THEORETICAL LOCAL HEAT TRANSFER COEFFICIENT AGAINST DISTANCE ALONG THE SURFACE AT THE INDICATED ROTATIONAL SPEED IN R.P.M.

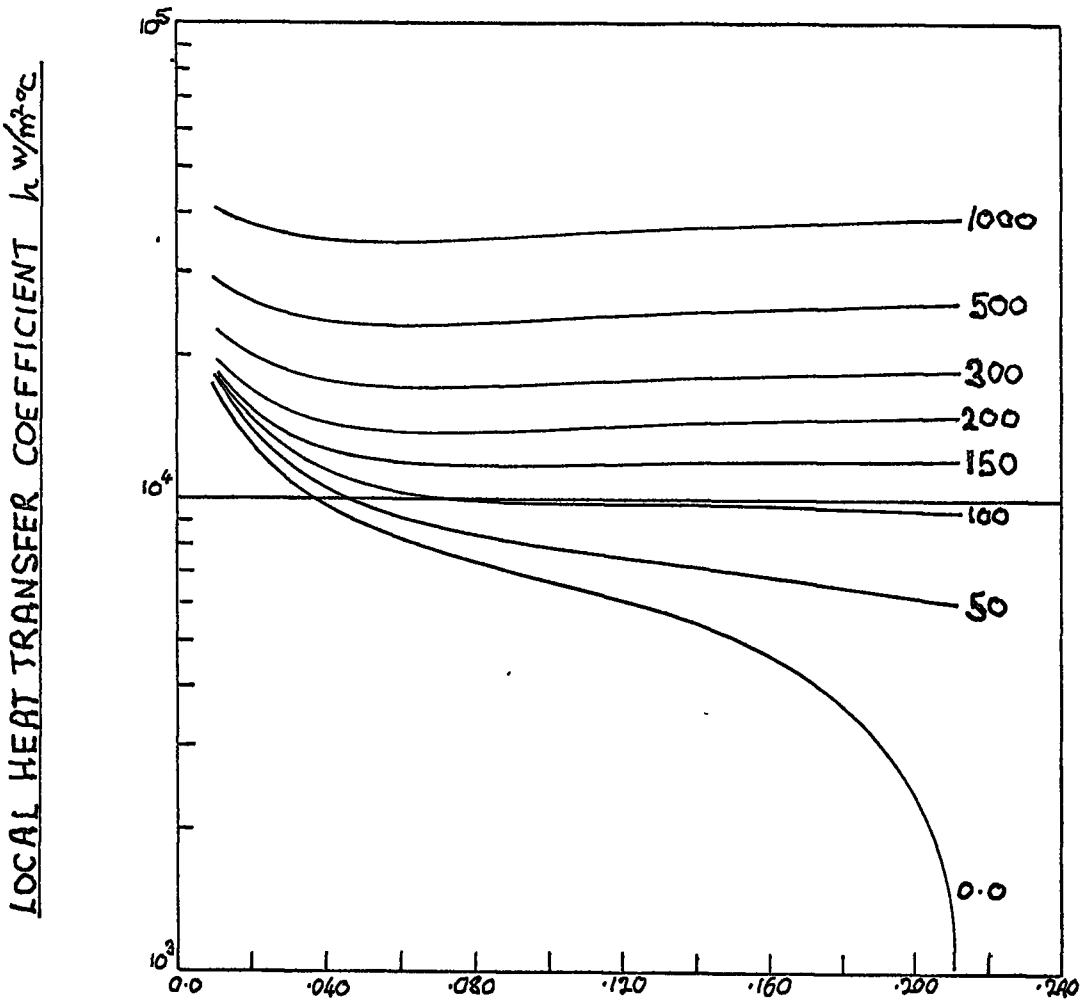

FIG. 13

LOCAL HEAT TRANSFER COEFFICIENT AGAINST DISTANCE ALONG SURFACE

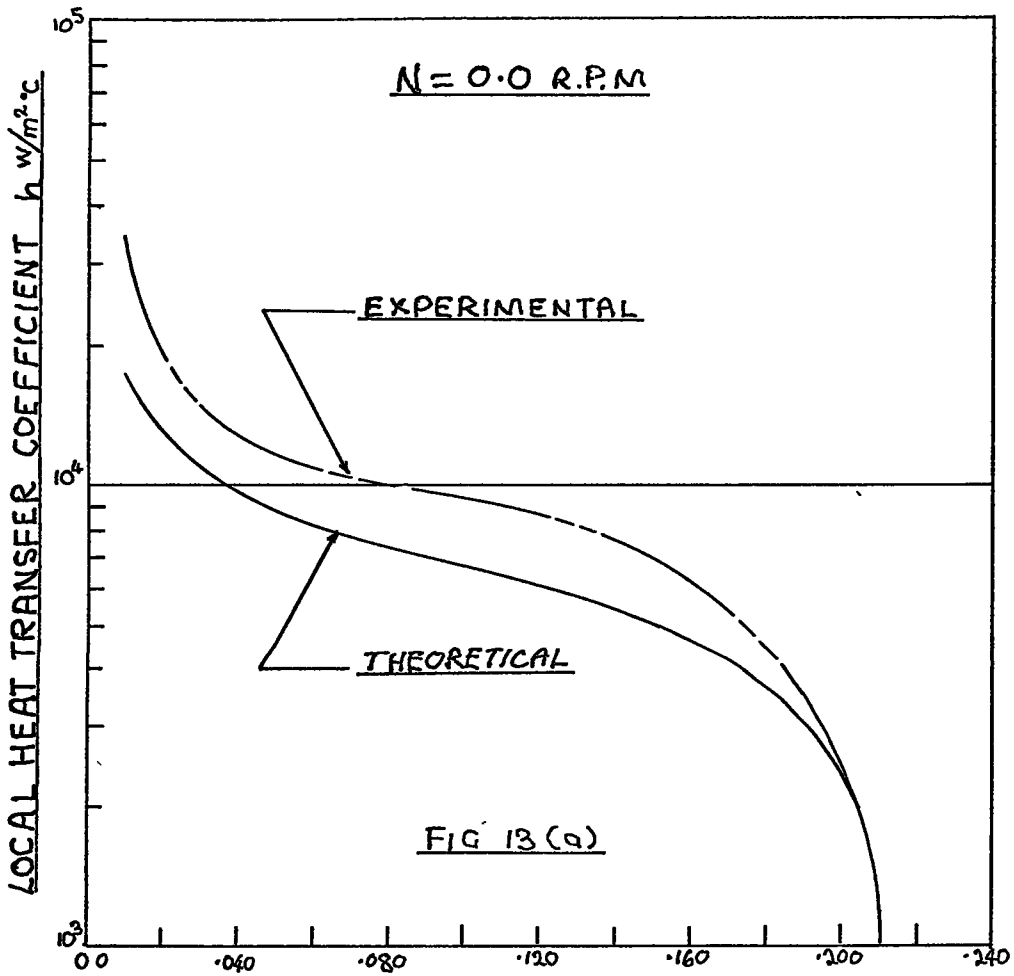

FIG 13 (a)

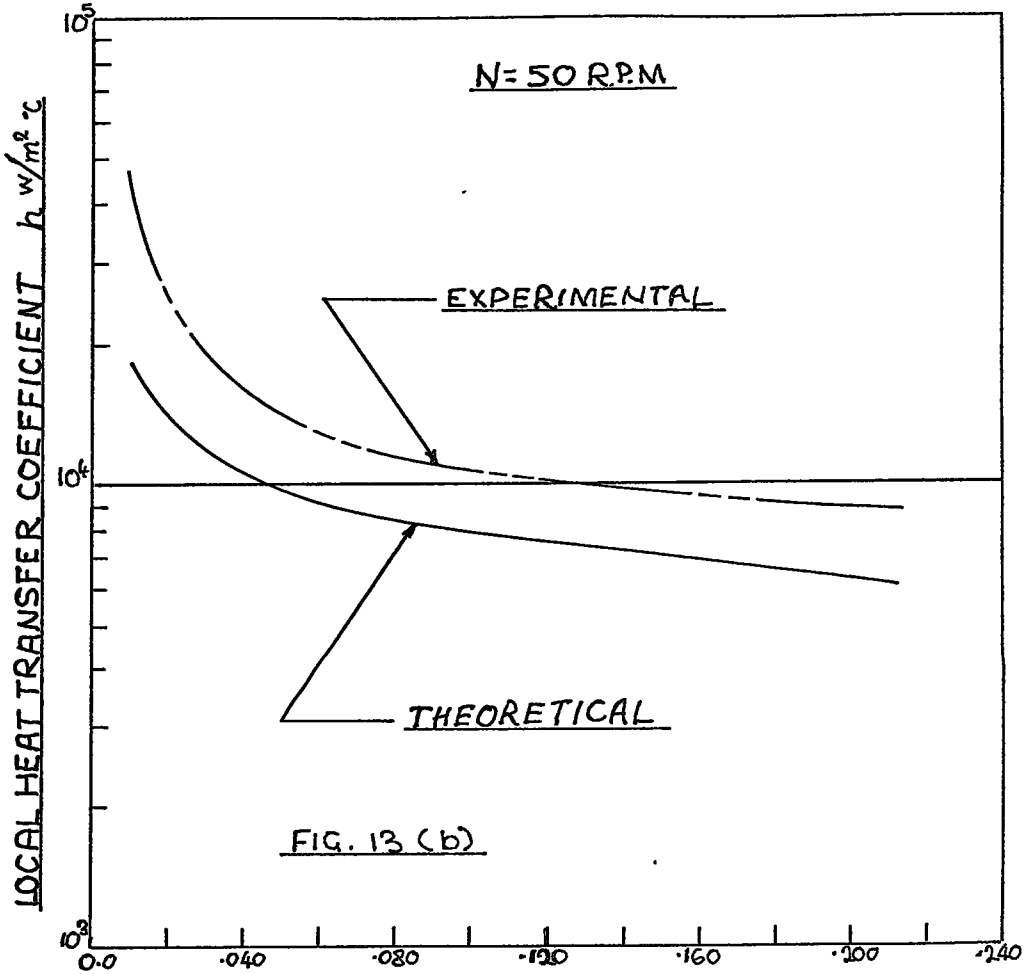

FIG. 13 (b)

LOCAL HEAT TRANSFER COEFFICIENT AGAINST DISTANCE ALONG SURFACE

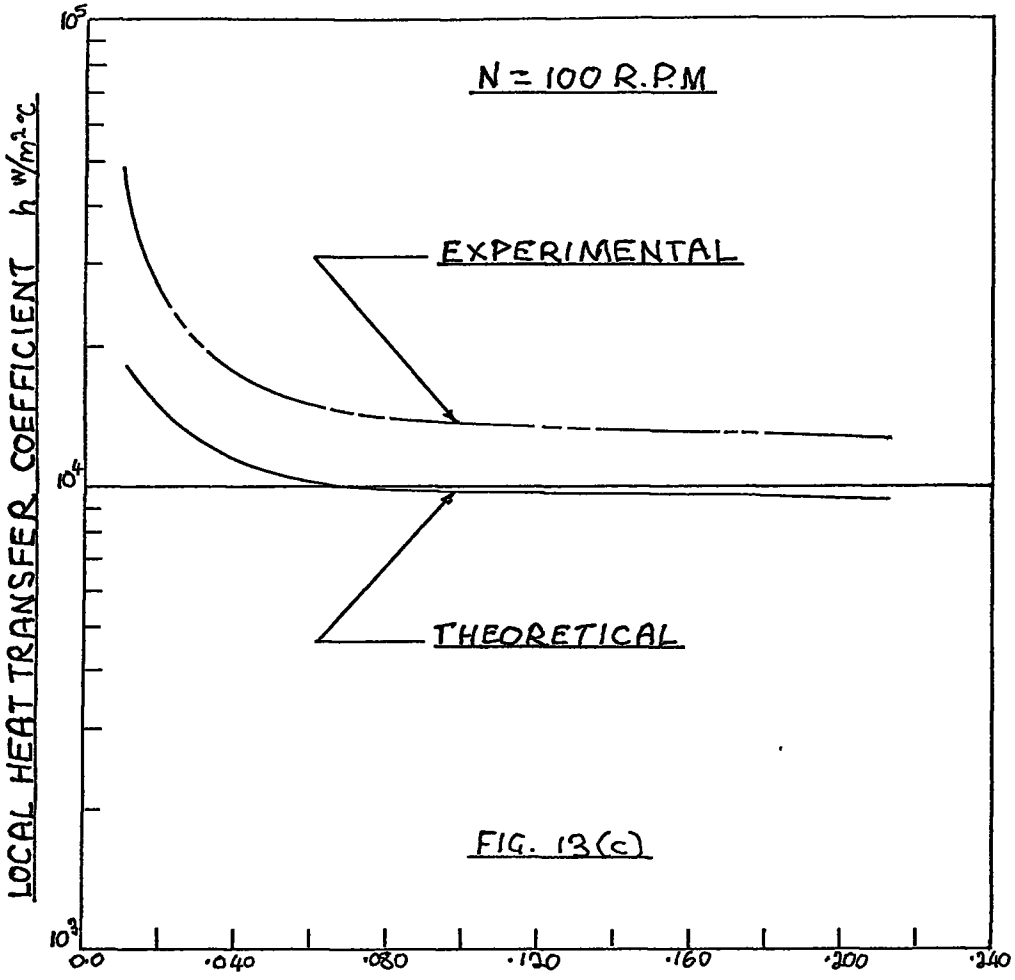

FIG. 13(c)

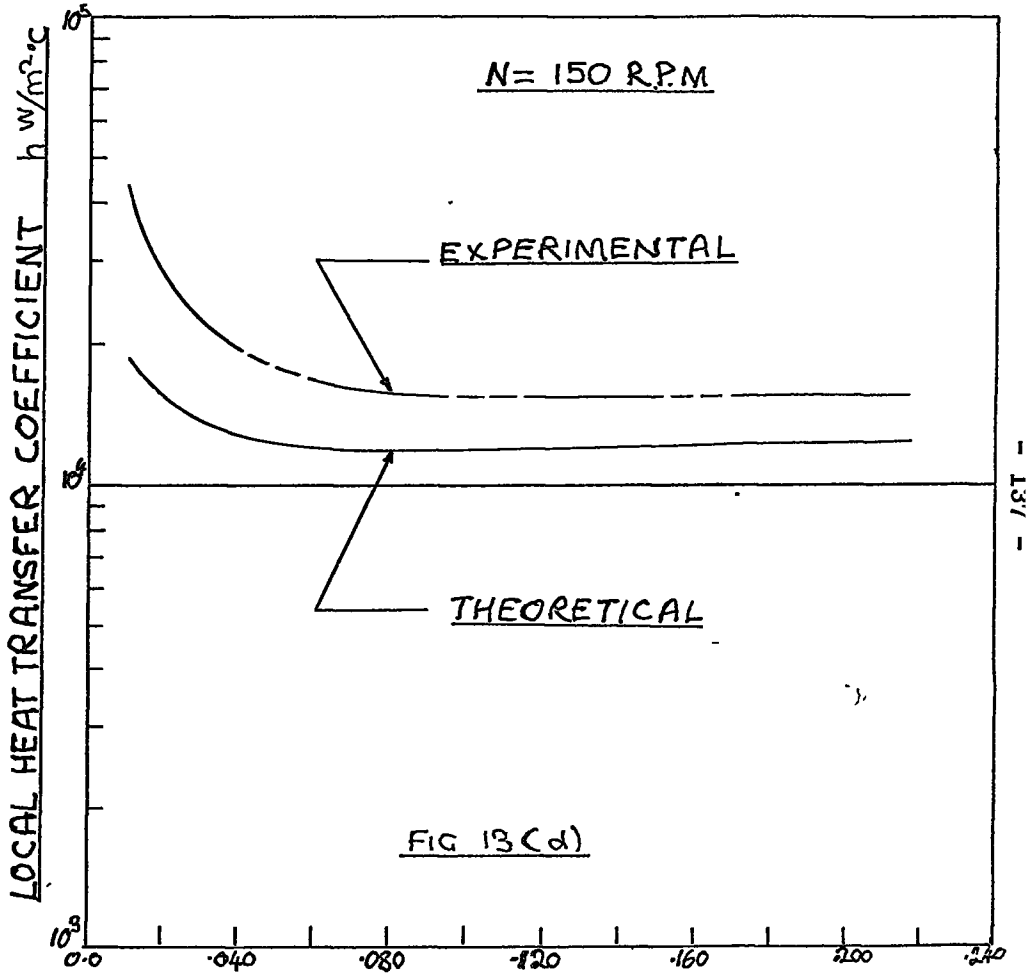

FIG 13(d)

LOCAL HEAT TRANSFER COEFFICIENT AGAINST DISTANCE ALONG SURFACE

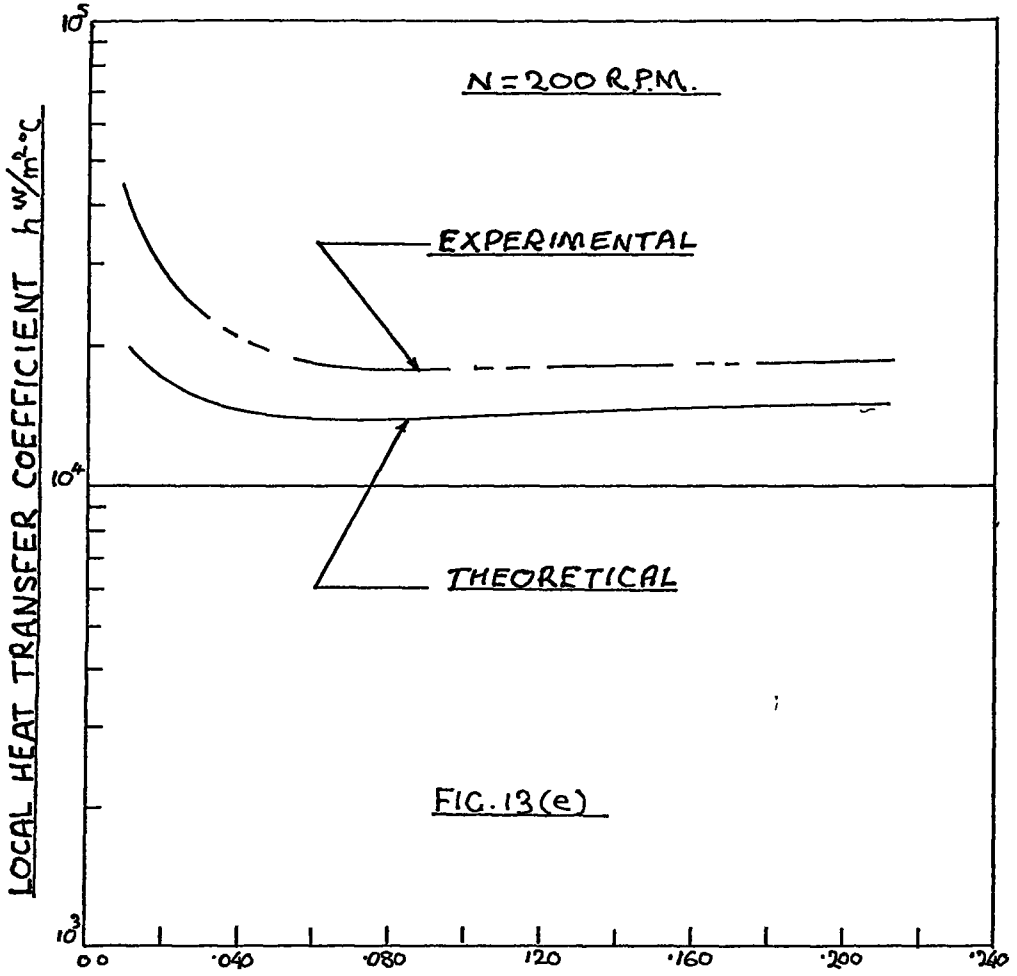

FIG. 13(e)

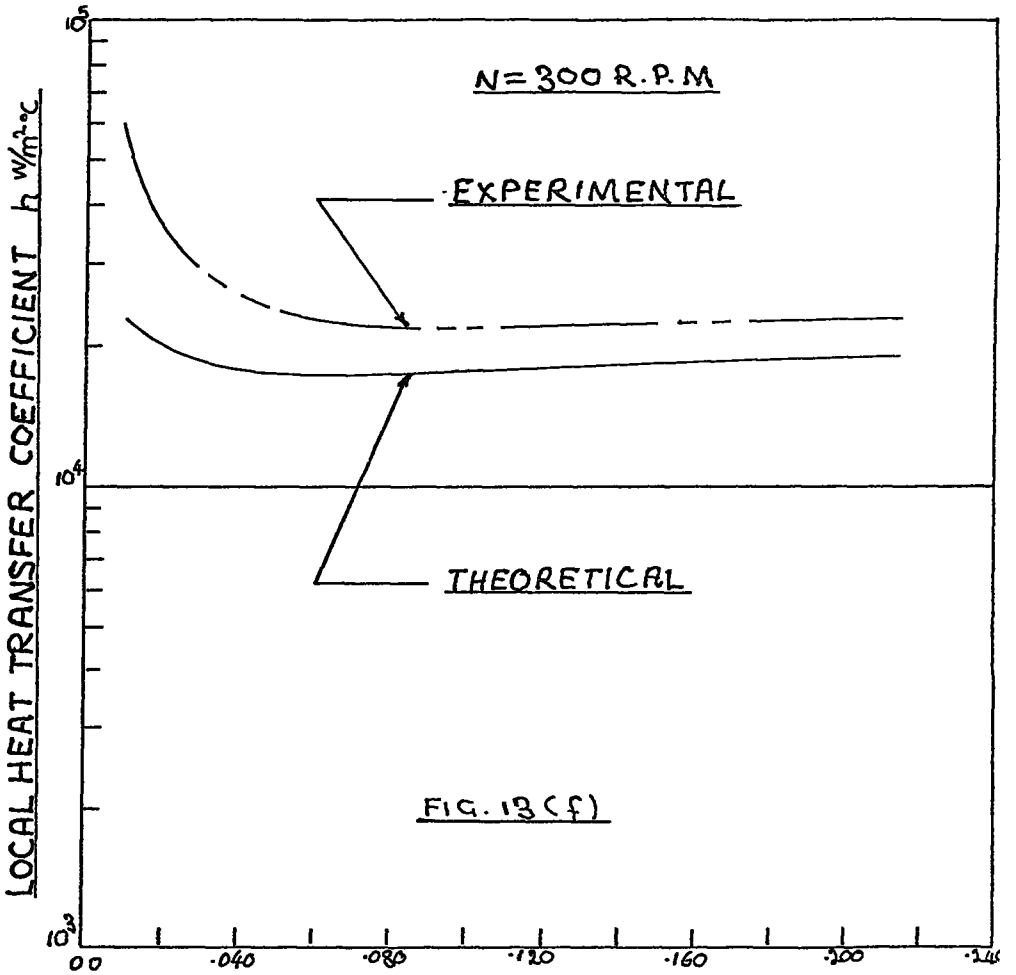

FIG. 13(f)

LOCAL HEAT TRANSFER COEFFICIENT AGAINST DISTANCE ALONG SURFACE

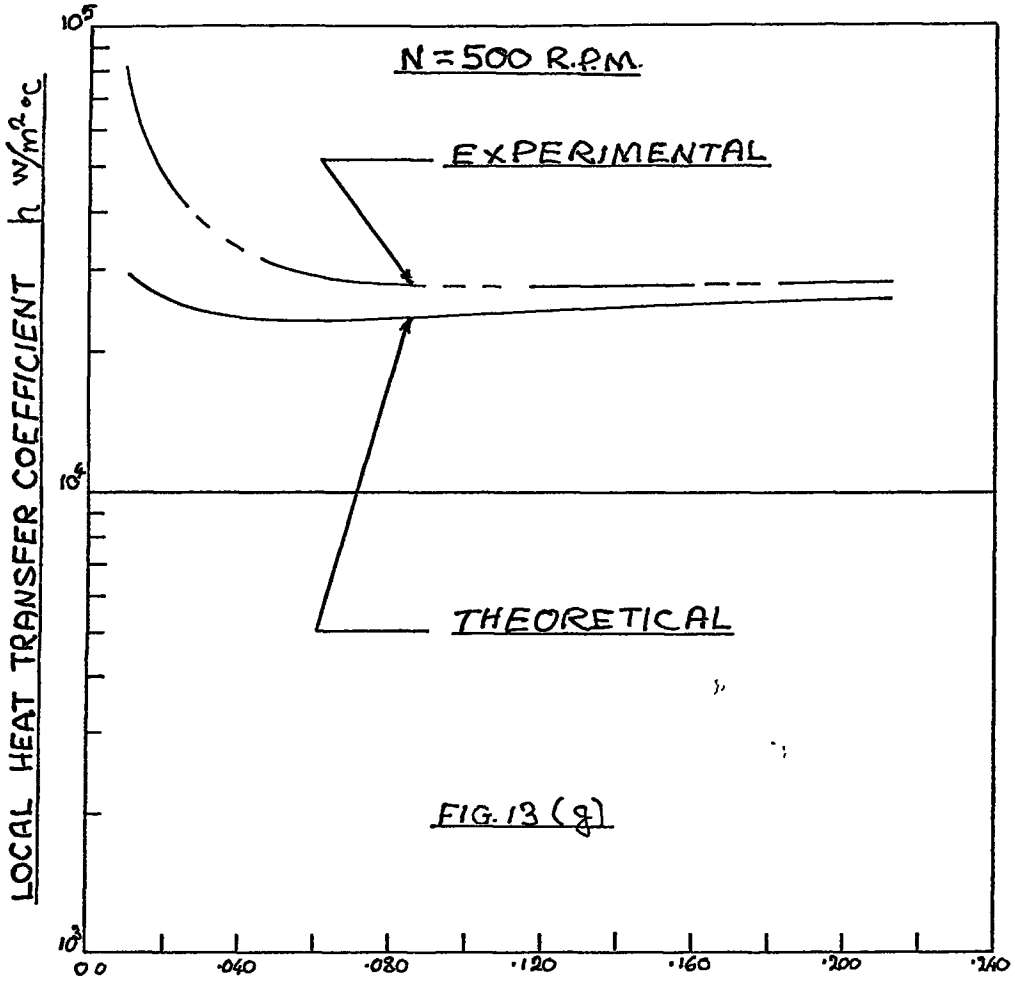

FIG. 13 (g)

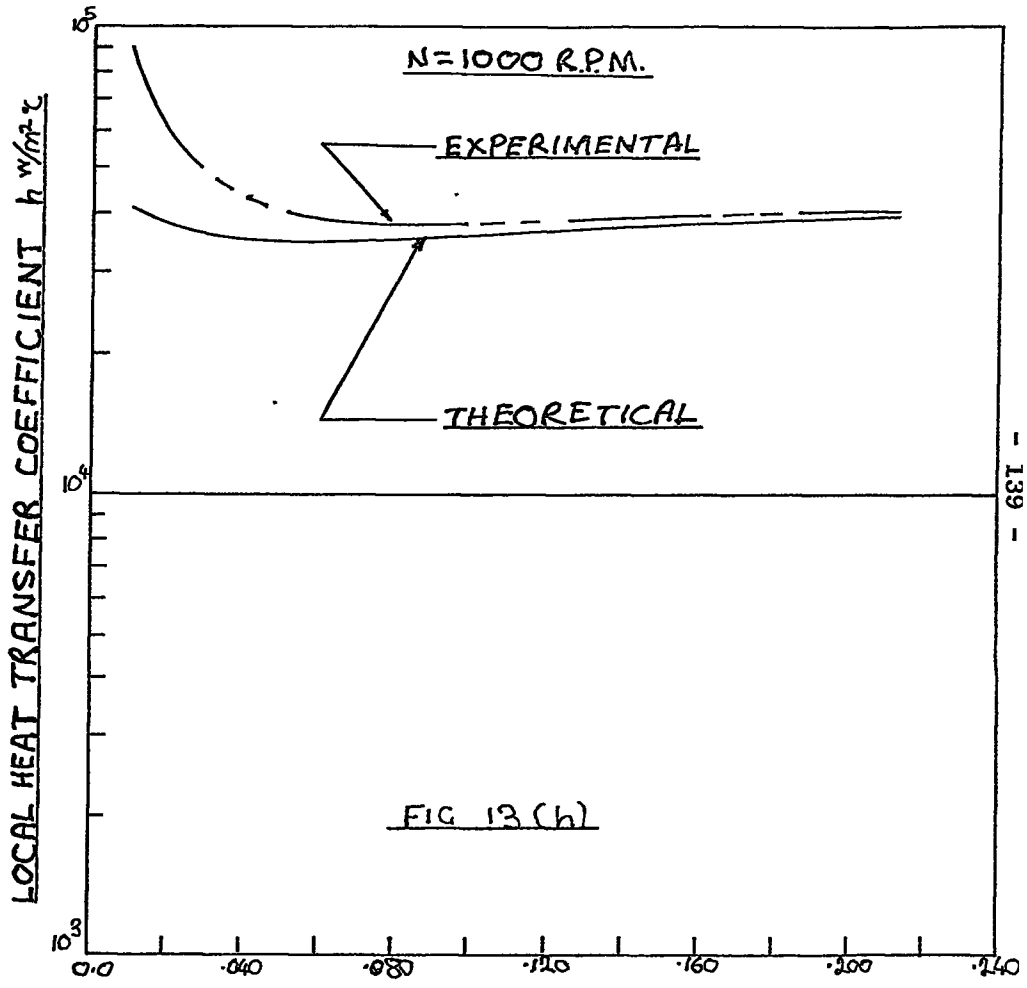

FIG 13 (h)

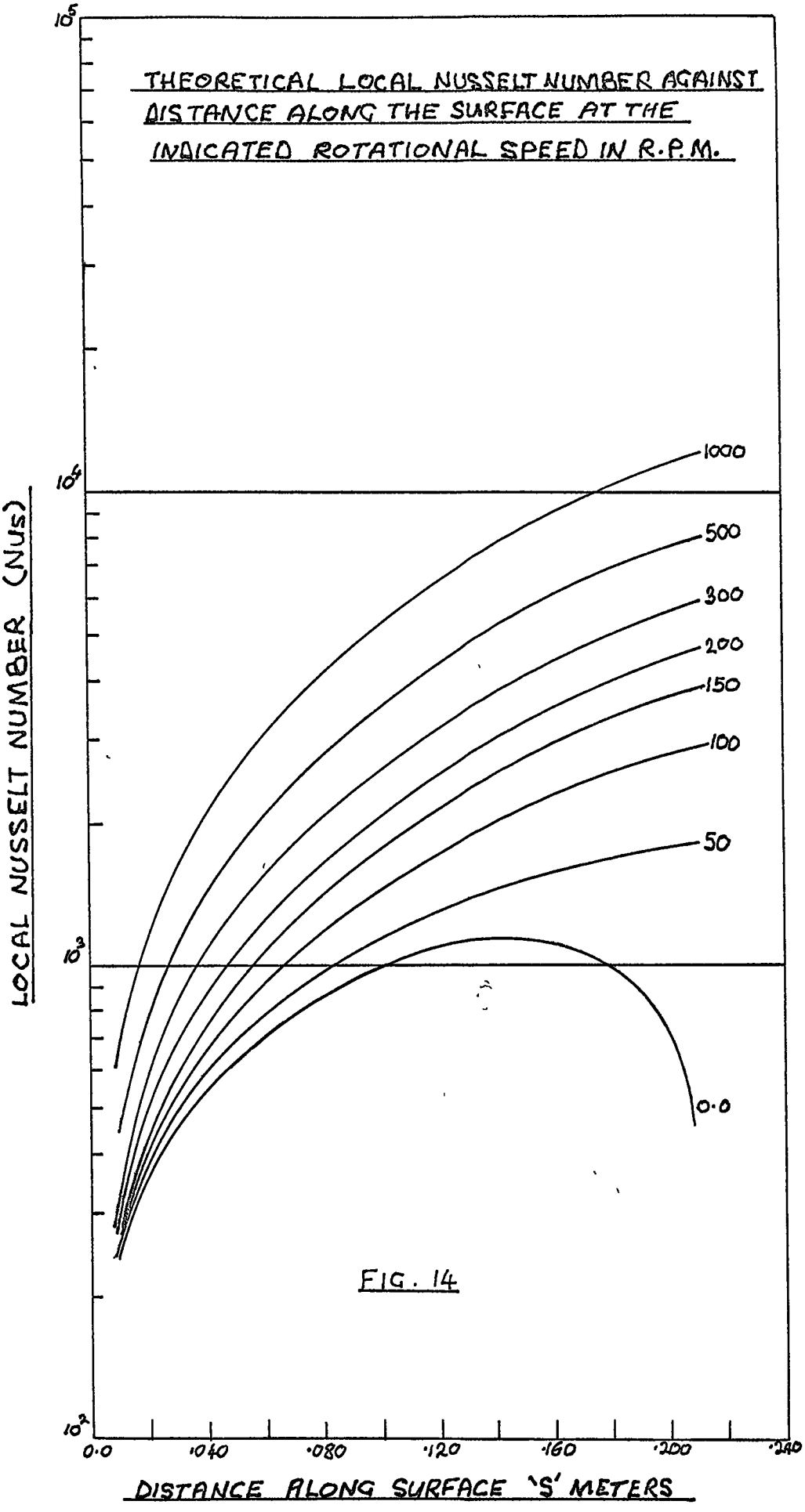
THEORETICAL LOCAL NUSSELT NUMBER AGAINST DISTANCE ALONG THE SURFACE AT THE INDICATED ROTATIONAL SPEED IN R.P.M.
LOCAL NUSSELT NUMBER (Nus)
10^5
10^4
10^3
10^2
1000
500
300
200
150
100
50
0·0
0·0
·040
·080
·120
·160
·200
·240
DISTANCE ALONG SURFACE 'S' METERS

FIG. 14

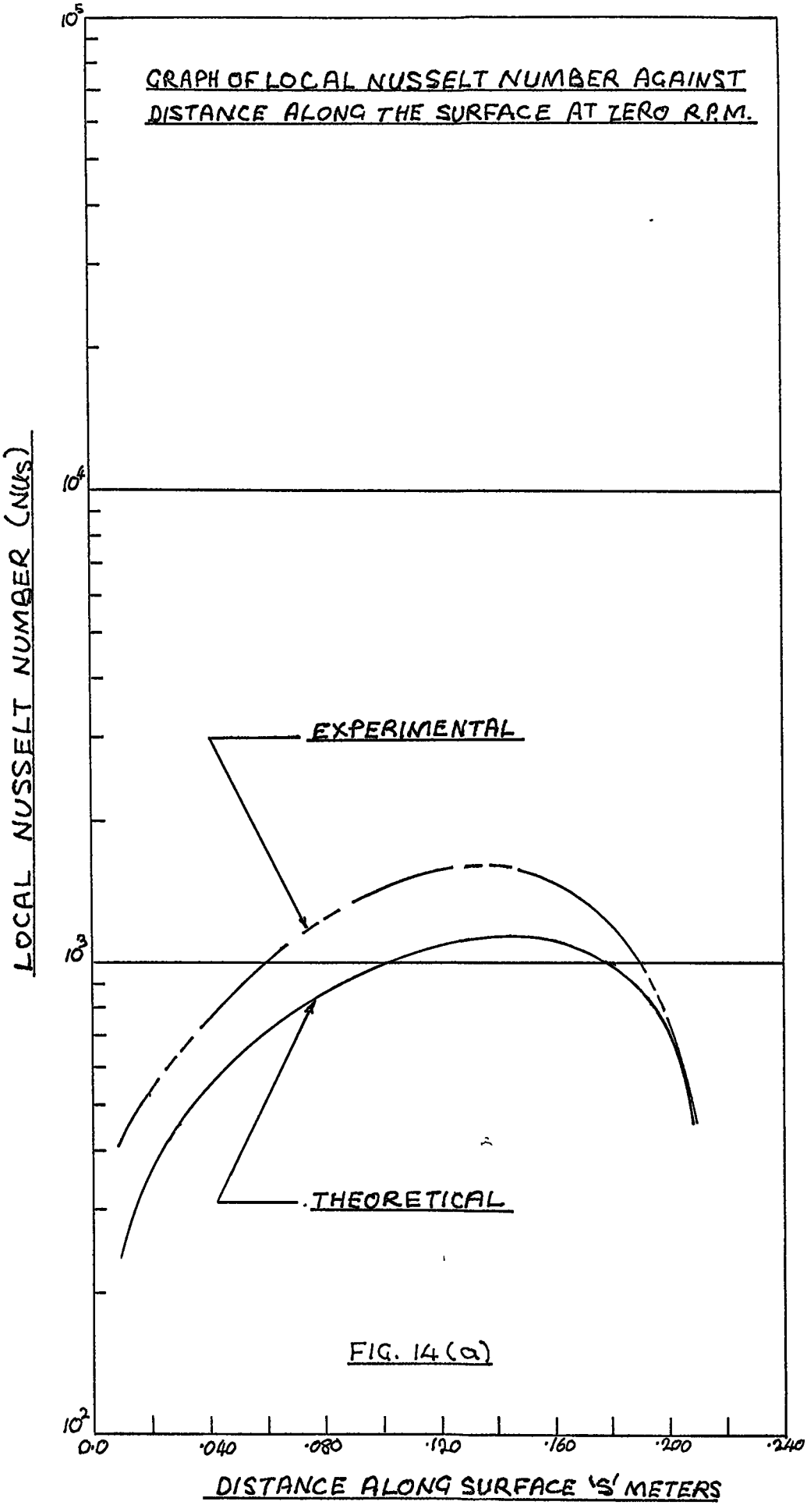
GRAPH OF LOCAL NUSSELT NUMBER AGAINST DISTANCE ALONG THE SURFACE AT ZERO R.P.M.
LOCAL NUSSELT NUMBER (Nus)
10^5
10^4
10^3
10^2
EXPERIMENTAL
THEORETICAL
0·0
·040
·080
·120
·160
·200
·240
DISTANCE ALONG SURFACE 'S' METERS

FIG. 14 (a)

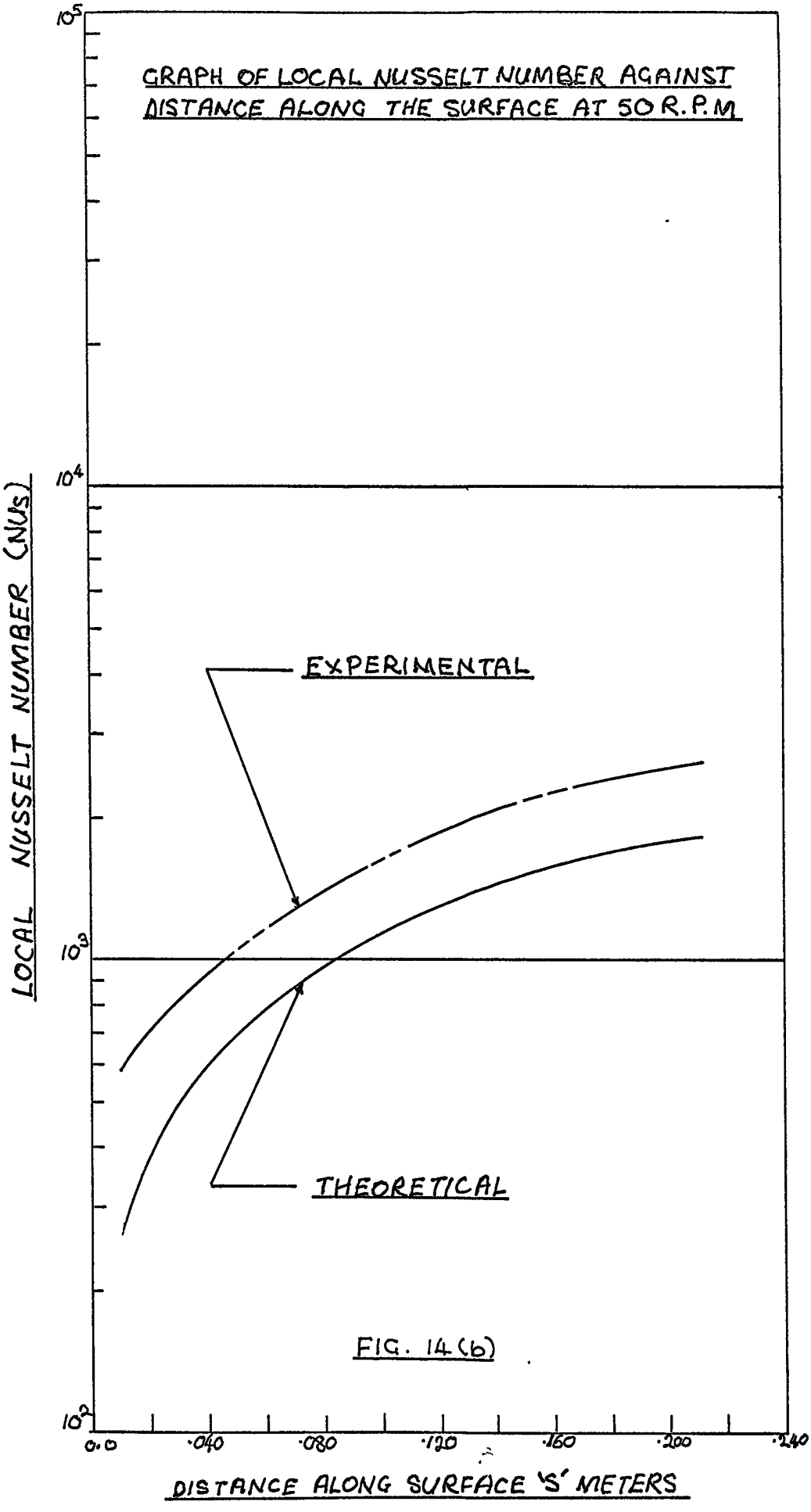
GRAPH OF LOCAL NUSSELT NUMBER AGAINST DISTANCE ALONG THE SURFACE AT 50 R.P.M
LOCAL NUSSELT NUMBER (Nus)
10^5
10^4
10^3
10^2
EXPERIMENTAL
THEORETICAL
0.0
·040
·080
·120
·160
·200
·240
DISTANCE ALONG SURFACE 'S' METERS

FIG. 14(b)

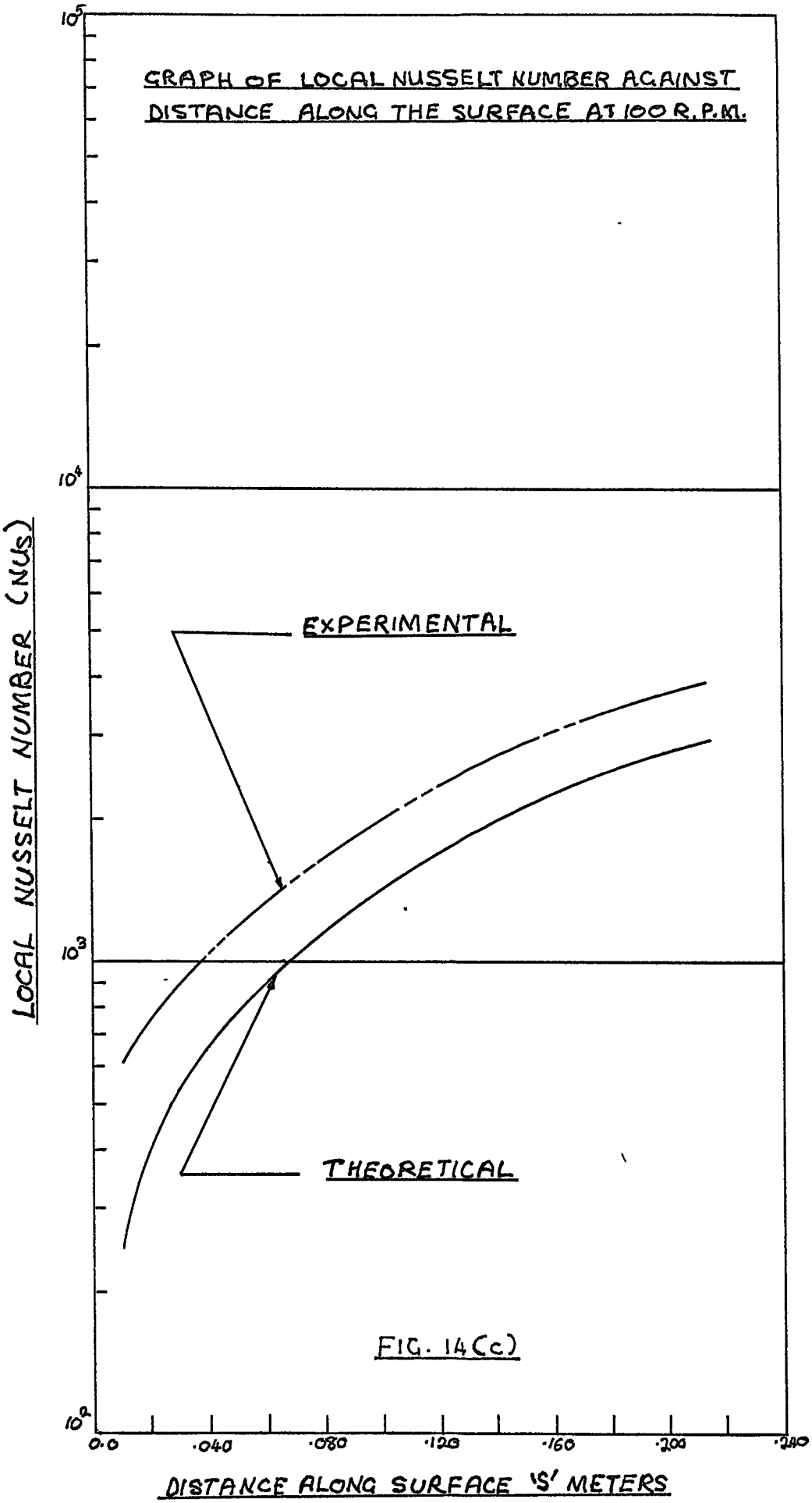
GRAPH OF LOCAL NUSSELT NUMBER AGAINST DISTANCE ALONG THE SURFACE AT 100 R.P.M.
LOCAL NUSSELT NUMBER (Nus)
10^5
10^4
10^3
10^2
EXPERIMENTAL
THEORETICAL
0.0
.040
.080
.120
.160
.200
.240
DISTANCE ALONG SURFACE 'S' METERS

FIG. 14(c)

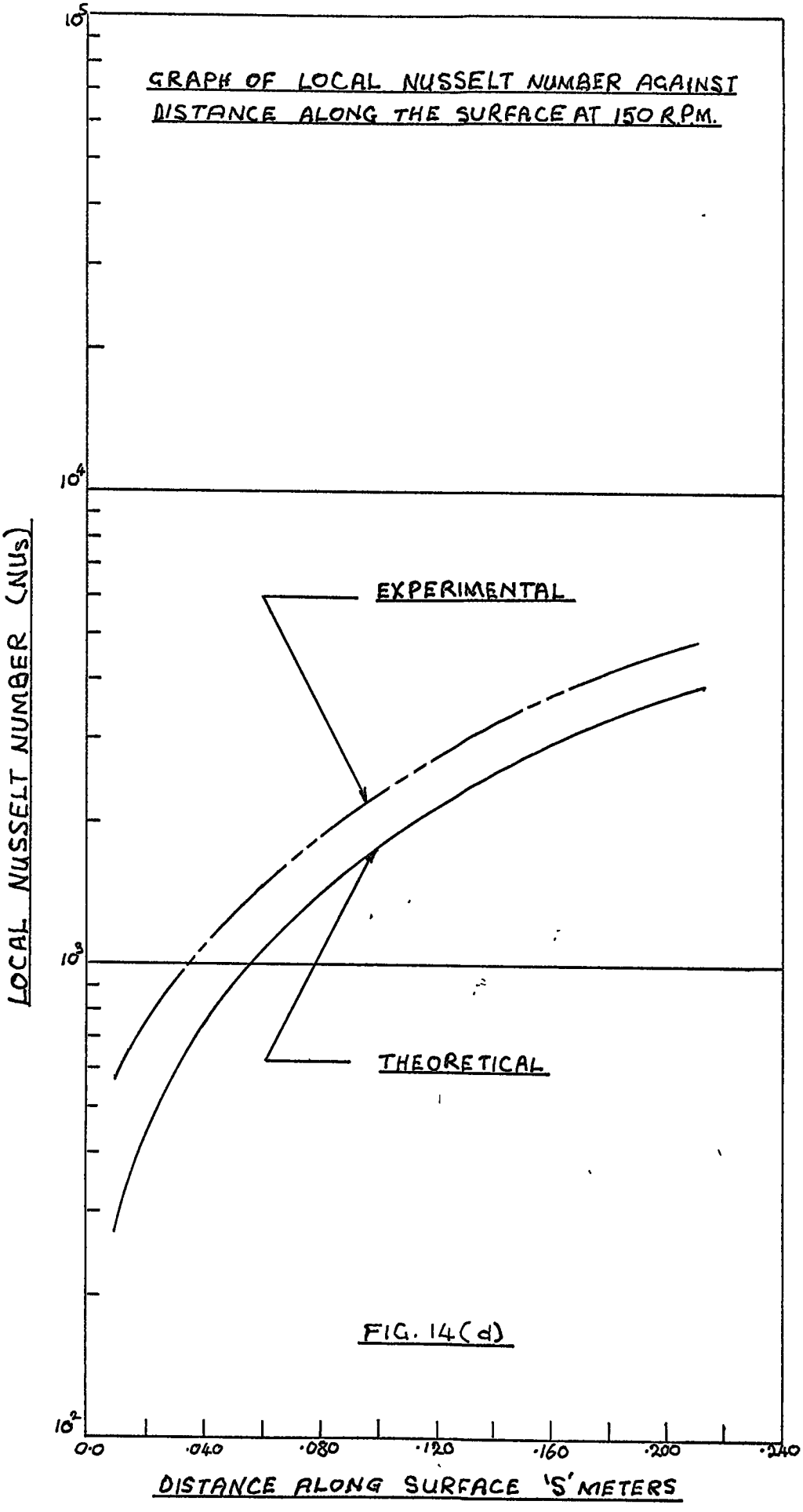
GRAPH OF LOCAL NUSSELT NUMBER AGAINST DISTANCE ALONG THE SURFACE AT 150 R.P.M.
LOCAL NUSSELT NUMBER (NUs)
10^5
10^4
10^3
10^2
EXPERIMENTAL
THEORETICAL
0·0
·040
·080
·120
·160
·200
·240
DISTANCE ALONG SURFACE 'S' METERS

FIG. 14(d)

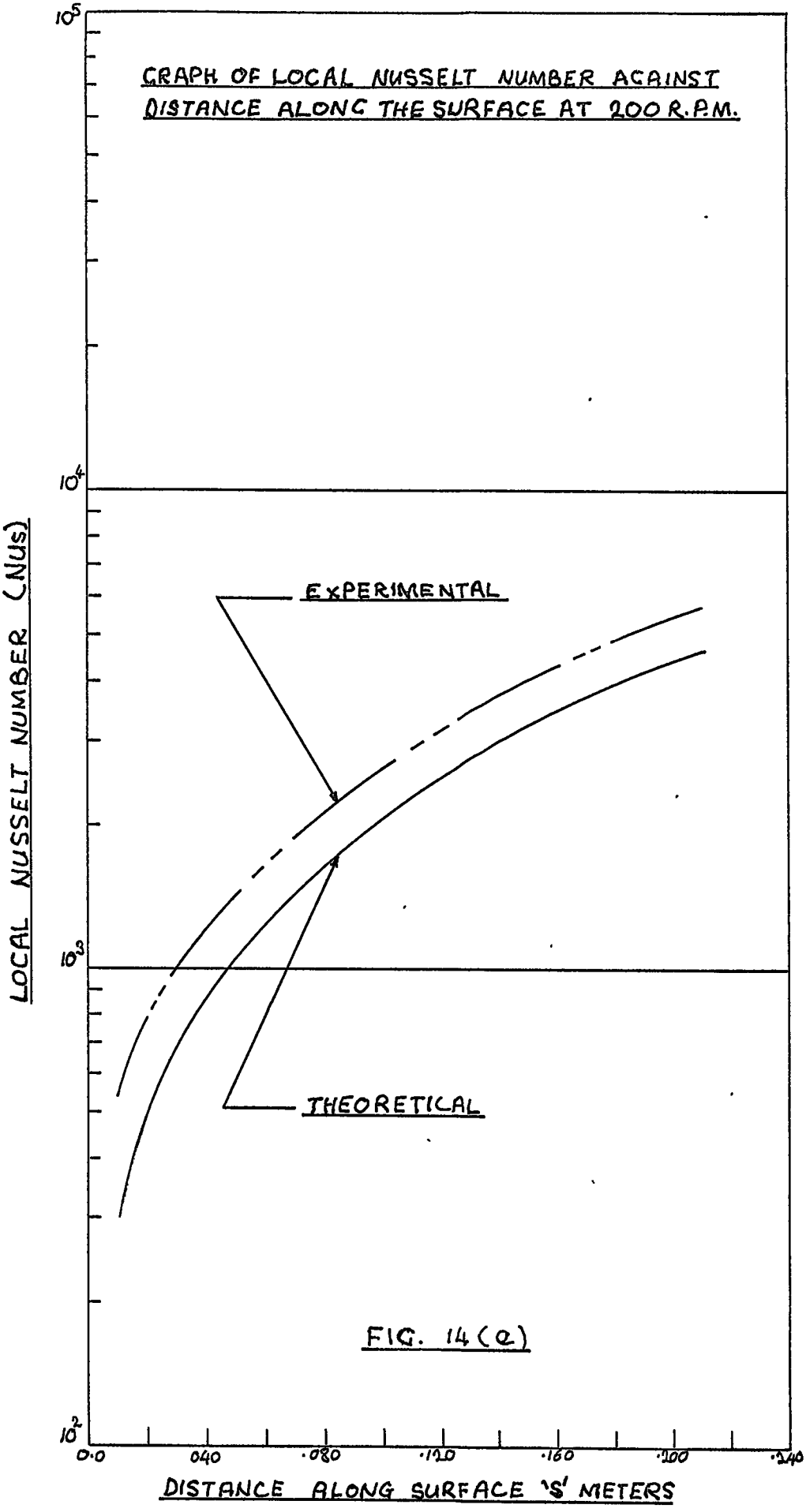
GRAPH OF LOCAL NUSSELT NUMBER AGAINST DISTANCE ALONG THE SURFACE AT 200 R.P.M.
LOCAL NUSSELT NUMBER (Nus)
10^5
10^4
10^3
10^2
EXPERIMENTAL
THEORETICAL
0·0
·040
·080
·120
·160
·200
·240
DISTANCE ALONG SURFACE 'S' METERS

FIG. 14 (c)

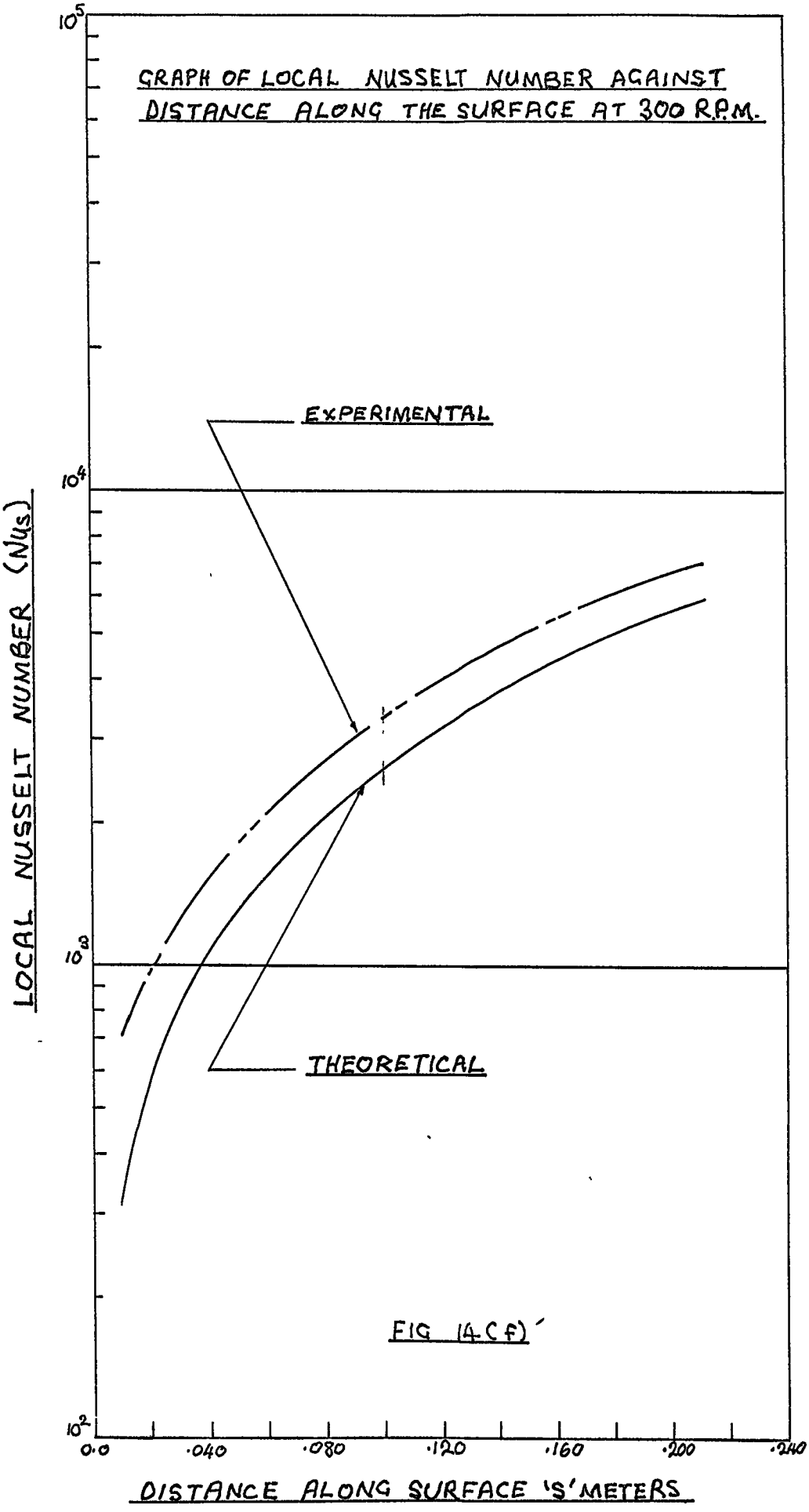
GRAPH OF LOCAL NUSSELT NUMBER AGAINST DISTANCE ALONG THE SURFACE AT 300 R.P.M.
EXPERIMENTAL
THEORETICAL
LOCAL NUSSELT NUMBER (Nus)
10^5
10^4
10^3
10^2
0·0
·040
·080
·120
·160
·200
·240
DISTANCE ALONG SURFACE 'S' METERS

FIG 14.C f)

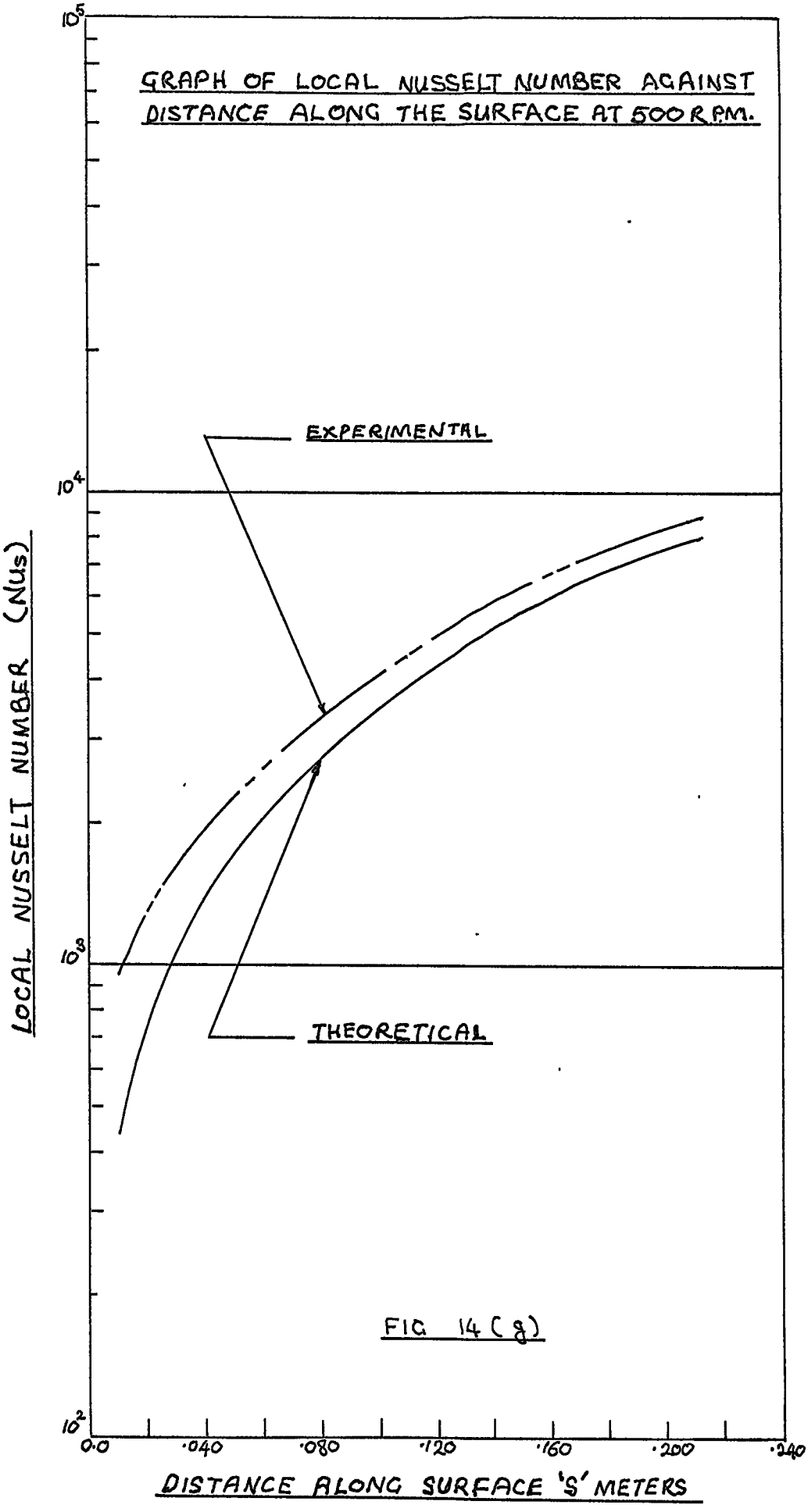
GRAPH OF LOCAL NUSSELT NUMBER AGAINST DISTANCE ALONG THE SURFACE AT 500 R.P.M.
EXPERIMENTAL
THEORETICAL
LOCAL NUSSELT NUMBER (Nus)
10^5
10^4
10^3
10^2
0·0
·040
·080
·120
·160
·200
·240
DISTANCE ALONG SURFACE 'S' METERS

FIG 14 (g)

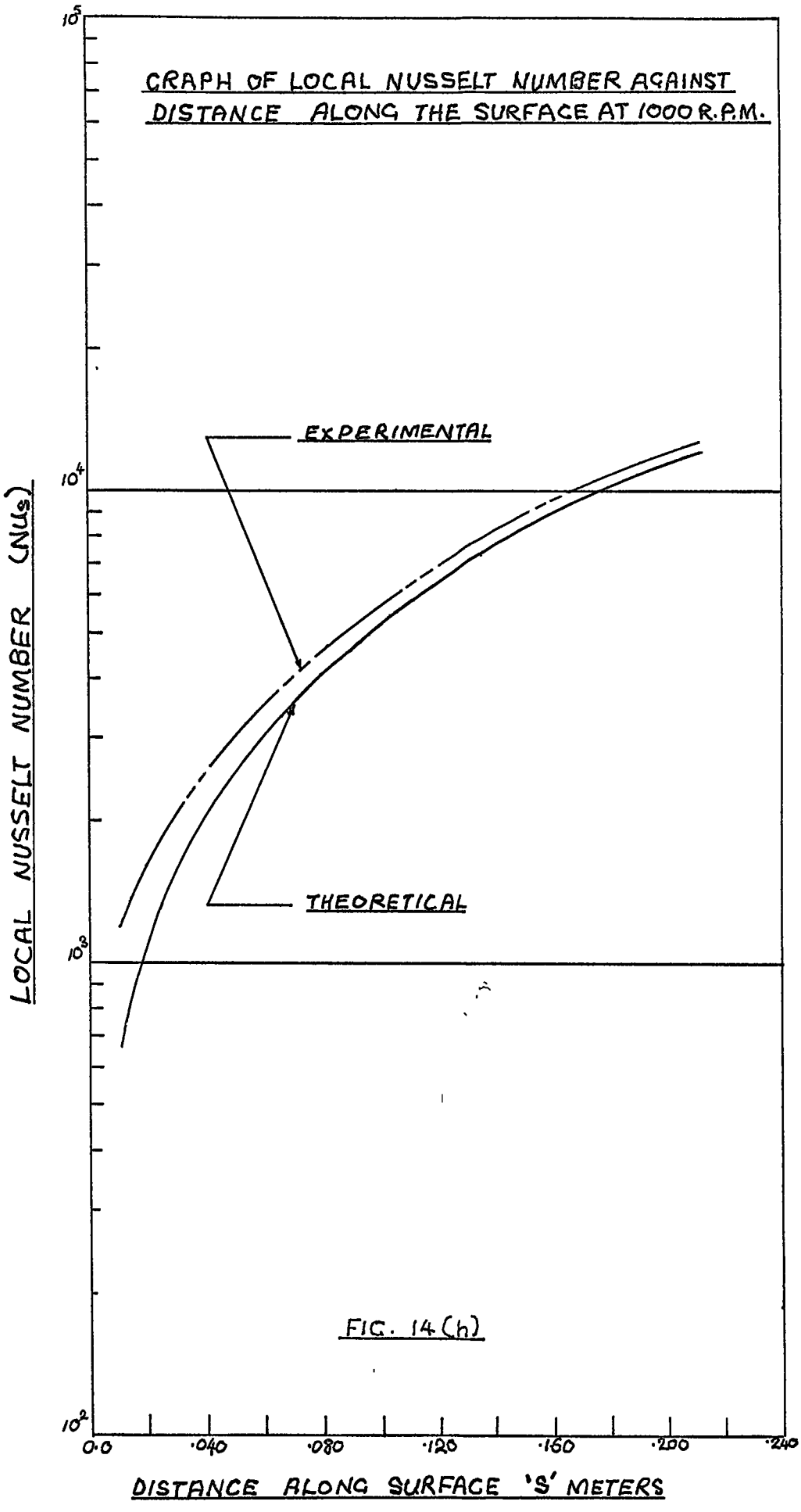
GRAPH OF LOCAL NUSSELT NUMBER AGAINST DISTANCE ALONG THE SURFACE AT 1000 R.P.M.
EXPERIMENTAL
THEORETICAL
LOCAL NUSSELT NUMBER (Nus)
10^5
10^4
10^3
10^2
0·0
·040
·080
·120
·160
·200
·240
DISTANCE ALONG SURFACE 'S' METERS

FIG. 14(h)

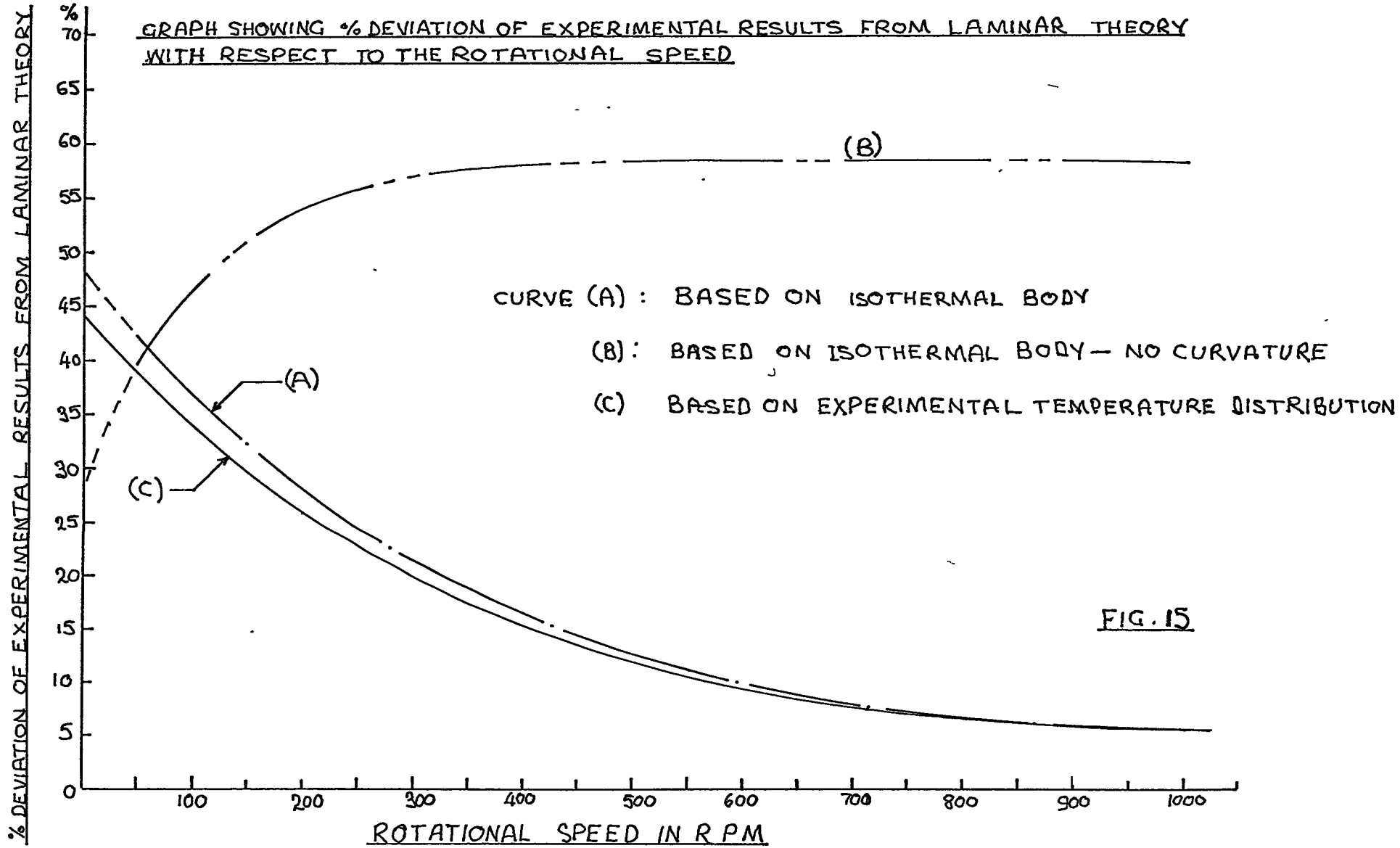
GRAPH SHOWING % DEVIATION OF EXPERIMENTAL RESULTS FROM LAMINAR THEORY WITH RESPECT TO THE ROTATIONAL SPEED
% DEVIATION OF EXPERIMENTAL RESULTS FROM LAMINAR THEORY
%
70
65
60
55
50
45
40
35
30
25
20
15
10
5
0
100
200
300
400
500
600
700
800
900
1000
ROTATIONAL SPEED IN R P M
(A)
(B)
(C)
CURVE (A) : BASED ON ISOTHERMAL BODY
(B) : BASED ON ISOTHERMAL BODY — NO CURVATURE
(C) BASED ON EXPERIMENTAL TEMPERATURE DISTRIBUTION

FIG. 15

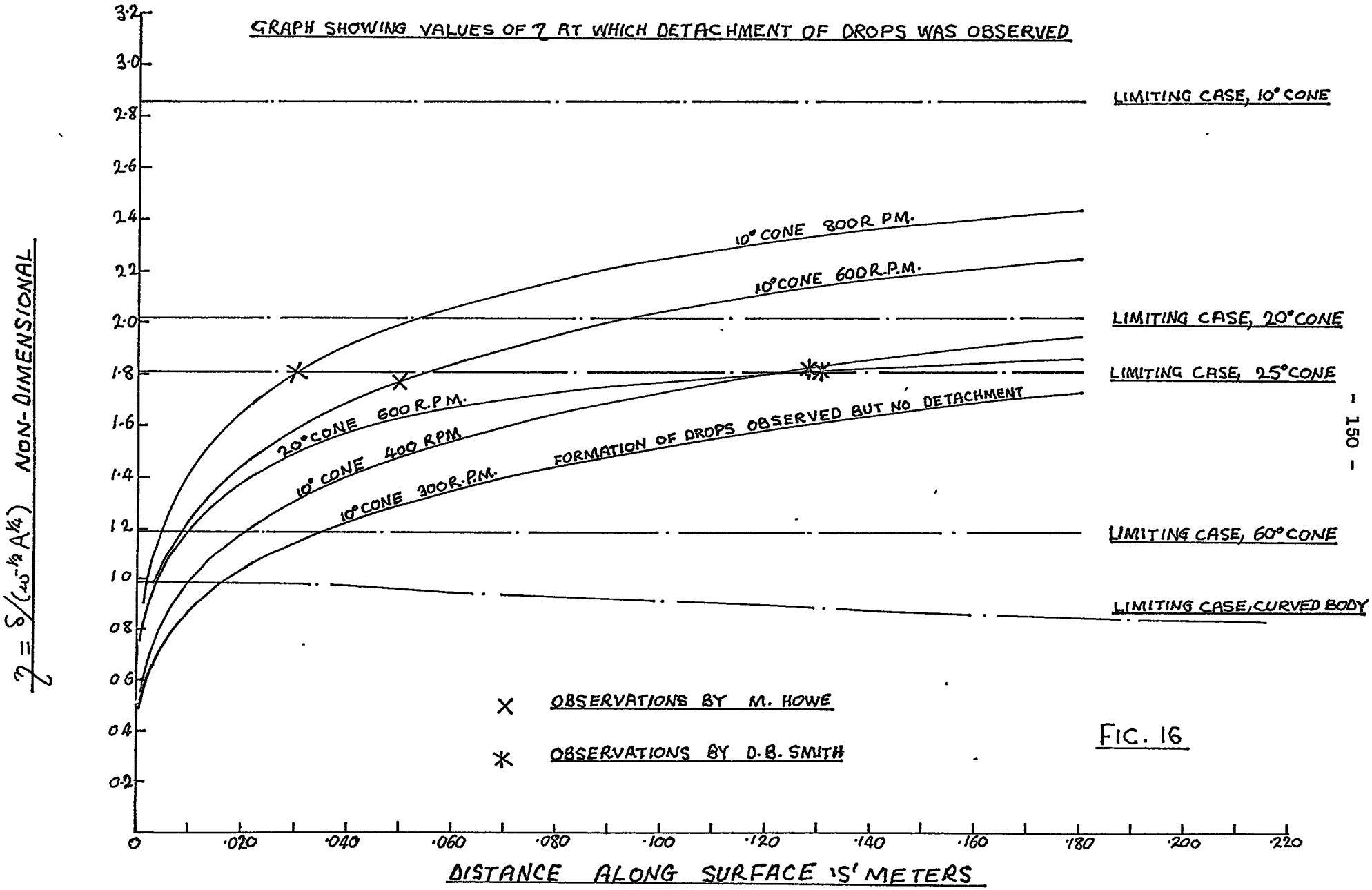
GRAPH SHOWING VALUES OF η AT WHICH DETACHMENT OF DROPS WAS OBSERVED
η = δ/(ω^-½ A^¼) NON-DIMENSIONAL
3·2
3·0
2·8
2·6
2·4
2·2
2·0
1·8
1·6
1·4
1·2
1·0
0·8
0·6
0·4
0·2
0
·020
·040
·060
·080
·100
·120
·140
·160
·180
·200
·220
DISTANCE ALONG SURFACE 'S' METERS
LIMITING CASE, 10° CONE
LIMITING CASE, 20° CONE
LIMITING CASE, 2·5° CONE
LIMITING CASE, 60° CONE
LIMITING CASE, CURVED BODY
10° CONE 800 R.P.M.
10° CONE 600 R.P.M.
20° CONE 600 R.P.M.
10° CONE 400 RPM
10° CONE 300 R.P.M.
FORMATION OF DROPS OBSERVED BUT NO DETACHMENT
× OBSERVATIONS BY M. HOWE
* OBSERVATIONS BY D.B. SMITH

FIG. 16

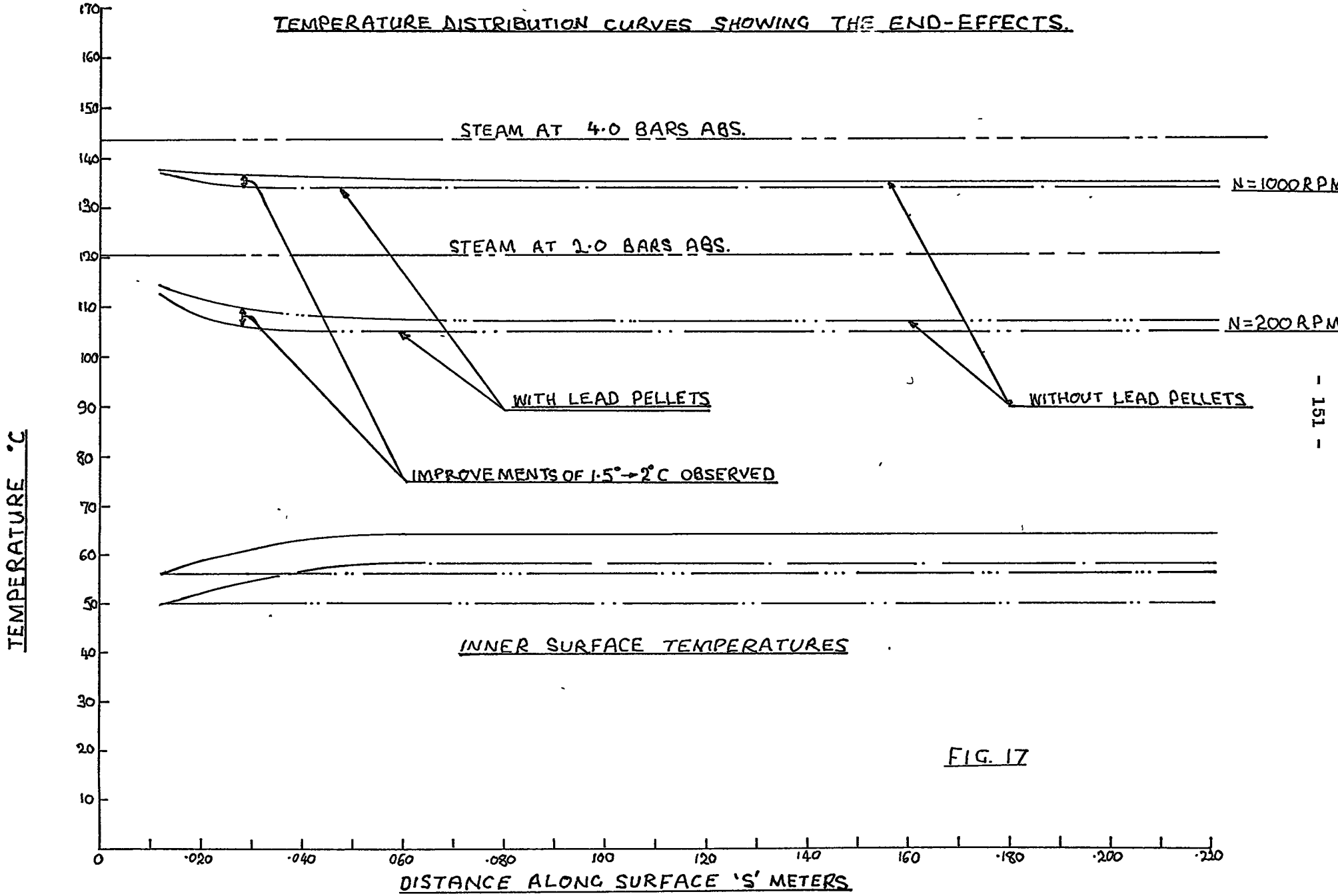
TEMPERATURE DISTRIBUTION CURVES SHOWING THE END-EFFECTS.
STEAM AT 4·0 BARS ABS.
STEAM AT 2·0 BARS ABS.
N=1000 RPM
N=200 RPM
WITH LEAD PELLETS
WITHOUT LEAD PELLETS
IMPROVEMENTS OF 1·5°→2°C OBSERVED
INNER SURFACE TEMPERATURES
TEMPERATURE °C
DISTANCE ALONG SURFACE 'S' METERS
0
·020
·040
060
·080
100
120
140
160
·180
·200
·220
10
20
30
40
50
60
70
80
90
100
110
120
130
140
150
160
170

FIG. 17

DIAGRAMMATIC ARRANGEMENT OF THE APPARATUS FOR DETERMINING THE THERMAL CONDUCTIVITY OF THE BODY WALL BY ELECTRICAL METHOD

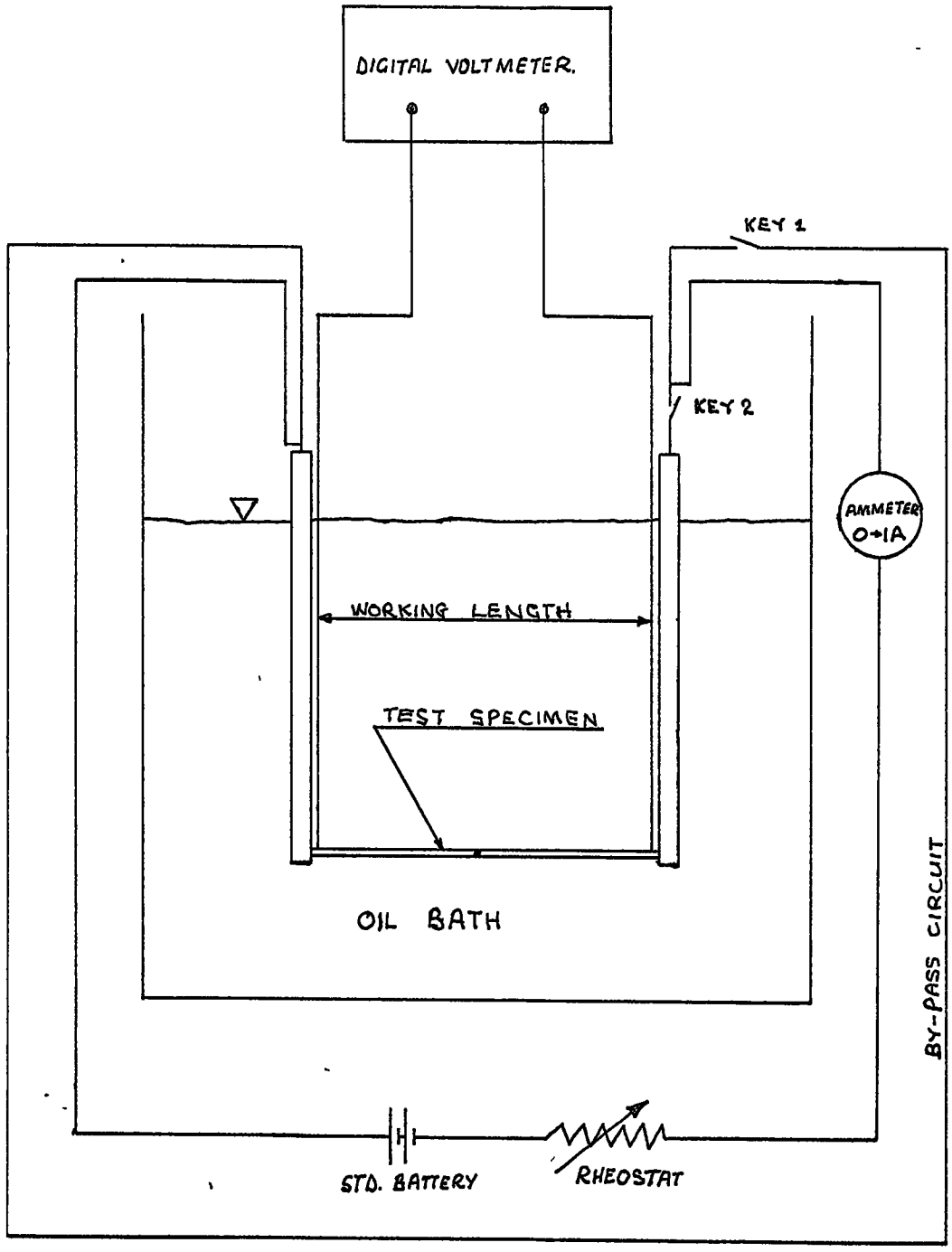

FIG. A1

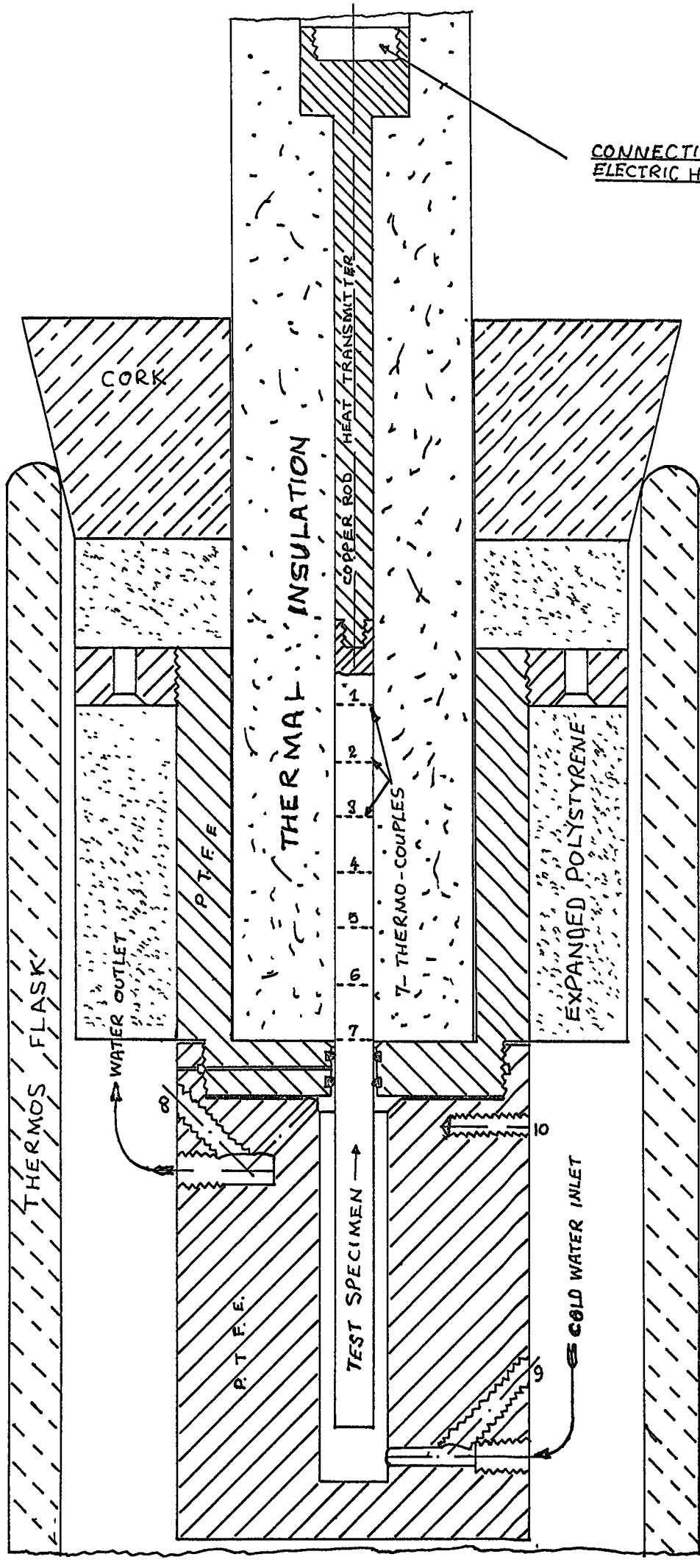

THERMO-COUPLES

1-7 SPECIMEN

8 WATER OUTLET

9 WATER INLET

10 WATER VESSEL WALL.

FIG. A2

VARIATION OF THERMAL CONDUCTIVITY OF THE BODY MATERIAL WITH TEMPERATURE AS MEASURED BY THE ELECTRICAL METHOD AND BY THE DIRECT METHOD.

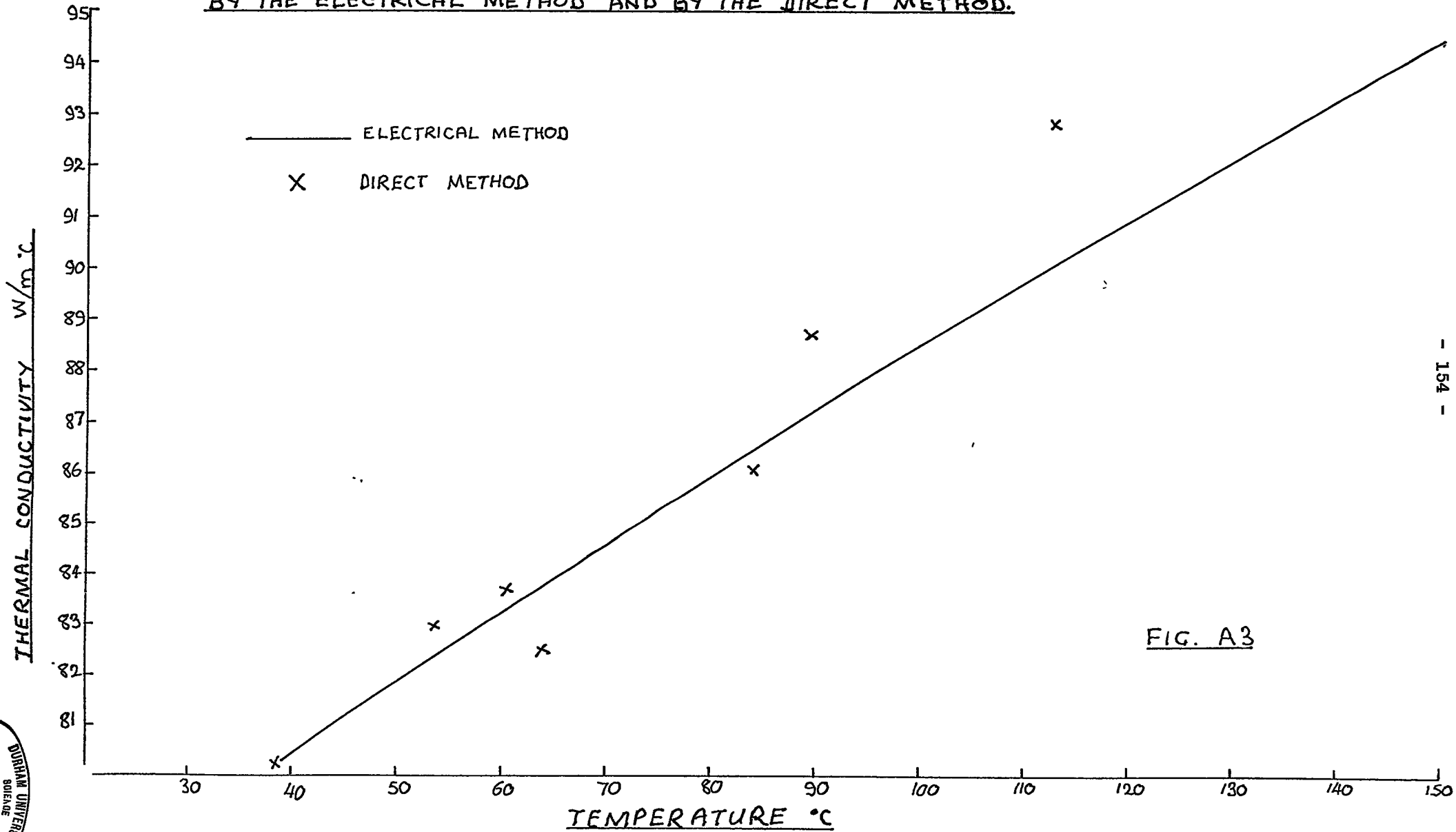

FIG. A3

PLATE 1 Full scale photograph at 0.0 rev/min.

PLATE 2 Full scale photograph at 50 rev/min.

PLATE 3 ·Full scale photograph at 100 rev/min.

PLATE 4 Full scale photograph at 150 rev/min.

PLATE 5 Full scale photograph at 200 rev/min.

PLATE 6 Full scale photograph at 300 rev/min.

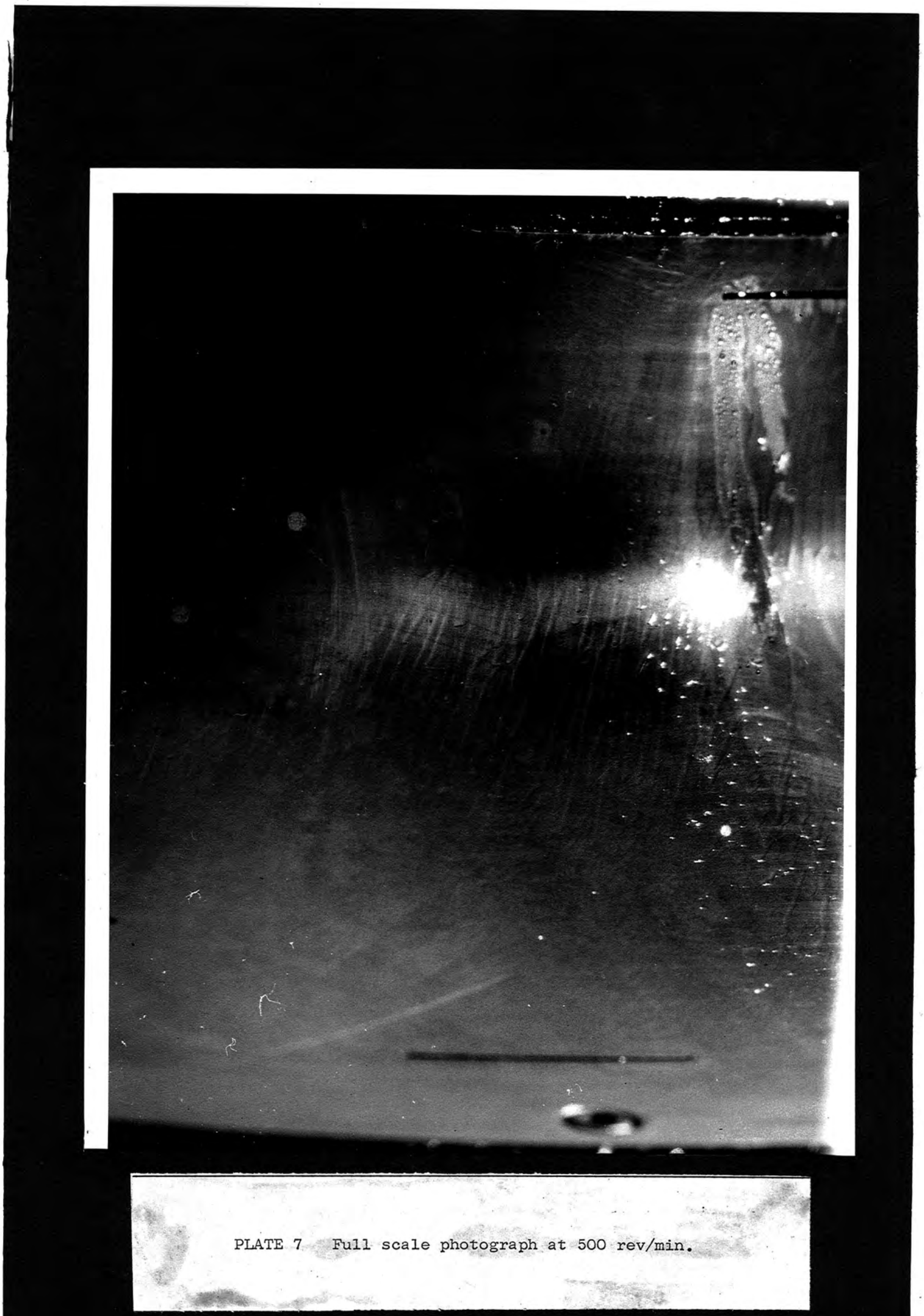

PLATE 7 Full scale photograph at 500 rev/min.

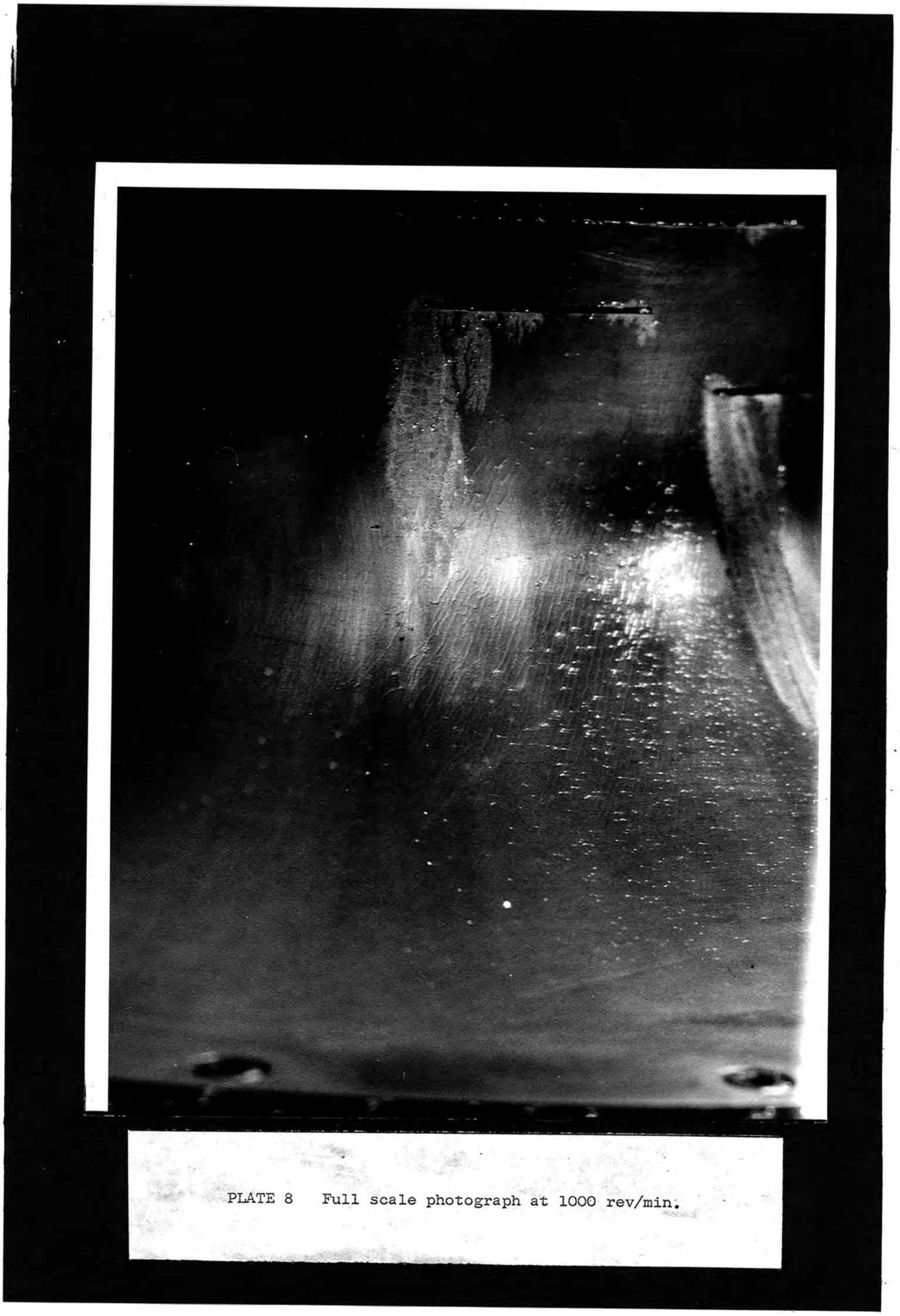

PLATE 8 Full scale photograph at 1000 rev/min.

PLATE 9 Curved body at 100 rev/min. No drops.

PLATE 10 Curved body at 150 rev/min. Drops at base

PLATE 11 Curved body at 1000 rev/min. Drops at base